



---

**Programme Area:** Carbon Capture and Storage

**Project:** Storage Appraisal

**Title:** Storage Capacity in Large Open Aquifers Exemplar

---

**Abstract:**

This document is a supporting document to deliverable MS6.1 UK Storage Appraisal Final Report.

**Context:**

This £4m project produced the UK's first carbon dioxide storage appraisal database enabling more informed decisions on the economics of CO<sub>2</sub> storage opportunities. It was delivered by a consortium of partners from across academia and industry - LR Senenergy Limited, BGS, the Scottish Centre for Carbon Storage (University of Edinburgh, Heriot-Watt University), Durham University, GeoPressure Technology Ltd, Geospatial Research Ltd, Imperial College London, RPS Energy and Element Energy Ltd. The outputs were licensed to The Crown Estate and the British Geological Survey (BGS) who have hosted and further developed an online database of mapped UK offshore carbon dioxide storage capacity. This is publicly available under the name CO<sub>2</sub> Stored. It can be accessed via [www.co2stored.co.uk](http://www.co2stored.co.uk).

---

**Disclaimer:**

The Energy Technologies Institute is making this document available to use under the Energy Technologies Institute Open Licence for Materials. Please refer to the Energy Technologies Institute website for the terms and conditions of this licence. The Information is licensed 'as is' and the Energy Technologies Institute excludes all representations, warranties, obligations and liabilities in relation to the Information to the maximum extent permitted by law. The Energy Technologies Institute is not liable for any errors or omissions in the Information and shall not be liable for any loss, injury or damage of any kind caused by its use. This exclusion of liability includes, but is not limited to, any direct, indirect, special, incidental, consequential, punitive, or exemplary damages in each case such as loss of revenue, data, anticipated profits, and lost business. The Energy Technologies Institute does not guarantee the continued supply of the Information. Notwithstanding any statement to the contrary contained on the face of this document, the Energy Technologies Institute confirms that the authors of the document have consented to its publication by the Energy Technologies Institute.

**UKSAP**

## **Appendix A5.4**

# **Storage Capacity in Large Open Aquifer Exemplar: Base Case Simulation and Sensitivities to Top Surface and Heterogeneity**

Conducted for

**The Energy Technologies Institute**

By

Imperial College London

Authors Aaron Goater, Branko Bijeljic and  
Martin Blunt  
.....

Technical Audit .....

Quality Audit .....

Release to Client Grahame Smith  
.....

Date Released 28<sup>th</sup> October 2011 (final)  
.....

The Consortium has made every effort to ensure that the interpretations, conclusions and recommendations presented herein are accurate and reliable in accordance with good industry practice and its own quality management procedures. The Consortium does not, however, guarantee the correctness of any such interpretations and shall not be liable or responsible for any loss, costs, damages or expenses incurred or sustained by anyone resulting from any interpretation or recommendation made by any of its officers, agents or employees.

Appendix A5.4 - Storage Capacity in Large Open Aquifers Exemplar - Base Simulation Sensitivities to  
Top Surface and Heterogeneity.doc File Location

## **Executive Summary**

One of the three main types of saline aquifer store relevant to UK CO<sub>2</sub> storage capacity that this project identified were „open aquifers“. In order to obtain more reliable storage capacity estimates for open aquifers, dynamic modelling was performed by numerical simulation using two classes of model: simplified generic models, termed „Representative Structures“ (see section 5.3.1 in the main report and Appendix A5.3), and more detailed models of selected regions of actual UKCS aquifer units, termed „Exemplars“.

A specific Exemplar aquifer was modelled to investigate issues not practical for investigation at the Representative Structure level. The principal aims of the Exemplar were to demonstrate the storage feasibility of an open aquifer with a realistic model case, to ascertain the impact of geological features such as top-surface structure and heterogeneity and to substantiate the Representative Structure storage regime 1, 2 and 3 results (Appendix A5.3). The Forties sandstone was identified as a suitable formation to situate the Exemplar, based upon a preliminary assessment of the permeability and dip of open aquifers available in CarbonStore.

A geological model for this region was constructed and a channelised sandstone and shale facies model was built using PETREL™. The final geo-cellular model consisted of 1.7 million cells, however the majority of modelling work was carried out with a 450,000 cell upscaled version to yield manageable simulation times. A grid sensitivity study showed the change in estimated storage capacity due to the upscaling was acceptable. The dynamic model was constructed in ECLIPSE 100™ into which the geological model was imported. Residual and dissolution trapping were modelled and structural trapping was calculated.

A multi-well injection scenario was created, applying the constraints on storage security and migration speed after 1000 years and pressure during injection, as listed in section 5.3.1 in the main report. The number and location of wells were selected to promote maximum storage potential. Under this „base case“ scenario the storage capacity of the Exemplar model was 471 Mt, representing a pore volume utilisation of 3.5%. The model arithmetic average permeability was 11 mD, at the lower end of the range for the whole Forties sandstone. The relatively low permeability required a higher number of injection wells, but also reduced migration velocities, providing good storage security.

To investigate the effect of the Exemplar heterogeneity and top-surface topography, models were run first with their full geological description, then without heterogeneity and then with the top-surface structure removed, to recreate a homogeneous smooth-topped model more comparable to the Representative Structure models. This analysis was then applied to cases with adjusted average dip and permeability with the well locations fixed in each case but injection from each well adapted to ensure that the storage constraints were met. These dip and permeability sensitivities confirmed the significance of permeability and dip upon pore volume utilisation shown in the simpler Representative Structure modelling, whether with a structured top-surface and heterogeneity or not.

The investigation of the effect of top-surface topography saw that its addition to the smooth model introduced structural traps and regions with locally higher or lower dip than the model average. It was found that this can increase or decrease pore volume utilisation relative to the smooth top-surface Representative Structure modelling, depending upon the strength of competing effects from structural trapping and the introduction of regions with higher and

lower dip. The relative importance of these effects was found to be dependent upon the storage regime of the smooth model.

In cases representative of storage regime 3, introducing top-surface topography:

- Increased pore volume utilisation through the addition of structural trapping of CO<sub>2</sub> and regions with lower dip characteristic of storage regime 2
- Maintained low pore volume utilisation typical of storage regime 3 in areas with increased dip.

In cases representative of storage regime 2, introducing top-surface topography:

- Again increased pore volume utilisation through the addition of structural trapping of CO<sub>2</sub>
- Maintained high pore volume utilisation typical of storage regime 2 where low dip was maintained
- Significantly reduced pore volume utilisation to levels typical of storage regime 3 where new localised high dip regions were introduced.

For the particular Exemplar top-surface topography studied, in cases representative of storage regime 2 the result of these competing effects saw a decrease in pore volume utilisation. These Exemplar results emphasise that real stores are likely to include both storage regimes 2 and 3 and consequently the utilisation is likely to be some combination of the storage regime 2 and 3 values, which was not seen in the Representative Structure modelling.

The introduction of heterogeneities influenced pore volume utilisation through its effect on injectivity and reservoir sweep during injection. In the cases investigated, heterogeneity, such as shale layers within the model, was found to increase lateral migration of the CO<sub>2</sub> plume, increasing the reservoir contact around the wells, and therefore the amount of residual trapping at deeper depths. In these scenarios increased CO<sub>2</sub> was stored residually at these depths while similar amounts were stored in the shallower layers near the top-surface to the homogeneous scenarios. As a result, the additional residual trapping meant increased pore volume utilisation was achieved in these cases. Different heterogeneity, not modelled in this study, could lead to channelling that reduces sweep, however other literature (e.g. Lengler et al. 2010) shows that this is rarely the case with permeability heterogeneity on a number of different length-scales.

A second effect of heterogeneity, and in particular the impermeable shales, was to increase local pressure build up in the Exemplar model. Where injectivity was found to be a limiting factor on the pore volume utilisation this injectivity reduction decreased the utilisation further.

Appendix A5.4 is organised as follows: *Introduction* addresses previous modelling work in open aquifers on the key parameter in the storage capacity estimates – pore volume utilisation factor, or storage efficiency –, states the need for dynamic modelling work for better storage capacity estimates, and defines the aims of the Exemplar study. *Exemplar Model and Methods* describe the geocellular and the dynamic model used in simulation, as well as the methodology used for calculating storage capacity. This is followed by *the Base case*

*Storage Capacity in Large Open Aquifer Exemplar: Base Case Simulation and Sensitivities to Top Surface and Heterogeneity*

---

*Exemplar results, and the results on the impact of top-surface and heterogeneity (sensitivity). The significance of the storage capacity results for the UKSAP project is discussed and conclusions are drawn.*

# Contents

Executive Summary .....	iii
1 Introduction .....	1
1.1 General Framework for Capacity Estimation in Open Aquifers .....	1
1.2 Volumetric Storage Capacity Estimation Projects and Studies .....	2
1.3 Storage Capacity Estimation Projects and Studies based on Dynamic Models ..	4
1.4 The Effect of Geological Features upon CO <sub>2</sub> Capacity and the Distribution of CO <sub>2</sub> .....	8
1.5 Aims of the Exemplar Study.....	10
2 Exemplar Model and Methods .....	13
2.1 Geocellular Model of the Forties-based Storage Unit .....	13
2.2 Construction of the Dynamic Model .....	17
2.3 Base Case Injection Set-up .....	19
2.4 Storage Security and Trapping Assessment .....	20
2.5 Sensitivity Models for Studying the Impact of Top Surface and Heterogeneity ..	22
2.6 Methodology for Calculating Storage Capacity – Optimising Injection and Well Location .....	24
2.7 Alternative Simulations using Streamlines.....	27
3 Base Case Exemplar Results .....	28
3.1 Base Case Exemplar Storage Appraisal .....	28
3.2 Base case Exemplar – Storage Capacity and Trapping Mechanism.....	29
3.3 Base Case Exemplar Verification.....	31
3.3.1 Sensitivity to Grid Resolution.....	31
3.3.2 Sensitivity to Boundary Condition .....	35
3.4 Base case Exemplar Sensitivity to Reservoir Dip and Permeability .....	37
3.4.1 Base case Exemplar sensitivity to permeability.....	37
3.4.2 Base Case Exemplar Sensitivity to Dip.....	39
3.4.3 Conclusions and Analysis of the Dip and Permeability Sensitivity and Storage Regime Results.....	40
4 Impact of Top-Surface Structure and Heterogeneity – Sensitivity Results.....	46
4.1 Effect of Top-surface Structure upon Storage Capacity.....	46
4.1.1 Effect upon Models with Injectivity Limited Storage Capacity (storage regime 1) .....	46
4.1.2 Effect upon Models Characterised by Storage Regime 2 .....	48
4.1.3 Effect upon Models Characterised by Storage Regime 3 .....	49
4.1.4 Conclusions on the Effect of Top-surface Structure.....	51
4.2 Effect of Heterogeneity upon Storage Capacity.....	52
4.2.1 Effect upon models with Injectivity Limited Storage Capacity (storage regime 1) .....	52
4.2.2 Effect upon Models Characterised by Storage Regimes 2 & 3 .....	53
4.2.3 Conclusions on the Effect of Heterogeneity .....	54
5 Discussion.....	55
6 Conclusions.....	58
7 Acknowledgements .....	59
8 References.....	60

## List of Tables

Table A2.1: Initial conditions and parameters for the Exemplar base case simulation.....	18
Table A3.1: Storage pore volume utilisation (PVU) results .....	45

## List of Figures

Figure A1.1: Open aquifer storage regimes as described in section 5.3.1 in the main report... 7	
Figure A1.2: Sketch of a dipping open aquifer (left) versus a large-scale structural closure (right). It is assumed that the structural closure has closure in all directions. ....	10
Figure A2.1: Location of the Forties Sandstone member and the Forties geological model. Areal extent of the Forties geological model is identified by black rectangle .....	13
Figure A2.2: Top Forties seismic interpretation in depth. The location of the Forties geological model and wells are also shown .....	14
Figure A2.3: Facies Model at Layer 1 (top) and Layer 90 (bottom). Higher shale proportion is seen at base Forties.....	15
Figure A2.4: Porosity model at Layer 1 (top) Forties Exemplar base case geological model. ....	16
Figure A2.5: Permeability model at Layer 1 (top) Forties Exemplar base case geological model.....	16
Figure A2.6: Viking 2 relative permeability and capillary pressure used in the Exemplar base model simulation .....	17
Figure A2.7: Overpressure contours for the Forties Sandstone member. Forties base case geological model area is shown in red .....	19
Figure A2.8: Map of cells on the top layer which are structurally closed. Due to the buoyancy of CO <sub>2</sub> , once within these structurally closed cells it will stay there until dissolved .....	21
Figure A2.9: Permeability maps for (from left to right) base case 11mD permeability and two permeability sensitivities 145mD and 1D. Figures show top layer of model viewed from above .....	22
Figure A2.10: Porosity maps for the different dip sensitivity models. The base case has dip 0.27° and two sensitivity cases have dips 1° and 3°. Models are viewed from the west and vertically exaggerated by a factor of 15.....	23
Figure A2.11: Simplification of base case model by removing heterogeneity then top-surface structure. Figures show permeability in mD, are viewed from the south and are exaggerated by a factor 15 in the vertical direction.....	23
Figure A2.12: Locations of the eleven horizontal wells used for the base case and sensitivity scenarios. Viewed from above.....	25
Figure A2.13: General methodology for calculating the capacity of each model.....	26
Figure A3.1: Pressure (bars) profile at top layer at 50 years in a preliminary 6 well injection scenario. Purple 'specs' are shales that were treated as inactive cells in early simulations. Pressures around 400bars (=40MPa) and below indicate some limited pressure space, suggesting that using more wells would lead to higher storage capacities. Wells are shown in black .....	28
Figure A3.2: The total mass of CO <sub>2</sub> (Mt) injected into the base case geological model per decade using 11 wells .....	29
Figure A3.3: CO <sub>2</sub> saturation in Forties base case model at 1000 years. Maximum gas saturation is 0.577. Model length 36km, viewed from south and vertically exaggerated by a factor of 15. Wells are shown in black.....	30
Figure A3.4: Mechanisms trapping CO <sub>2</sub> in the base case model at 1000 years. Percentages show the proportion of the total amount trapped by different mechanisms.....	30
Figure A3.5: Mechanisms trapping CO <sub>2</sub> at 1000 years and 10,000 years.....	31
Figure A3.6a: Porosity distribution for 1,733,400 (left) and 450,450 (right) cell models .....	32
Figure A3.7: Permeability (mD) map for 1,733,400 (left) and 450,450 (right) cell models viewed from above .....	32

Figure A3.8: Saturation profiles at 10000 years for 1,733,400 (left) and 450,450 (right) cell models. Top models show top layer viewed from above. Wells are shown in black. Bottom models show saturation intersections around injection well INJ12 ..... 33

Figure A3.9: Pressure (in bars) profiles on top layer at 40 years for 1,733,400 (left) and 450,450 (right) cell models. Higher localised pressure is visible in the 450,450 cell model.... 34

Figure A3.10: Mass (Mt) of CO<sub>2</sub> stored with different grid resolutions at 1000 years ..... 34

Figure A3.11: Scenario 3 - The cells at the boundary had large pore volumes to represent the volume of aquifer attached to the model. Visually these boundary cells appear with the same area as their neighbours, however their pore volume is larger. To test the effect of the resolution of these boundary cells, such as the one highlighted they were refined. This can be seen by the range of colours inside. This refinement allowed the pressure to be resolved more accurately..... 35

Figure A3.12: Sensitivity of injected CO<sub>2</sub> volume to changes in boundary condition..... 36

Figure A3.13: Sensitivity of base case storage pore volume utilisation (PVU) to permeability..... 37

Figure A3.14: Top layer saturation profile at 1000 years for 145mD permeability sensitivity. The injection scenario shows injected CO<sub>2</sub> equal to 4% of the storage unit pore volume. 0.4% of the injected left the model – meeting the 99% storage constraint; however the migration velocity constraint was failed. Wells are shown in black ..... 38

Figure A3.15: Top layer saturation profile at 1000 years for 145mD permeability sensitivity. The injection scenario shown injected CO<sub>2</sub> equal to 2% of the storage unit pore volume and met the storage constraints. Wells are shown in black ..... 39

Figure A3.16: Sensitivity of base case storage pore volume utilisation (PVU) to reservoir dip ..... 39

Figure A3.17: Sensitivity of storage pore volume utilisation (PVU) due to changes in permeability in the 0.270 smooth heterogeneous model..... 40

Figure A3.18: Top layer saturation profile for at 1000 years for 145mD permeability smooth homogeneous model..... 41

Figure A3.19: Sensitivity of the stored mass (Mt) of 'Low velocity CO<sub>2</sub>' to permeability in a 0.27° dip, smooth homogeneous scenario. Low velocity CO<sub>2</sub> is defined in Section 2.4 ..... 42

Figure A3.20: Saturation profile in the top layer of a smooth, homogeneous 1 Darcy model at 1000 years. Most gas saturation is seen to be near residual ..... 43

Figure A4.1: Change in storage pore volume utilisation (PVU) due to the introduction of top-surface structure and heterogeneity to the 11mD 0.27° smooth homogeneous case ..... 46

Figure A4.2: Saturation profile showing the top layer of a smooth homogeneous 11mD model with a dip of 0.27° at 1000 years..... 47

Figure A4.3: Saturation profile showing the top layer of 11mD, 0.27° dip homogeneous model with top-surface structure at 1000 years ..... 47

Figure A4.4: Change in storage pore volume utilisation (PVU) due to the introduction of top-surface structure and heterogeneity to the 145mD 0.27° smooth homogeneous case ..... 48

Figure A4.5: Saturation of a homogeneous 145mD, 0.27° dip model with top-surface structure at 1000 years. Model viewed from south and exaggerated by factor 15 in the vertical direction ..... 49

Figure A4.6: Change in storage pore volume utilisation (PVU) due to the introduction of top-surface structure and heterogeneity to the 1 Darcy 0.27° smooth homogeneous case ..... 50

Figure 4.7: Change in storage pore volume utilisation (PVU) due to the introduction of top-surface structure and heterogeneity to the 145mD, 1° smooth homogeneous case ..... 51

Figure A4.8: Pressure (in bars) profile around well INJ10 in heterogeneous (left) and homogeneous (right) cases at 50 years. The intersections show that localised high pressure can build up in the heterogeneous model whereas it spreads further in the homogeneous model..... 53

Figure A4.9: Saturation intersections to show wider lateral migration under shales in the heterogeneous model (left) compared to the homogenous model (right) at 1000 years. Both models have 145mD permeability and 0.27° dip ..... 53

Figure A4.10: Gas saturation intersection around well INJ2 to show structural trapping under shales at 1000 years for the 11mD heterogeneous case..... 54

Figure A5.1: Range of potential general effects of the introduction of top-surface structure to storage regimes 2 and 3..... 56

# 1 Introduction

In the next section the previous modelling work in open aquifers on the key parameter in CO<sub>2</sub> storage capacity estimates – pore volume utilisation, or storage efficiency factor is addressed. Dynamic modelling in this context is reviewed in detail and the key objectives of the Exemplar study are stated.

The simplest approach to estimating storage capacity is to multiply the estimated pore volume of the aquifer by some (small) constant that represents the fraction of the pore space that CO<sub>2</sub> is likely to occupy. This constant can be estimated using two generic approaches. The first uses the compressibility of the resident brine and the formation to find the maximum volume change over the whole storage unit that would limit the average pressure increases to some threshold – usually so that the pressure stays below the fracture pressure of the rock. This is easy to do, but assumes an average pressure everywhere and takes no account of the dynamics of the process and the migration paths of the injected CO<sub>2</sub>. The second approach simulates the injection of CO<sub>2</sub> and does study the CO<sub>2</sub> migration and the dynamic pressure response, using this to assess capacity. The geological model used can be homogeneous and structurally simple - as in the work on Representative Structures described in Appendix A5.3. In this Exemplar modeling study, however, a structurally realistic heterogeneous reservoir model is used, with a geologically realistic subsurface model to study constraints on injection rate and total storage capacity, investigating both pressure response and the movement of injected CO<sub>2</sub>.

## 1.1 General Framework for Capacity Estimation in Open Aquifers

In recent years (CSLF, 2008; Vangkilde-Pedersen et al., 2009; USDOE, 2010) a simple type of volumetric equation, of which there are variations, has been used across a wide range of national capacity studies to form the framework for capacity estimation in aquifers. In particular this form is used to estimate the 'Effective Storage Capacity' as defined by Bradshaw et al. (2007). This represents the capacity of potential storage sites to store CO<sub>2</sub> when a range of geological and engineering effects are taken into account such as quality of the reservoir and seal, pressure regimes and size of the pore volume of the reservoir or trap. This measure does not however consider all technical, legal, regulatory and general economical barriers to CO<sub>2</sub> storage.

There are three main variations of this form of volumetric equation [1.1-1.3], each evaluating how much of the pore volume can be occupied by CO<sub>2</sub>:

Vangkilde-Pedersen et al. (2009) present the equation used in the EU GeoCapacity project for calculating capacity in saline aquifers:

$$M_{CO_2} = S_{eff} NGAh\phi\rho_{CO_2} \quad (1.1)$$

$A$  and  $h$  are the regional or trap area and average thickness, respectively,  $\phi$  is average porosity,  $NG$  is the net to gross ratio of the regional trap,  $\rho_{CO_2}$  is the density of the CO<sub>2</sub> and  $S_{eff}$  is the 'storage efficiency factor', or pore volume utilisation factor – the term that will be used throughout this work.

The U.S. Department of Energy (USDOE) present their methodology (USDOE, 2010) for calculating CO<sub>2</sub> storage capacity:

$$M_{CO_2} = EAh\phi\rho_{CO_2} \quad (1.2)$$

$A$  and  $h$  are the formation area and average formation thickness respectively,  $\phi$  is average porosity and  $E$  is the storage efficiency factor.

The Carbon Sequestration Leadership Forum (CSLF) presented a number of formulae to estimate the volume of CO<sub>2</sub> stored through the different mechanisms of structural, residual, solubility and mineral trapping (CSLF, 2008). At the national scale and for estimating effective capacity the structural trapping equation is to be used:

$$M_{CO_2} = C_c(1 - S_{wirr})Ah\phi\rho_{CO_2} \quad (1.3)$$

$A$  and  $h$  are the structural trap area and average thickness, respectively,  $S_{wirr}$  is the average irreducible water saturation and  $C_c$  is the 'capacity coefficient'. The capacity coefficient takes into account the impact of heterogeneity, CO<sub>2</sub> buoyancy and sweep efficiency. The CSLF methodology also proposes a range for the CO<sub>2</sub> density between the density of CO<sub>2</sub> at the initial formation pressure and at the maximum allowable formation pressure, since the formation pressure is not known until injection finishes. A key difference between this and the other equations is in that the CSLF method is defined for estimating storage capacity within structural closures. Bachu et al. (2007) define hydrodynamic trapping as a combination of all storage mechanisms occurring while a plume of injected CO<sub>2</sub> migrates within an unconfined aquifer. CO<sub>2</sub> stored through this hydrodynamic trapping definition may best compare to the CO<sub>2</sub> evaluated through the USDOE and EU GeoCapacity methodologies.

Each of these equations represents approximately the same approach with a parameter that measures the storage efficiency (pore volume utilisation) within a storage unit. The differences are that the CSLF method takes into account the irreducible water saturation explicitly in a separate parameter as does the EU GeoCapacity method with the net to gross ratio. Furthermore the CSLF method is designed for estimating storage in structural closures.

These equations provide a framework for capacity estimation. It is either possible to use the equations with fixed storage efficiency parameter values, or if further analysis suggests, vary these values for different regions, basins or storage units. In the next section the values of these storage efficiency parameters that have been applied in previous studies, where one value was applied universally to all open aquifers, are reviewed.

## 1.2 Volumetric Storage Capacity Estimation Projects and Studies

Over the past 10 years there have been numerous storage capacity studies at the national scale using various estimation methodologies that are described with varying clarity. A number of studies applied the above equations with fixed efficiency parameters:

Vangkilde-Pedersen et al. (2009) present the EU GeoCapacity preliminary estimate for European CO<sub>2</sub> storage capacity in all open and closed aquifers as 325Gt. Within this work a number of countries produced estimates using the EU GeoCapacity formula. To determine the storage efficiency factor they distinguish between storage capacity estimates for regional

aquifers and estimates for individual structures and stratigraphic traps. For regional open aquifers they suggest using a uniform storage efficiency factor of 2% based upon the work of USDOE. For individual structural or stratigraphic traps they suggest values from 3% to 40% for semi-closed low quality and open high quality reservoirs, respectively. Within this study Radoslaw et al. (2009) calculated the CO<sub>2</sub> storage capacity for a mixture of open aquifers, geological structures and hydrocarbon fields in Poland. They calculate that Poland's total aquifer capacity is 78Gt, the capacity of selected structures is 3.5Gt, and the capacity of hydrocarbon fields is 0.8Gt. The constant storage efficiency factor of 2% was used in the regional aquifers and 20% was used in the structural traps.

Lewis et al. (2009) presented an application of the CSLF methodology to estimate storage capacity in onshore and offshore Ireland. Under this methodology they estimate theoretical, effective or practical storage capacities based upon data available. Keeping consistency with the CSLF methodology they only estimate the capacity of structures within the reservoirs. For the aquifers where sufficient data was available they calculate the capacity in structures as 3.5Gt using the CSLF method with  $C_c (1 - S_{wirr}) = 0.4$ . This figure was based upon a numerical simulation of filling a structure within a closed reservoir.

Ogawa et al. (2011) presented work on the Japanese national CO<sub>2</sub> storage capacity assessment. The saline aquifers were first classified into two categories for storage capacity assessment in terms of the type of geological structure present. Aquifers or hydrocarbon fields with structural traps were found to have 30Gt storage capacity and aquifers without geological structural closure 116Gt, providing a total storage capacity of 146Gt. They calculate CO<sub>2</sub> capacity by mass using a formula broadly similar to those presented above with parameters to account for heterogeneity and CO<sub>2</sub> saturation. For the open units without structural traps their storage efficiency factor under the USGS method was in the range 0.025-0.05 dependent upon the sand/clay ratio present within a reservoir. Under the GeoCapacity formula, which includes a net/gross ratio, this is equivalent to a storage efficiency factor  $S_{eff}$  of 0.125 with the net to gross values from 0.2 to 0.4. For the structural closures the equivalent storage efficiency factor under the GeoCapacity formula was 0.25.

Bradshaw et al. (2011) evaluated the effective storage capacity in thirty six basins including aquifers, oil and gas fields and coal seams in Queensland, Australia. These came from the results of the Queensland CO<sub>2</sub> Geological Storage Atlas. Under their methodology, in addition to calculating storage capacities of a mixture of open and closed units, they also introduced a point system to rank the suitability of sites. The factors taken into account in measuring suitability were bulk seal effectiveness, faults through seal, porosity, permeability and depth at base of seal.

Other studies have run preliminary assessments for national storage capacity, but require further work to produce national capacities, such as work on the Indian subcontinent by Holloway et al. (2009). Li et al. (2009) and Dahowski et al. (2009) both present work on Chinese theoretical capacity estimation based on a volumetric formula  $V_{CO_2} = SAh\phi$  to calculate the capacity of each basin, where  $S$  is the solubility of CO<sub>2</sub> in deep saline formations. Using this calculation and summing together all of the aquifers they found 3066Gt of storage, representing over 99% of China's total potential capacity. However, since this represents a theoretical estimate of capacity in the capacity scale of Bradshaw et al. (2007) it is expected that the effective capacity estimate is to be lower.

In the UK, Holloway (2009) reviews CO<sub>2</sub> storage capacity estimates up to 2008 for oil and gas fields. The total CO<sub>2</sub> storage capacity in the UK oil fields, as estimated by the old Department for Trade and Industry, is approximated to be 1.2Gt. These estimates are considered to fit into the matched capacity in the capacity scale of Bradshaw et al. (2007) due to the level of technical detail from industry put into these. The total CO<sub>2</sub> storage capacity of the southern North Sea gas fields is estimated as 3.9Gt CO<sub>2</sub> and gas fields in the East Irish Sea Basin are estimated as 1Gt CO<sub>2</sub>. Studies into the capacity of saline aquifers in the Southern North Sea basin indicate several Gt of CO<sub>2</sub> storage capacities; however it was suggested that none of these studies take into account all the major factors influencing capacity estimates and that studies for aquifers needed to be revisited. In particular, it would be desirable to take into account the dynamics of flow within reservoirs.

### 1.3 Storage Capacity Estimation Projects and Studies based on Dynamic Models

A number of projects and studies have developed methodologies that try to account more explicitly for the dynamics of flow within reservoirs. All the estimates reviewed in section 1.2 assume a volumetric (static) capacity and do not take into account how fast CO<sub>2</sub> can be injected. Within these, the storage efficiency parameters are usually still used or calculated but are not always fixed and can be given different values depending upon the basin's characteristics.

Van der Meer and Yavuz (2009) estimated the capacity in the Dutch subsurface using a mixture of fixed parameter analyses and a more dynamic approach. First they use the EU GeoCapacity formula with the 2% storage efficiency factor finding a total capacity of 438Mt, although they apply this to "areas comprising partly/fully dip-closed structures or fault-bounded structures" measuring the areal extent of these by determining the location of spilling points. They then take into account the effect of limited injectivity into these formations after which the capacity is found to be 104Mt. The injectivity analysis takes into account the homogenous porosity and permeability and thickness of five large zones that construct the total capacity. In their analysis they represent zones by connected aquifer portions and within these zones determine the number of traps and their spill points. Kopp et al. (2009) proposed using the Doughty et al. (2001) framework in their model, which under the CSLF capacity equation constructs the capacity coefficient  $C_c$  from three factors:

$$C_c = C_i C_g C_h \tag{1.4}$$

where  $C_i$  is the intrinsic capacity coefficient, which accounts for the 1D displacement efficiency,  $C_g$  is the geometric capacity coefficient, which accounts for partially penetrating well, gravity segregation and dipping aquifers, and  $C_h$  is the heterogeneity capacity coefficient. They ran sensitivities to various parameters to investigate their effect on the capacity coefficients in two open models without structure. The two cases were a 1D idealised gravity-free reservoir and a 3D radially symmetric domain. The parameters investigated were reservoir depth, geothermal gradient, relative permeability, permeability, capillary entry pressure and injection rate. In both the 1D and 3D case injection continued until CO<sub>2</sub> reached a spill-point a set distance from the well. In the 3D case this is set 1km from the well – equivalent to the field scale.

In the 1D case, their median reservoir had  $C_i = 0.323$ , the lowest value was 0.245 for a shallow reservoir and the greatest value was 0.505 for a basal relative permeability with low CO<sub>2</sub> residual. Since these efficiencies were calculated during injection it seems that this analysis is best suited to injection in a structural trap. Otherwise over a full post-injection period one would expect the case with low residual saturation to travel further, as opposed to during injection where it was possible to displace water with more efficient, higher and slower leading CO<sub>2</sub> saturation.

In the 3D case, Kopp et al. (2009) find values for  $C_i$  ranging from 0.2150 to 0.4868 for the same sensitivities as the 1D test and values of  $C_g$  ranging from 0.1978 to 0.6334 for the slow rate and the low permeability case respectively. In conclusion they find that deep cold and/or low permeability reservoirs are more favourable for efficient utilisation of the available storage volume. Their results provide CSLF type capacity coefficients in the range 7.1% – 18%. Their study did not include heterogeneity, structure, dip, dissolution of CO<sub>2</sub> into brine and the effects of relative permeability hysteresis. They comment that their horizontal cap and one injection well and lack of dissolution may lead to conservative results but that lacking heterogeneity may lead to optimistic results.

Szulczewski and Juanes (2009) and Juanes et al. (2010) present an analytic approach for calculating CO<sub>2</sub> storage capacity in open aquifers at the basin scale. The model uses simplifying assumptions to take into account dynamic phenomena such as gravity override and residual trapping in open aquifers that have a horizontal top surface without structure. The outcome is a simple equation to calculate storage efficiency factor under the US-DOE definition using constant values for mobility, reservoir volume, CO<sub>2</sub> density, and water and CO<sub>2</sub> residual saturations. In an example basin they obtain storage efficiency factor from 0.8% to 1.6%, depending upon the amount of residual trapping. These factors are calculated at the time when all CO<sub>2</sub> is residually trapped. This work has been extended in Macminn et al. (2010) to account for dip analytically, although rather than a single form, a set of closed forms and approximations are now provided. Furthermore Macminn et al. (2011) account for dissolution and in this case the problem is solved numerically.

Goodman et al. (2011) present a description of the USDOE methodology for estimating CO<sub>2</sub> storage capacity, which expands the USDOE definition of storage efficiency given in equation (1.2). They calculate the storage efficiency factor  $E$  for saline aquifers with the proposed formula:

$$E = E_{An/At} E_{hn/hg} E_{\theta_e/\theta_{tot}} E_A E_L E_g E_d \quad (1.5)$$

where the net-to-total area ratio  $E_{An/At}$  is the fraction of the total basin or region area that is suitable for CO<sub>2</sub> storage. The net-to-gross thickness ratio  $E_{hn/hg}$  is the fraction of the geologic unit that meets their minimum porosity and permeability requirements for injection. The effective-to-total porosity ratio  $E_{\theta_e/\theta_{tot}}$  is the fraction of total interconnected porosity. The areal displacement efficiency  $E_A$  is the fraction of planar area surrounding the injection well that CO<sub>2</sub> can contact. The vertical displacement efficiency  $E_L$  is the fraction of vertical cross section that can be contacted by the CO<sub>2</sub> plume from a single well. The gravity displacement

efficiency  $E_g$  is the fraction of net thickness that is contacted by CO<sub>2</sub> as a result of CO<sub>2</sub> buoyancy. The microscopic displacement efficiency  $E_d$  is the fraction of the CO<sub>2</sub> contacted, water-filled pore-volume that can be replaced by CO<sub>2</sub>.

In their calculations Goodman et al. (2011) treat systems as open at the boundaries and note that closed systems could in theory have their pressure build-up remediated. Structural and hydrodynamic trapping are the focus of their methodology for estimating aquifer capacity at the basin scale, although it is not clear at what timescale the parameters are estimated. Within their analysis they do not take into account injection rate or pressure, the number of wells drilled, type of well and other economic and regulatory considerations. They use Monte Carlo simulation to account for uncertainty in a variety of parameters and find efficiency factors range between 0.4 and 5.5% over the 10<sup>th</sup> to 90<sup>th</sup> percentile. In particular they produce distributions for each of the above parameters for three geological settings – clastics, dolomite and limestone.

Gorecki et al. (2009), who present work from IEAGHG (2009), set out to use both numerical simulations and available field-data to build upon the storage coefficients built by USDOE. For basin-scale open aquifers, efficiencies were evaluated and presented with the storage efficiency factor  $E$  and the volumetric and microscopic displacement efficiencies from the USDOE work. The volumetric efficiency was taken as the product of the areal, vertical and gravity displacement efficiency, as defined by Goodman et al. (2011).

Gorecki et al. (2009) produced a homogenous base case model which had permeability 230mD, salinities of 53,000 ppm, pressures of 23.9MPa, depths of 2338m, temperatures of 75°C, thickness of 26m, permeability anisotropy  $K_v/K_h = 0.1$  and a halfdome structure. To determine which key parameters most strongly affect the storage efficiency factor they ran sensitivities to structure, depth, temperature, permeability anisotropy, relative permeability and injection rate in a homogeneous model. The structures compared included domes, anticlines and flat models. In all sensitivity cases they injected 0.91Mt for 1 year so that all cases obeyed a bottom-hole pressure constraint. The storage coefficient was then calculated at the end of injection using a minimal volume block enclosing the free phase CO<sub>2</sub> saturation plume to measure the total pore volume.

In general, tightly closed structures, increased depth and lower temperatures, low ratios of vertical-to-horizontal permeability, and high injection rates all increased the storage efficiency. Structure had the strongest effect, promoting higher volumetric and macroscopic displacement efficiency and storage efficiency rising from 0.15 and 0.25 in the most curved formations. Rate, depth and permeability anisotropy ( $K_v/K_h$ ) and temperature lead to variation in storage efficiency of 0.07, 0.06, 0.05 and 0.03 respectively, while relative permeability had a smaller effect. As in other studies, it is noted that calculating storage efficiency at the end of injection is best suited to the structurally secure models, and may give high values to basins without significant structure.

They also studied 195 heterogeneous models using three lithologies, five structural settings and ten depositional environments. Each lithology was assigned specific parameter distributions for  $K_v/K_h$ , relative permeability, porosity and permeability and the injection rate for all cases was reduced to 0.18Mt/yr. Based upon this methodology, they found that lithology had an effect on storage coefficient with P10/P50/P90 ranges at the formation scale

of 1.86/2.70/6.00, 2.58/3.26/5.54 and 1.41/2.04/3.27 % for clastics, dolomites and limestone respectively.

Finally, they demonstrated the effect of the boundary condition on the storage efficiency. Comparing a closed system against the open systems they found storage efficiency reduced by a factor of 25 for the closed system, demonstrating the effect of the boundary condition as the key factor and signifying that if boundary conditions are known, a suitable open or closed methodology should be used.

In the dynamic modeling section 5.1 in the main report storage units are either classified as closed or open and within the open units where potential structural traps are known to be large and therefore important in terms of overall UK storage capacity they are separated out. The remaining open aquifer area is assumed to have smooth structural topography. Storage pore volume utilisation values under the USDOE definition are then calculated at the storage unit scale at 1000 years. To calculate these, structurally smooth, homogeneous simulation models were constructed and used to investigate the effect of various parameters including horizontal and vertical permeability, porosity, thickness, dip, brine salinity and trapped gas saturation (Appendix A5.3). This work showed that reservoir top-surface dip and permeability had strongest influences on storage pore volume utilisation because they determine the velocity at which CO<sub>2</sub> flows and the injectivity of a model. From this conclusion three storage regimes were identified as shown in **Figure A1.1** with different distributions of storage pore volume utilisation for each storage regime (see section 5.3.1 in the main report).

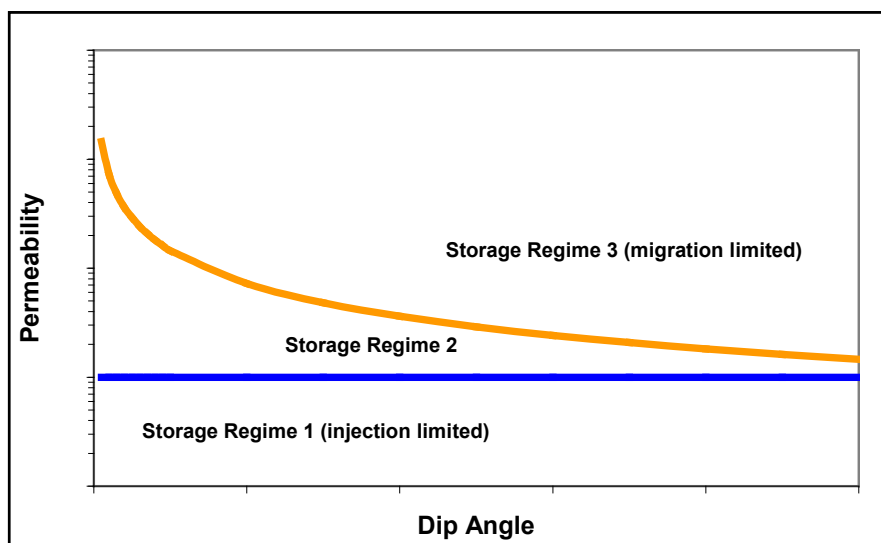


**Figure A1.1: Open aquifer storage regimes as described in section 5.3.1 in the main report**

The storage regimes are described as:

**Regime 1** has poor well injectivity but good storage security and is characterised by a low representative permeability.

**Regime 2** is characterised by both good CO<sub>2</sub> injectivity and good storage security and therefore typically has higher storage capacities.

**Regime 3** has good CO<sub>2</sub> injectivity, but storage capacities are strongly constrained by the tendency of CO<sub>2</sub> to migrate updip due to buoyancy forces. Such stores are characterised by either a high representative permeability or significant mean dip, or both.”

Storage regime 2 and 3 are separated by a boundary that estimates the characteristic migration velocity associated with a field.

The work carried out hereafter shall consider the storage regimes further in sections 3 and 4 of this report.

The work described to date considers analytical or simple numerical models to describe storage capacity but do not address the impact of key factors such as reservoir top-surface structure and heterogeneity. Hence, the studies that are more focussed on reservoir top-surface structure and heterogeneity are discussed in the next section.

## 1.4 The Effect of Geological Features upon CO<sub>2</sub> Capacity and the Distribution of CO<sub>2</sub>

In addition to this broad set of studies designed to use or improve the storage efficiency results, there has also been a lot of simulation work at the field or storage site scale focusing on the effect of geological features upon either storage capacity or the distribution of CO<sub>2</sub> that can have an impact on the storage capacity.

Doughty et al. (2001) assessed the capacity of the saline heterogeneous Frio formation in Texas using Equation (1.4) to define a capacity coefficient. They used TOUGH2 to model 20 years injection and 40 years post-injection period in an open 1km x 1km x 100m aquifer model. The formation heterogeneity is described by transition probability geostatistics and the top-surface structure is smooth and flat. They then consider a homogeneous model and then a model with no gravity, to examine the effect of heterogeneity and gravity respectively. During injection they allow fluid to leave the boundaries freely and consider the storage pore volume utilisation at 20 years and 60 years. In their models they found heterogeneity enhanced capacity by counteracting gravity. They acknowledge that the volumes over which capacity coefficients are evaluated and time at which they are evaluated are important.

Obi and Blunt (2006) used a one million cell model of CO<sub>2</sub> storage into an open heterogeneous 5km x 9km x 200m North Sea aquifer with a smooth top-surface. They found that advective transport of CO<sub>2</sub> was dominated by high-permeability channels and that this led to storage efficiency of around 2% evaluated at 200 years using the smallest box volume that contained the CO<sub>2</sub> plume. Qi et al. (2009) considered a similar heterogeneous setup, but explored the injection of water with CO<sub>2</sub> to enhance residual trapping. They found that storage efficiency could be increased from 3% to 9% by optimizing the injection strategy. This storage efficiency was assessed at the end of 20 years injection, when due to extra residual trapping over 90% of the CO<sub>2</sub> was either residually trapped or dissolved.

Flett et al. (2007) considered the impact of heterogeneity on containment and trapping. They used an open 5km x 10km areal scale model with a smooth dipping top-surface and notional yet realistic geological heterogeneity and compared against a homogeneous model. Flow was modelled for 1000 years with injection for the first 50 years. They found that with increasing net-to-gross ratio vertical flow was progressively inhibited, promoting lateral flow. This resulted in increased tortuosity of the CO<sub>2</sub> pathway and improved reservoir contact and

increased dissolution. In addition, they found that the increase in the tortuosity of the CO<sub>2</sub> pathways delayed residual gas trapping.

Kuuskräa et al. (2009) considered how reservoir architecture could be used to maximise storage capacity. They created an open radial base case model with a flat topography using layering from field data containing multiple shale breaks. To investigate the effects of reservoir architecture and properties on plume dynamics they simulated a number of scenarios. These included the base case shale model, a homogeneous model and a model with “leaky” 1mD shales each having 4 years injection and modelled for 100 years after injection. A final scenario with 40 years injection was also modelled. They found that when impermeable layers – which extended across the model – were included, the reservoir contact was increased and they expected a plume of less than half the extent of that in the homogenous model.

Jin et al. (2010) considered two geological models of aquifers with dimensions of the order 10km x 10km x 300m, one with a simpler tilted geology and the other a more complex structure including an anticline and two deep synclines. They considered open and closed forms of these models. For the first model it was found that storage efficiency values at the end of injection varied from 0.5% to 1% depending upon whether the system was open or closed at the boundaries, although significant CO<sub>2</sub> was still mobile at this time. The end of injection period was determined in each case by reaching a pressure limit, but they also modelled storage for a further 5000 years. In the second model they found storage efficiencies up to 2.75% at the end of injection. Both geological systems showed that the migration of CO<sub>2</sub> is strongly influenced by the local topography of the upper surface, although there is not an analysis of the effect. Pickup et al. (2011) looked at the second model considered by Jin et al. (2010) comparing its results against the results on a simplified smooth top version of the model. They observed that the CO<sub>2</sub> migration was influenced strongly by topography.

Ukaegbu et al. (2009) used a 5km x 5km x 80m heterogeneous model with dip and found the highest amount of dissolved CO<sub>2</sub> in models with the highest permeability anisotropy.

Lengler et al. (2010) investigated the impact of spatial variability of the petrophysical properties using a stochastic approach. Their model concentrated upon a 50m long 6m deep 2D section that had a smooth horizontal top-surface and was open at the boundaries. The permeability heterogeneity for a number of models was created geo-statistically with different correlation lengths, anisotropy ratios, upscaling, and variances of the permeability distribution. Each of these sensitivities had 29 different realizations. In the heterogeneous cases CO<sub>2</sub> was seen to arrive at the boundary 50m from the injection well later more often than earlier. The result of this is that storage capacity was underestimated by the homogeneous model. On the other hand, it was observed that generally injectivity decreased with increasing heterogeneity.

Finally, Hayek et al. (2009) provide some analytic insight into vertical flow of CO<sub>2</sub> where high and low permeability layers exist in a model. They solve the 1D vertical Riemann problems and propose semi-analytical solutions describing the CO<sub>2</sub> evolution and showing why saturation discontinuities arise under low permeability layers.

Although much of this work does not directly apply its conclusions to considering storage efficiency, the understanding of these results is valuable in studying storage capacity. The effect of heterogeneity has been considered in a number of ways including its impact on dissolution, residual trapping, reservoir contact, breakthrough time and capacity. A number of

studies have concluded that heterogeneity increases reservoir contact and leads to better storage efficiencies by suppressing gravity over-ride, an initially surprising and important finding that will be considered in later sections. Work considering the presence of top-surface in open aquifers has been sparser. Some studies (Jin et al., 2010; Pickup et al., 2011) have suggested that topography strongly influences CO<sub>2</sub> migration. In addition, there has been some consideration of various simple structures (Gorecki et al., 2009), however mainly those with total structural closure. The results obtained in this project on Representative Structures (see Appendix A5.3) have indicated that dip, which represents a form of structure, can have a significant role upon storage pore volume utilisation. Elsewhere there seems to be little further evaluation or consideration of the impact of top-surface structure, which is not entirely structurally closed.

## 1.5 Aims of the Exemplar Study

This literature survey has shown that a range of influences on the dynamics of storage can have a considerable impact on storage pore volume utilisation (storage efficiency), with estimates ranging from much less than 1% to over 10% of pore volume dependent on the reservoir structure, heterogeneity and injection design. The dynamics are especially important when assessing the capacity of open as opposed to closed aquifers. In open aquifers the dynamics control both pressure response and the time needed for CO<sub>2</sub> to reach a storage boundary, which represents a potential constraint on capacity, whereas in closed aquifers the less dynamically-dependent pressure build-up generally constrains capacity.

A number of the above studies (Gorecki et al., 2009; Kopp et al., 2009; Goodman et al., 2011), as well as the study presented in Appendix A5.3, have started to account for the differing dynamics of flow in different fields or basins and consequently applied different storage efficiencies for these. In this work the focus is on developing further understanding of how the dynamics of flow can affect storage capacity and pore volume utilisation in open aquifers.

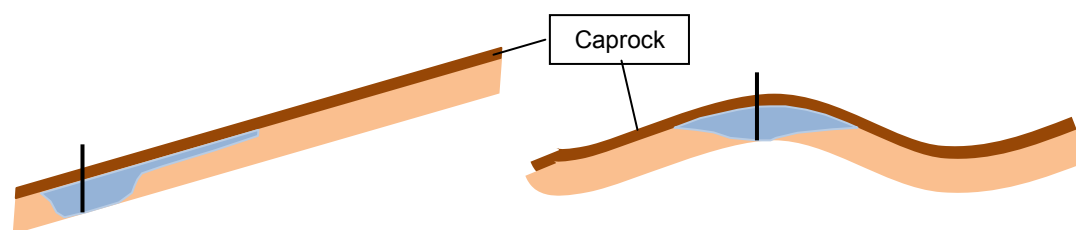


**Figure A1.2: Sketch of a dipping open aquifer (left) versus a large-scale structural closure (right). It is assumed that the structural closure has closure in all directions.**

In particular, the impact of dynamics upon flow in open aquifers that do not have significant large-scale structural closure like domes or fault sealing traps (herein called dipping open aquifers) will be studied. **Figure A1.2** shows a simple sketch of a dipping open aquifer as opposed to a large-scale structural closure. This type of aquifer has been seen to represent a significant proportion of storage capacity in the UK and worldwide (Holloway, 2009; Ogawa et al., 2011), making their capacity estimation important. In addition to this, a number of national scale storage estimation studies, including that of Ogawa et al. (2011) and the study presented in Appendix A5.3 of the main report have found it useful to implement separate capacity estimation methodologies for dipping open aquifers and the units with large-scale structural closures. Without these separate methodologies a potential difficulty is accounting

for the significant difference in storage pore volume utilisation between the units with large-scale structural closures, which tend to be significantly more efficient at storing CO<sub>2</sub> but generally, at the regional scale, have less volume, and dipping open aquifers with possibly lower storage pore volume utilisation but much larger pore volumes. In addition, the sensitivity of storage pore volume utilisation to certain characteristics in the two cases may be quite different making the design of a universal method difficult. Thus a separate understanding of each type is important and in particular here for the dipping open aquifers.

In order to produce methodologies to estimate storage capacity of dipping open aquifers, an understanding of which mechanisms are important for storage and whether storage pore volume utilisation is sensitive to variations in different characteristics is needed. There have been numerous dynamic studies modelling how dipping open aquifers store CO<sub>2</sub> (Doughty et al., 2001; Obi and Blunt, 2006; Flett et al., 2007; Gorecki et al., 2009; Kopp et al., 2009; Kuuskraa et al., 2009; Lengler et al., 2010; Jin et al., 2010; Juanes et al., 2010; Goodman et al., 2011), however fewer studies have looked into their sensitivity to parameter changes, and of those, results have often been more applicable to large-scale structural closures. For example, either a half dome has been assumed as the base case structure (Gorecki et al., 2009; Goodman et al., 2011) or results were assessed during injection thus not considering total migration (Kopp et al., 2009), a more important feature in dipping open aquifers. More recently however, the work presented in Appendix A5.3 of the main report has considered sensitivity of dipping open aquifers to various characteristics that influence dynamics producing three storage regimes that summarise storage pore volume utilisation based on two key parameters – average dip and permeability. In addition to this, other studies (Flett et al., 2007; Kuuskraa et al., 2009) have considered the sensitivity to heterogeneity.

These sensitivity studies offer important understanding that dip and permeability – simplified versions of top-surface structure and heterogeneity – are key sensitivities for dipping open aquifers. Within these sensitivity studies the effect of top-surface structure was not considered or the top-surface has been considered smooth. In the rare studies where top-surface structure has been introduced (Jin et al., 2010; Pickup et al., 2011) it was suggested that the characteristics of the CO<sub>2</sub> plume can be significantly affected by the topography of the top surface of a reservoir, but without further study or analysis.

Therefore a number of key issues will be studied in this work:

- Look at how top-surface structure can affect storage pore volume utilisation in a dipping open aquifer in Section 4.
- Investigate in Section 3.4 whether the storage regimes, as set in section 5.3.1 in the main report, are still a good approximation when top-surface structure and heterogeneity are present.
- Consider the effect of heterogeneity upon storage pore volume utilisation in a dipping open aquifer in Section 4.

To investigate the effect of top-surface structure and heterogeneity a number of issues will be studied in this work:

- Calculate the effective storage capacity (as defined by Bradshaw et al., (2007)) of reservoirs. Issues such as lack of data will not be considered.

- Use the Vangkilde-Pedersen et al. (2009) definition of their ‘storage efficiency factor’ as storage pore volume utilisation parameter used in this work. The use of ‘factor’ will be omitted and instead referred to as *the storage pore volume utilisation*.
- Measure CO<sub>2</sub> storage pore volume utilisation at 1000 years as opposed to at the end of injection or when CO<sub>2</sub> is all residually trapped. This follows the approach presented in Appendix A5.3 of the main report.
- Investigate a model at the scale of a potential ‘storage unit’. The scale is considered to be between basin scale ~ 100km x 100km and field scale ~1km x 1km. It will be referred to as the ‘*storage unit scale*’ ~10km x 10km.

As it will be seen later, this analysis uncovers some surprising general results. It will be shown that open aquifers of modest permeability can prove to be favourable storage sites with reasonable storage capacities. These aquifers limit the speed with which the CO<sub>2</sub> migrates, while the extensive open pore volume can help dissipate pressure, avoiding pressure problems associated with other types of storage site.

## 2 Exemplar Model and Methods

A specific exemplar field was modelled to investigate issues not practical for investigation using the homogeneous, smooth-top-surface representative structure models, and to demonstrate the storage feasibility realistic of an open aquifer with a realistic model scenario. The selection to have an Exemplar for open aquifers was made because they have potentially large storage (section 5.3 in the main report). Geocellular model was constructed by Senergy with engineering support from Imperial College.

### 2.1 Geocellular Model of the Forties-based Storage Unit

The Forties sandstone member of the Sele Formation was identified as a suitable storage unit to situate the Exemplar after a preliminary assessment of the permeability and dip of open aquifers available in CarbonStore. Within the Forties sandstone member an area of interest was selected for modelling that avoided hydrocarbon fields, significant structural closures, known faulting and communication with overlying formations. The area of interest – shown by the black box overlaying **Figure A2.1** – was 21.4km x 36km and a geo-cellular model was constructed in PETREL™ of this section of the Forties Sandstone Member. The model was orientated northwest to southeast and spans several blocks in Quadrant 22 of the Central North Sea.

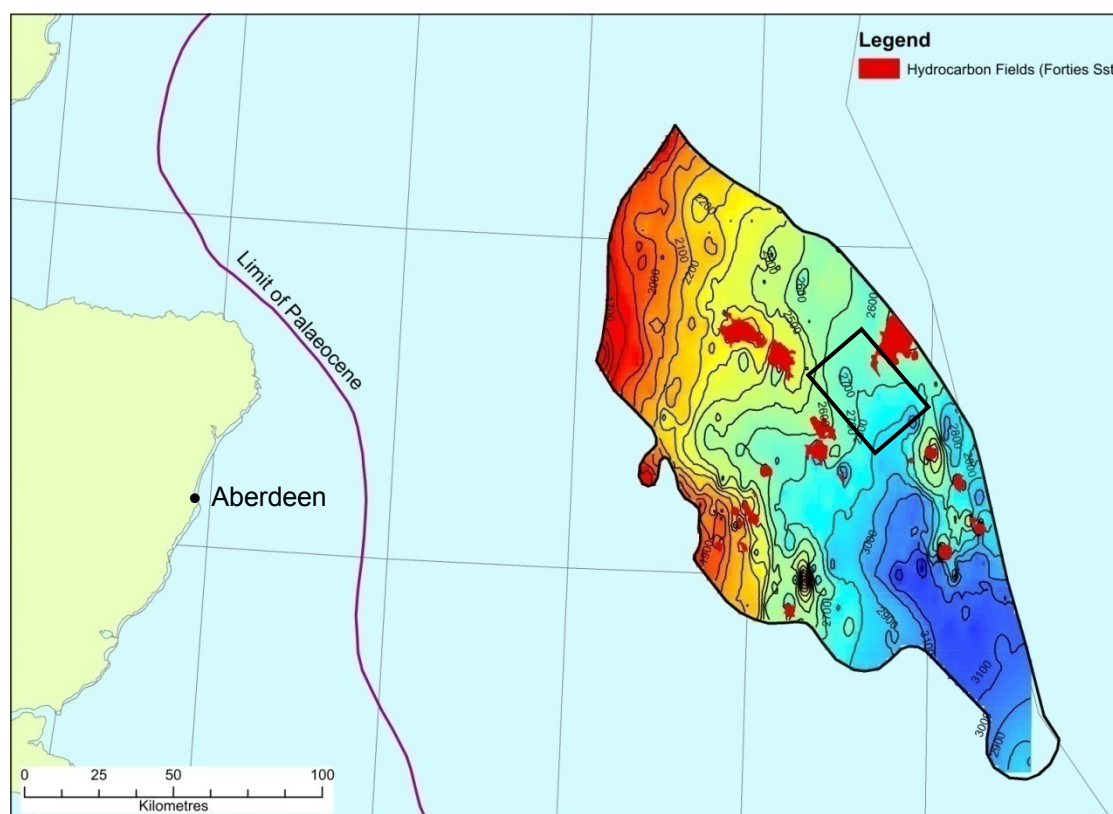


**Figure A2.1: Location of the Forties Sandstone member and the Forties geological model. Areal extent of the Forties geological model is identified by black rectangle**

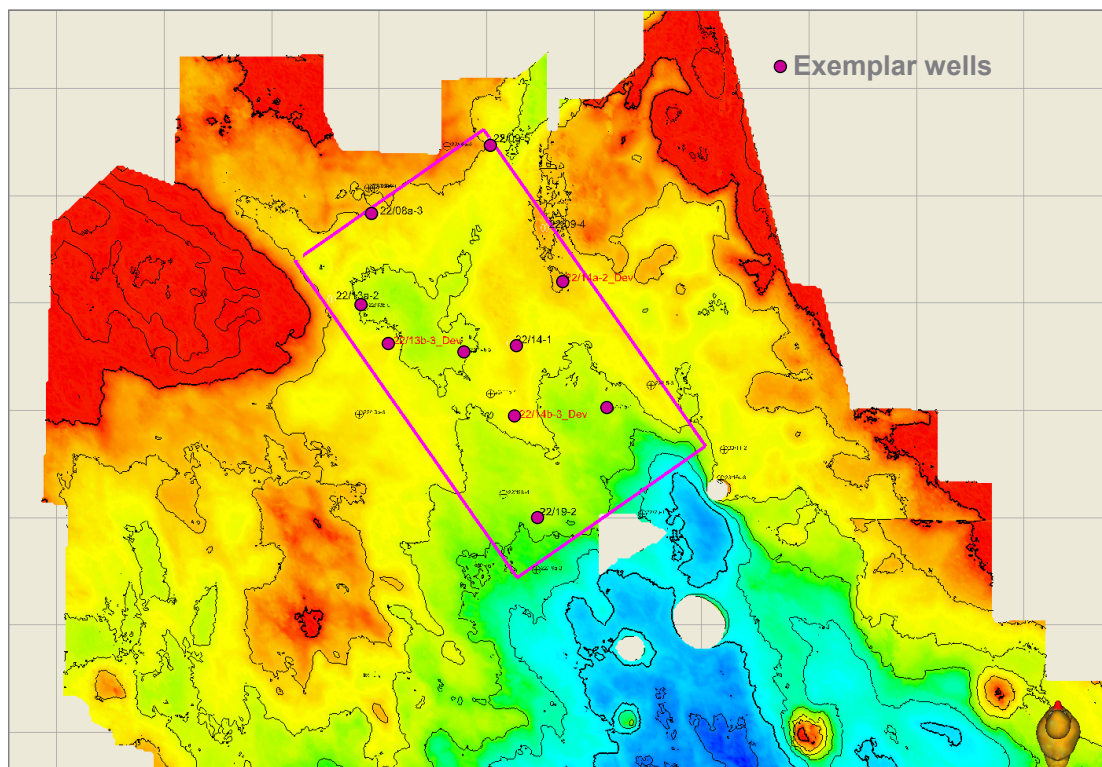


**Figure A2.2: Top Forties seismic interpretation in depth. The location of the Forties geological model and wells are also shown**

The grid dimensions of the model were 107 x 180 x 90 giving a total of 1,733,400 grid cells. The structural framework of the model is based on a top Forties seismic interpretation in depth (**Figure A2.2**) and well tops of the Andrew Sandstone Unit to define base Forties. To accommodate simulation requirements the reservoir is divided into three zones; a 2m 'roof' zone beneath top Forties with 4 layers, a 5m 'sub-roof' zone with 5 layers and the remaining Forties zone with 81 layers. To capture thin CO<sub>2</sub> tongues occurring towards the top of the storage unit, the vertical resolutions were from 0.5m to 1m towards the top of the Forties interval increasing to 3m at the base. This also allowed the intra-reservoir shales to be captured in the geological model provided, thus preserving enough meaningful vertical heterogeneity.

The porosity and permeability models were built upon a simple facies model describing cells as either channel or background (**Figure A2.3**) that was derived using data from 10 wells located in **Figure A2.2**. Porosity and permeability ranges from published data and local core analysis data were modeled directly into the channel facies and are shown in **Figures A2.4 & A2.5**. The background shales were modeled with near-zero porosity and permeability.

Storage Capacity in Large Open Aquifer Exemplar: Base Case Simulation and Sensitivities to Top Surface and Heterogeneity

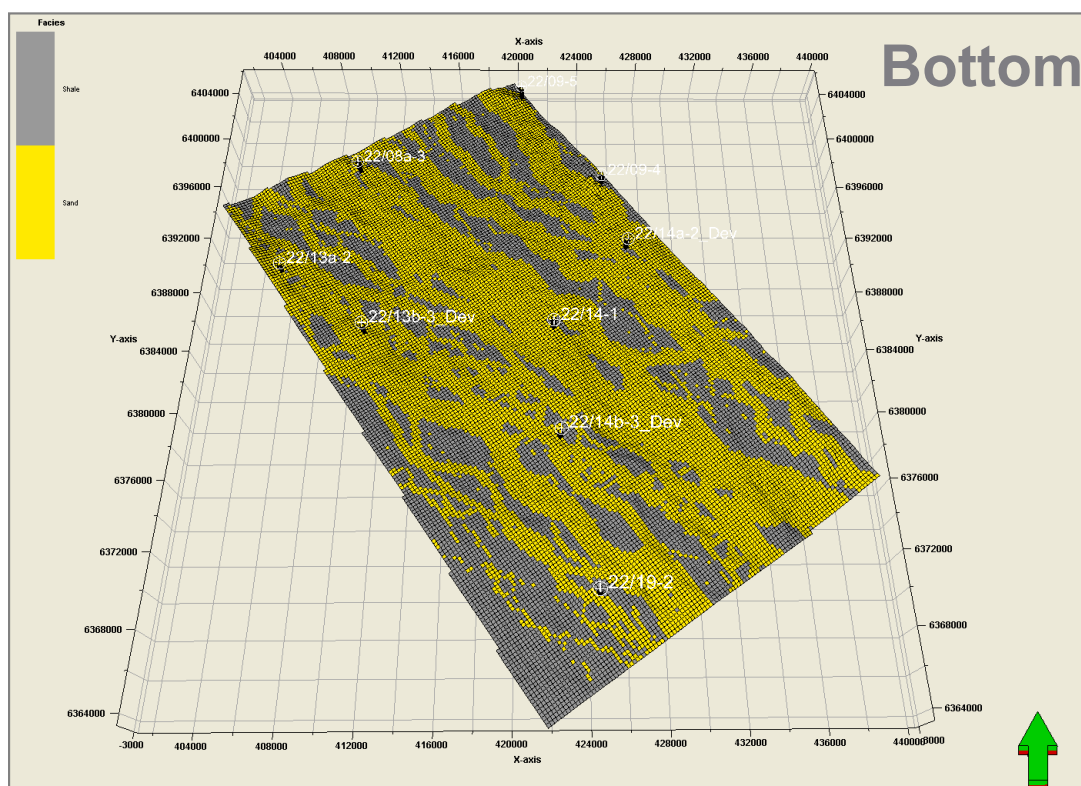
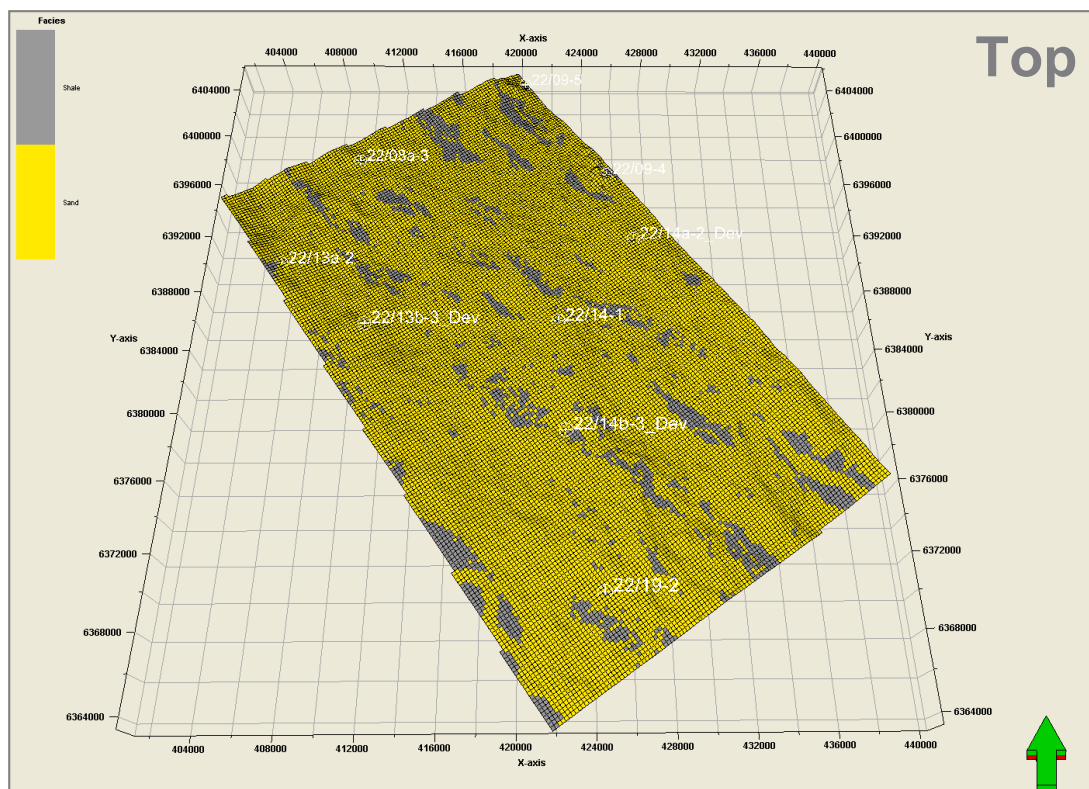


Figure A2.3: Facies Model at Layer 1 (top) and Layer 90 (bottom). Higher shale proportion is seen at base Forties

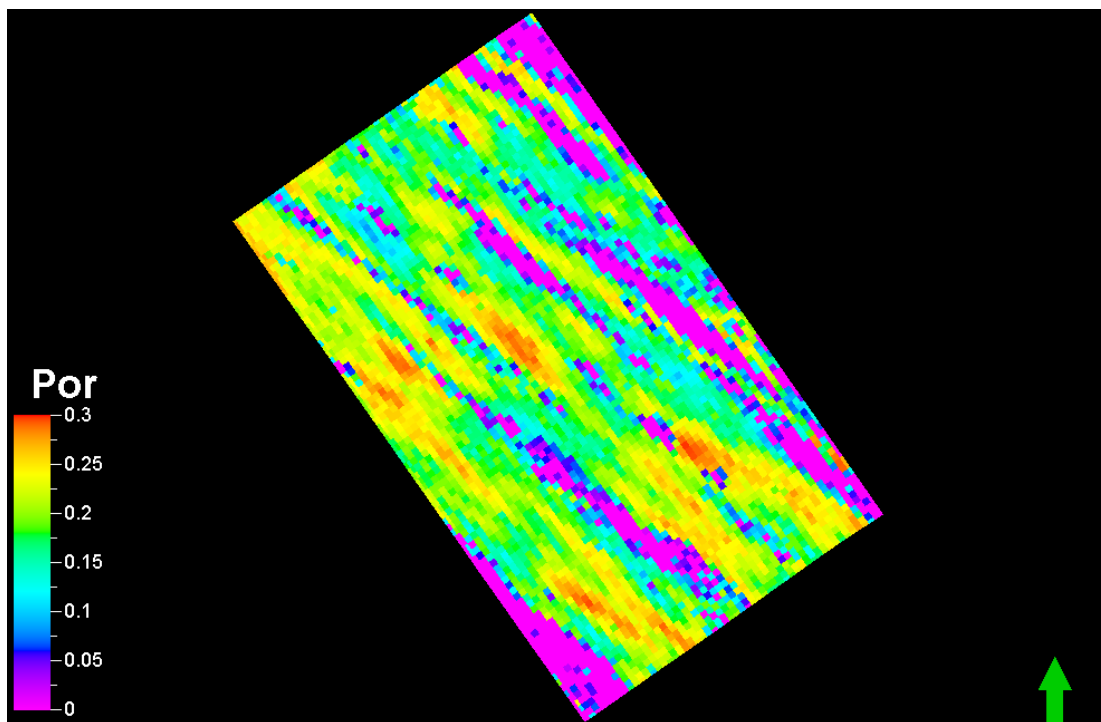


Figure A2.4: Porosity model at Layer 1 (top) Forties Exemplar base case geological model

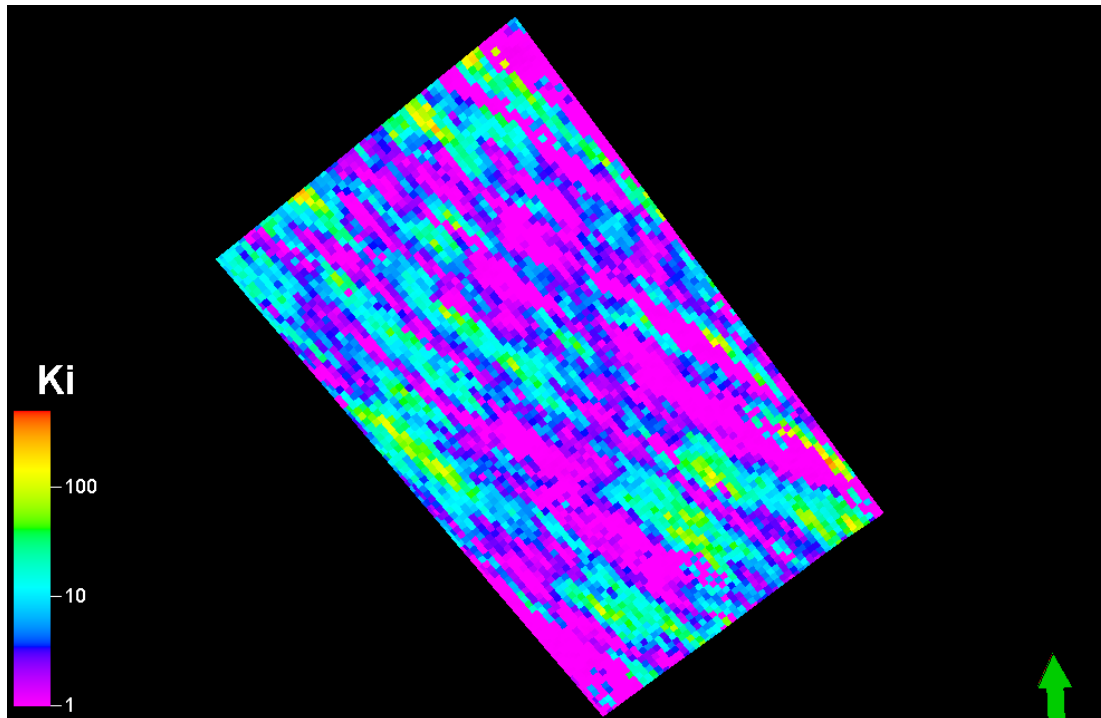
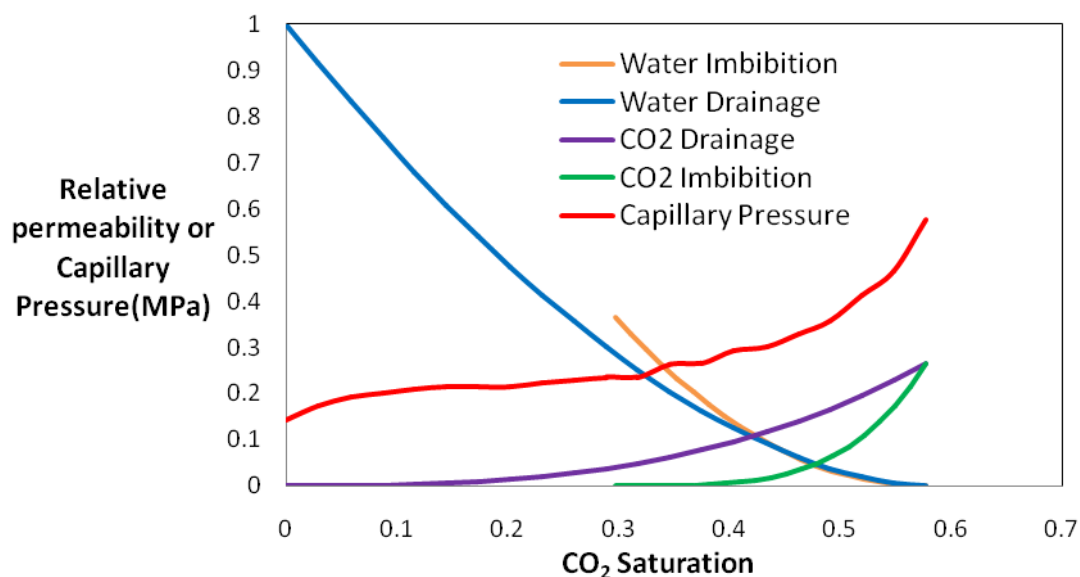


Figure A2.5: Permeability model at Layer 1 (top) Forties Exemplar base case geological model

## 2.2 Construction of the Dynamic Model

The dynamic model was constructed in ECLIPSE 100™. Rock properties from the geological model such as porosity and permeability models were imported. Drainage and imbibition relative permeability data as well as the capillary pressure data from the Viking 2 dataset (Bennion and Bachu, 2008), were used - see **Figure A2.6**. Relative permeability hysteresis was modelled using Carlson model (Carlson, 1981).



**Figure A2.6: Viking 2 relative permeability and capillary pressure used in the Exemplar base model simulation**

The 1,733,400 million cell geo-cellular model grid was upscaled to a 450,450 cell model to reduce simulation runtimes. Using the 450,450 cell model 1000 year simulation runtimes varied from 7 hours to 13 days using a fast workstation PC. Upscaling of the porosity and permeability fields was done using arithmetic averaging by a factor of 2 in the two horizontal directions. It was applied to the central 104 x 178 x 90 cells. The results of grid sensitivity are presented in section 3.3.1.

A summary of initial fluid and rock properties is given in **Table A2.1**. The initial pressures in the reservoir were calculated at hydrostatic equilibrium and temperature was calculated using a geothermal gradient of 35°C/km and surface temperature of 8°C, with rounding to the nearest 5°C to coincide with availability of PVT data. Water salinity was estimated as 89,000ppm; salinity was also rounded for the same reason to the nearest 50,000ppm.

Dissolution of CO<sub>2</sub> into the brine phase and vaporisation of water into the gas phase were both modelled. As in simulation model construction for Representative Structures (see Appendix A5.3, section 3), all density, pressure, viscosity and phase partitioning calculations during simulation were done using data provided from TOUGH2™ ECO2N Module (Pruess, 2005). Temperature was assumed constant in space and time in the simulations.

PARAMETER	VALUE	SOURCE
Reservoir datum depth	2800m	Geological model
Brine Salinity	100,000ppm	Gluyas and Hichens(2002)
Temperature	105°C	Evans et al. (2003)
Pressure at datum	32MPa	Calculated using water density
CO <sub>2</sub> density at datum	660kg/m <sup>3</sup>	TOUGH2™ PVT data
CO <sub>2</sub> viscosity at datum	0.0000546Pa.s	TOUGH2™ PVT data
Brine density at datum	1006kg/m <sup>3</sup>	TOUGH2™ PVT data
Brine viscosity at datum	0.000345Pa.s	TOUGH2™ PVT data
Rock compressibility	0.0000489MPa <sup>-1</sup>	CarbonStore
Porosity (arithmetic average)	0.16	Geological model
Permeability (arithmetic average)	11mD	Geological model
Volume of storage unit	2 x 10 <sup>10</sup> m <sup>3</sup>	Geological model
Volume of Forties sandstone member	3 x 10 <sup>11</sup> m <sup>3</sup>	CarbonStore
Fracture Pressure Gradient	0.0181MPa/m	UKSAP

**Table A2.1: Initial conditions and parameters for the Exemplar base case simulation**

To represent the pressure response from the volume of the Forties sandstone connected to the Exemplar but outside the model, significant additional pore volume was added around the boundaries of the model to make the total pore volume match 3 x 10<sup>11</sup> m<sup>3</sup> - the volume of the Forties sandstone member. The aquifer is believed to be open to flow beyond some of these boundaries, however this was not accounted for. Increases in the pore volume, presented in section 3.3.2, showed that adding more pore volume to account for this would make relatively little difference to the overall volume of CO<sub>2</sub> injected.

The inclusion of groundwater flow was considered and for this purpose the local change in overpressure across the field found from **Figure A2.7**. Based on this overpressure gradient, analytic estimates of groundwater flow velocities through the unit using Darcy's Law with permeability and viscosity values from **Table A2.1** were 0.04m/year. Over 1000 years this results in a migration distance of a tenth of one cell in the model used, and further flow through the higher permeability channels would only migrate around one cell over 1000 years; therefore groundwater flow was neglected.

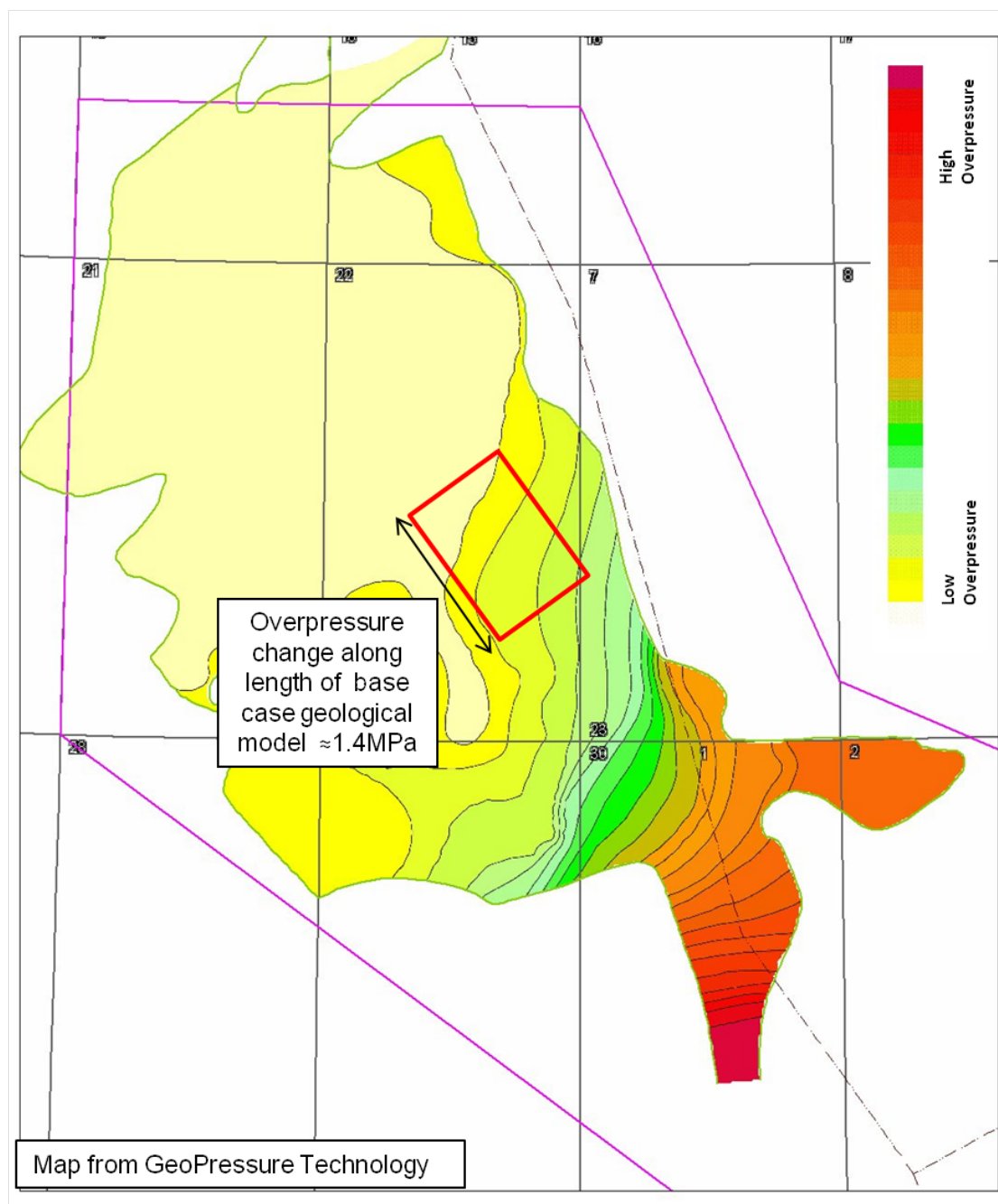


**Figure A2.7: Overpressure contours for the Forties Sandstone member. Forties base case geological model area is shown in red**

### 2.3 Base Case Injection Set-up

In the Exemplar base case model injection was simulated for 50 years and the post injection period was simulated for a further 1050 years in order to calculate the capacity of the section of the Forties sandstone member. Injection and the calculated capacity of models were constrained by the following three conditions as set out in section 5.3.1 of the main report, which interprets current EU regulation and IPCC suggestions:

- 99% of injected CO<sub>2</sub> must remain within the storage boundary after 1000 years - in further text this will be referred to as the '99% storage constraint';

- CO<sub>2</sub> migration velocities at 1000 years must be less than 10 metres/year and declining - the 'migration velocity constraint';
- Pressures must remain less than 90% of the estimated fracture pressure limit - the 'Bottom Hole Pressure (BHP) constraint'.

In addition a minimum well injection rate of 0.1Mt/year was also applied.

A small adaptation was made to the second condition to allow for features of flow in a heterogeneous media that do not represent an increase in the risk of leakage, as the original constraints were set to represent. This was introduced to allow for cases where either a single cell or a few cells situated significantly behind the maximum extent of the CO<sub>2</sub> plume, but with a locally high permeability and dip, produce mobile CO<sub>2</sub> velocity above 10m/year. As a result an extra practical allowance was used where up to 10 visually uncorrelated cells, generally away from the furthest extent of the CO<sub>2</sub> plume, were allowed velocities above 10m/year. This was useful for reducing the number of computationally intensive optimisation simulations used for very minimal changes in storage pore volume utilisation. The results are insensitive to the precise number of fast-moving cells allowed.

## 2.4 Storage Security and Trapping Assessment

Using the simulation setup described, residual, dissolution and structural trapping were all modelled. The key measures of storage security and trapping were defined and calculated for analysis as follows:

- **Escaped CO<sub>2</sub>**

CO<sub>2</sub> that reached the outer-most layers of cells at the side boundaries was summed together. Any CO<sub>2</sub> dissolved or free in these cells was counted as 'escaped'.

- **Dissolved CO<sub>2</sub>**

The total dissolved CO<sub>2</sub> was measured as all dissolved CO<sub>2</sub> within the boundaries of the model, but not within the outer-most layer of 'boundary' cells.

- **Structural trapping**

The total amount of structurally trapped CO<sub>2</sub> was measured as the total free phase (not dissolved) CO<sub>2</sub> within structural closures. An algorithm was written to calculate which cells were structurally closed. It calculated this using the definition that a cell "A" is structurally closed if there is a closed loop of top layer cells surrounding the cell of which all cells have depth deeper than cell "A". **Figure A2.8** shows the structurally closed cells in the base case model.

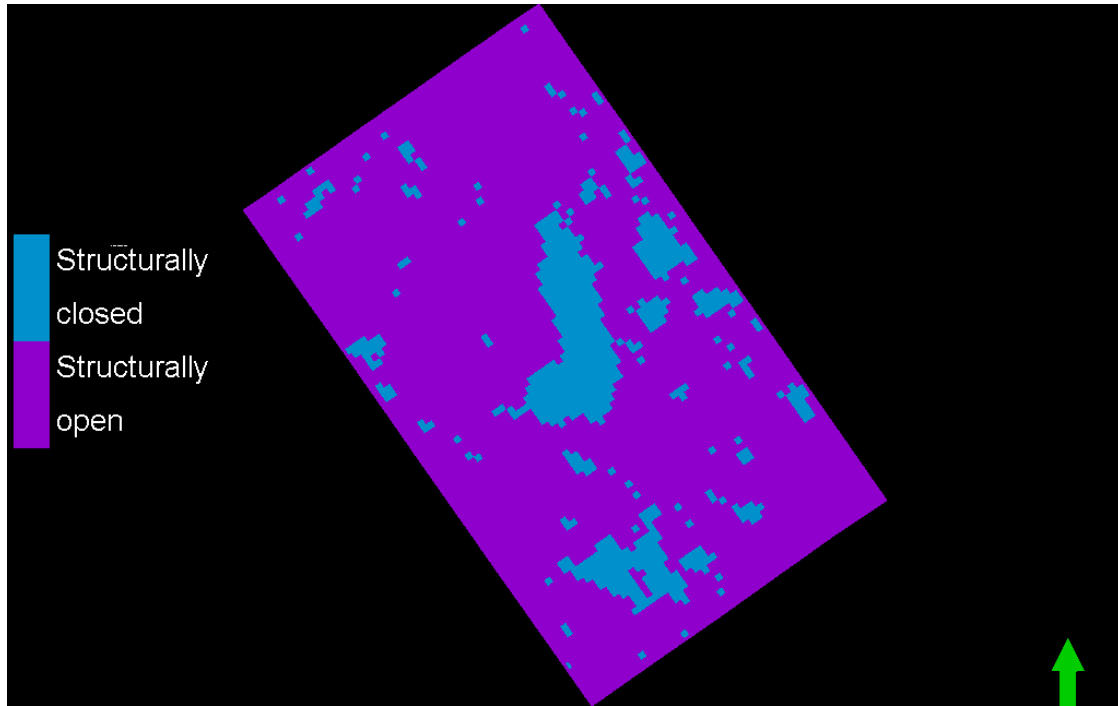


**Figure A2.8: Map of cells on the top layer which are structurally closed. Due to the buoyancy of CO<sub>2</sub>, once within these structurally closed cells it will stay there until dissolved**

- **Residual trapping**

For the purposes of analysis residual trapping was estimated using the Land trapping model (Land, 1968). This calculates the residual trapping in each cell using the equation:

$$S_{gr}^* = \frac{S_{gi}^*}{1 + S_{gi}^* \left( \frac{1}{(S_{gr}^*)_{\max}} - 1 \right)} \quad (2.1)$$

where all saturations  $S$  are normalised such that  $S^* = \frac{S}{1 - S_{wc}}$ ,  $S_{gi}^*$  is the normalised maximum historical gas saturation on a cell,  $S_{gr}^*$  is the normalised potential residual saturation and  $S_{wc}$  is the connate water saturation. Using this method an example cell with maximum historical CO<sub>2</sub> saturation  $S_{gi}^* = 0.6$  would have saturation  $S_{gr}^* = 0.3$  counted as residual since this CO<sub>2</sub> can never be displaced. Under this method all the CO<sub>2</sub> that is not counted will eventually leave the cell unless it becomes dissolved or is structurally trapped. CO<sub>2</sub> within structurally enclosed cells was not counted to avoid double counting.

An alternative approach considered was to measure residual as the volume of CO<sub>2</sub> present in the cells where the gas phase relative permeability  $K_{r,CO_2} < 0.0001$  and the cells are not structurally closed. Although this measure provides interesting information it was found to underestimate the amount of CO<sub>2</sub> that was unable to leave the model due to residual trapping, since it does not include any residual in the cells where  $K_{r,CO_2} > 0.0001$ .

- **Low migration velocity storage**

Any CO<sub>2</sub> that is still within the boundaries of the model and satisfying the velocity constraint at 1000 years and not trapped structurally, residually or by dissolution, is referred to as low velocity CO<sub>2</sub> and the storage mechanism is referred to as low migration velocity storage. Over time the low velocity CO<sub>2</sub> must eventually become either structurally or residually trapped, dissolved or escape the model boundaries.

- **CO<sub>2</sub> velocity**

ECLIPSE 100™ provides CO<sub>2</sub> flux in the I and J direction for each cell in surface m<sup>3</sup>/day. These values were converted to estimate the CO<sub>2</sub> migration velocity in m/year.

## 2.5 Sensitivity Models for Studying the Impact of Top Surface and Heterogeneity

The sensitivities studied were the presence of top-surface structure and heterogeneity, with variations in the reservoir dip and permeability. The aim was to ascertain the impact the top-surface structure and heterogeneity upon storage capacity and to substantiate the storage regime results presented in Appendix A5.3.

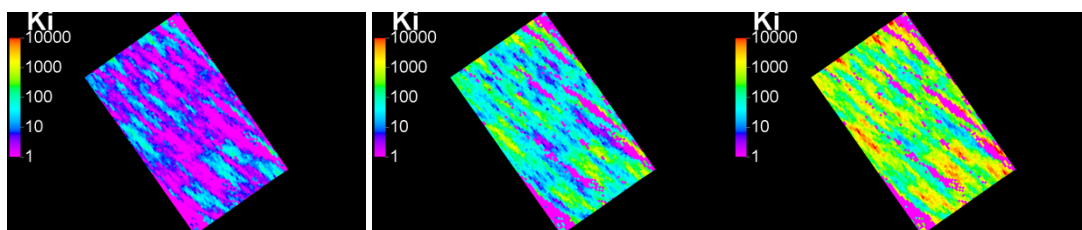


**Figure A2.9: Permeability maps for (from left to right) base case 11mD permeability and two permeability sensitivities 145mD and 1D. Figures show top layer of model viewed from above**

Firstly, to determine whether the storage regime results still applied when top-surface structure and heterogeneity were present, dip and permeability sensitivities were applied to the base case geological model. The sensitivity values used for dip were 1° and 3°, and for permeability were 145mD and 1D. The permeability and dip sensitivities applied to the 11mD 0.27° base case are shown in **Figure A2.9** and **Figure A2.10** respectively. These sensitivities allowed for looking at results representative of each of storage regime 1, 2 and 3.

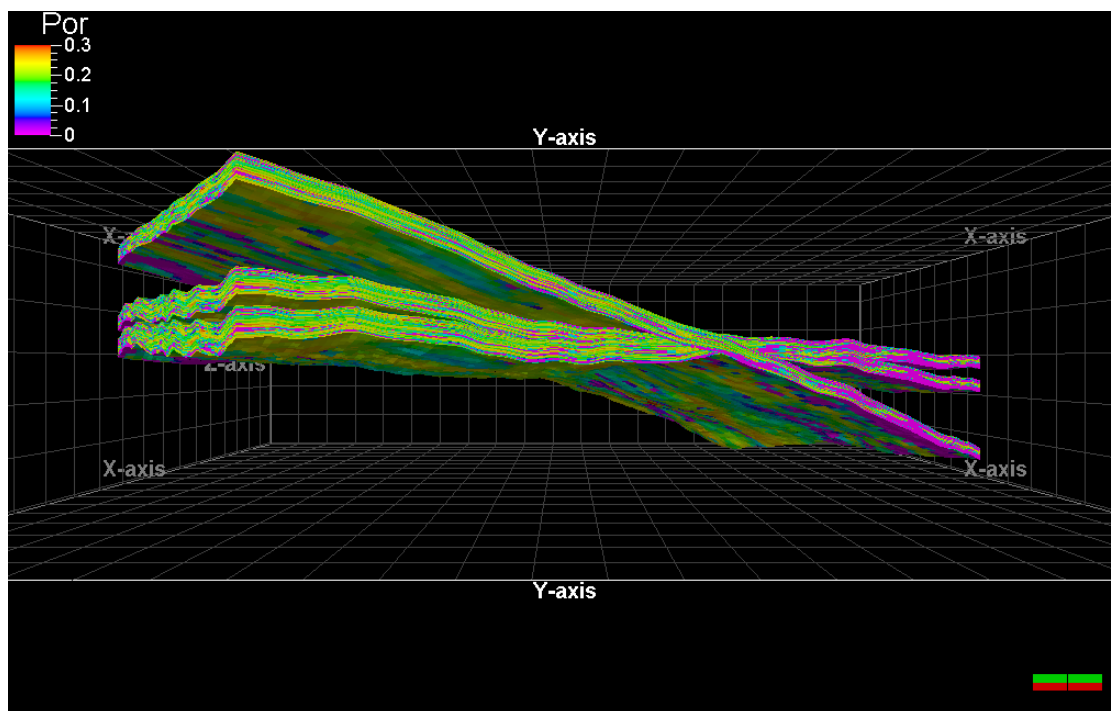


**Figure A2.10: Porosity maps for the different dip sensitivity models. The base case has dip  $0.27^\circ$  and two sensitivity cases have dips  $1^\circ$  and  $3^\circ$ . Models are viewed from the west and vertically exaggerated by a factor of 15**

To investigate the effect of the Forties geological model heterogeneity and top-surface structure, the same sensitivity study was run with geological models without heterogeneity and then with the top-surface structure removed thus creating homogeneous smooth-topped models. **Figure A2.11** shows the three different models with average horizontal permeability 11mD and dip  $0.27^\circ$ . In the homogeneous models the vertical to horizontal permeability ratio is set to 0.1 and porosities and permeabilities are set to the arithmetic average of the heterogeneous model. In the homogeneous models with and without top-surface structure the dip sensitivities were applied to the 145mD case to provide storage regime 3 dip scenarios. Using the results from the three dip-permeability sensitivity studies, the effect of adding and removing heterogeneity and top-surface structure could be observed.

In addition, the application of dip and permeability sensitivities to the cases without heterogeneity and/or top-surface structure was used for further substantiation of the storage regime results.

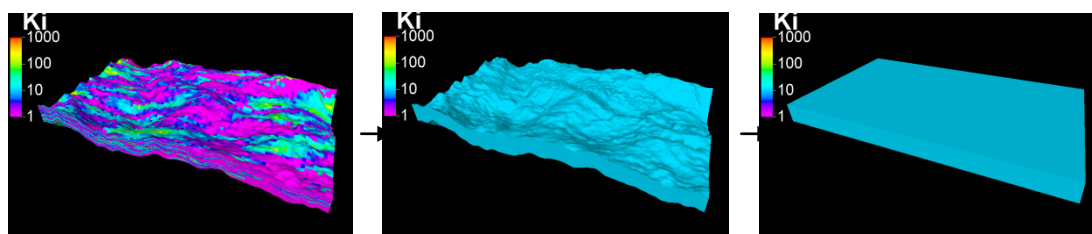


**Figure A2.11: Simplification of base case model by removing heterogeneity then top-surface structure. Figures show permeability in mD, are viewed from the south and are exaggerated by a factor 15 in the vertical direction**

## 2.6 Methodology for Calculating Storage Capacity – Optimising Injection and Well Location

In both base case Exemplar model and sensitivity models the storage capacity of units was estimated, while meeting the storage constraints introduced in section 2.3. To estimate these capacities a set of well placements and injection rates was required for each scenario.

It was decided that a single set of well placements would be used to keep the optimisation process feasible. However, these well placements were required to provide adequate well options to optimise storage capacity in a variety of different models with different flow behaviour. To achieve this, well locations would be designed to:

- have a reasonably even distribution,
- where possible be located preferentially down-dip,
- be located to avoid injection into shales in heterogeneous models,
- be given high enough well density for cases with lowest injectivity to inject maximally.

It was possible to satisfy these aims with a well placement setup used for the base case model, mainly because a large number of wells were required in this case, offering flexibility for the use of different numbers of wells in different locations in other scenarios. The exact placement of these wells was chosen by visual inspection aided by detailed numerical model visualisation of the permeability field and the local dip. The locations were optimised by gradually increasing or relocating wells in order to optimise injection into the base case. As explained further in section 3.1 the optimisation of the base case scenario involved particular effort to increase the number of wells so that any additional well increased total injection by at least 0.1Mt/yr.

The final well pattern from this process to be used for the base case and all sensitivities is shown in **Figure A2.12**. In order to find the final well pattern each of the points listed above were taken into consideration, although through its manual nature the process was not strictly rigorous. In the final setup it is noted that 2km long horizontal wells were used to help avoid injection near shale layers and also to assist with an improved areal spread of the CO<sub>2</sub> plume.

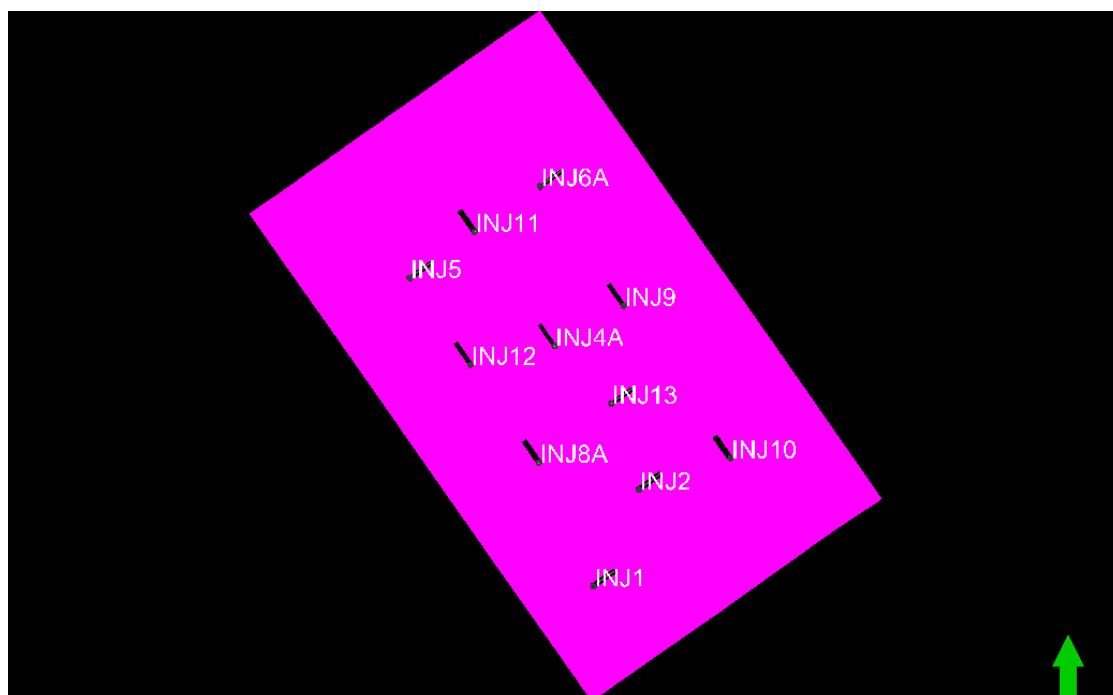


**Figure A2.12: Locations of the eleven horizontal wells used for the base case and sensitivity scenarios. Viewed from above**

With the well placement established, the storage capacity in each sensitivity model was estimated by running dynamic simulations and then increasing or reducing injection rates to meet the storage constraints. For each model setup this was achieved through an iterative process described by **Figure A2.13**. In this process the escaped CO<sub>2</sub> and CO<sub>2</sub> velocity at 1000 years were measured as explained in section 2.4 so that potential injection rate scenarios could be accepted or rejected under the 99% storage constraint or velocity constraint. The Bottom-Hole Pressure (BHP) constraint was applied directly through the simulation model set-up.

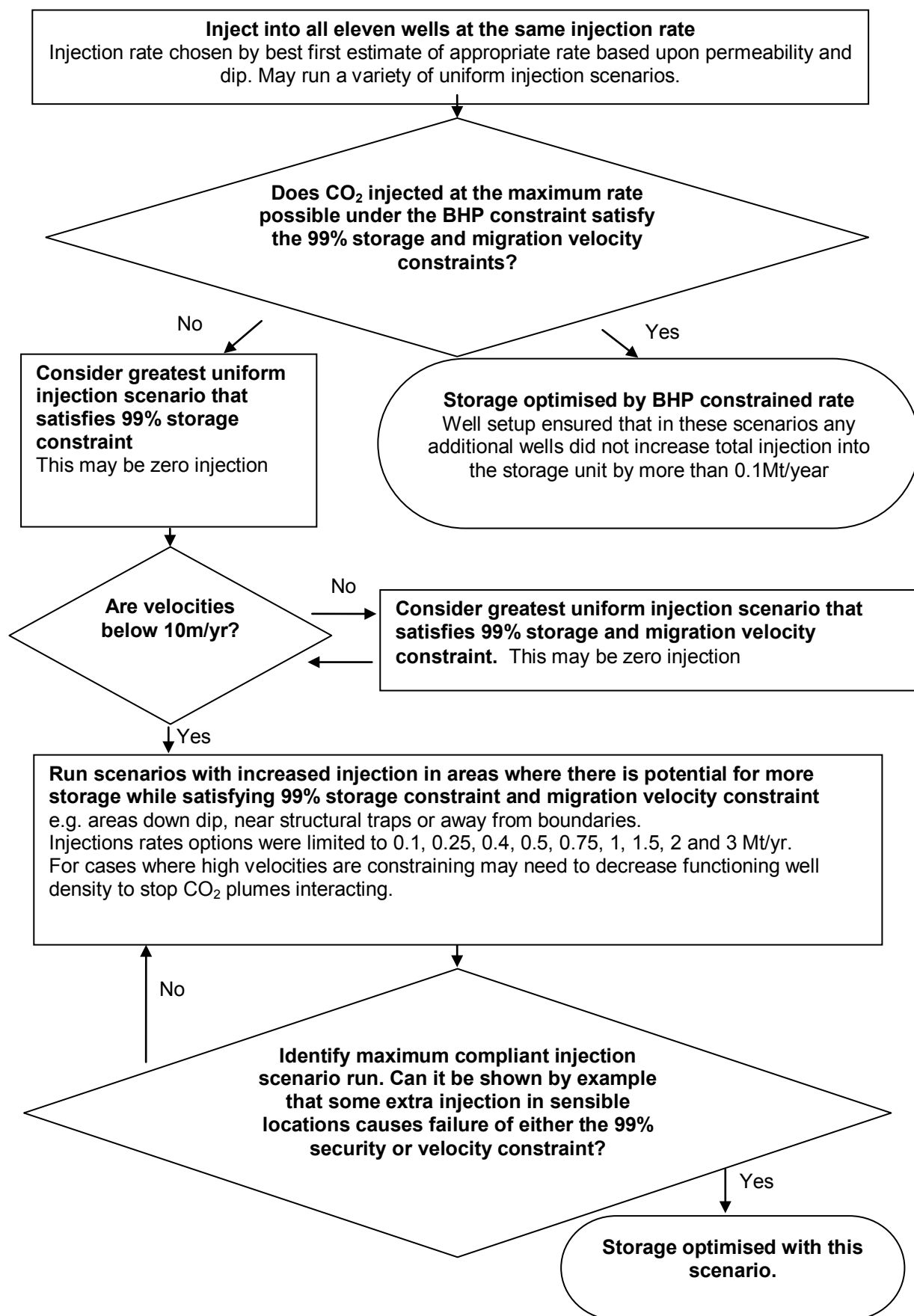


Figure A2.13: General methodology for calculating the capacity of each model

## 2.7 Alternative Simulations using Streamlines

Dynamic modeling using streamline simulation was undertaken to make use of their superior speed. Streamline simulation is a very efficient method for modelling advection-dominated, incompressible flow in a porous medium and makes higher resolution simulation of reservoir flow computationally feasible, and as a result it is particularly beneficial when finer-scale geological heterogeneity is to be investigated. Preliminary simulations were undertaken using two streamline-based reservoir simulators, a research streamline code from Imperial College and 3DSL™. Both codes were able to handle the 1,733,400 cell model with runtimes all under a day; however they each had issues leading to the final decision to use Eclipse 100™, even though this code is slower and required the use of an upscaled model.

The in-house research code was unable to handle corner point geometries. Further, due to the dip that would be investigated in some models, it was unable to produce an equivalent structure using a Cartesian grid without increasing the number of cells in the model to such an extent that simulation would be computationally unfeasible. Since one aim was to investigate the effect of structure this ruled out the Imperial College research code. 3DSL™ was able to handle corner-point geometries and also simulate compressible flow with runtimes still less than a day. However, it was not able to model relative permeability hysteresis and demonstrated significantly different results when using either the drainage or imbibition relative permeabilities, thus ruling out 3DSL™. In both cases, updating the simulators within the project time constraints was not possible.

### 3 Base Case Exemplar Results

The base case Exemplar model results are presented in three subsections: storage appraisal, storage capacity and trapping mechanism, and verification in terms of grid resolution sensitivity and pressure boundary conditions.

#### 3.1 Base Case Exemplar Storage Appraisal

The base case was first modelled in order to appraise the storage of a particular section of the Forties sandstone member. To appraise its storage, the location number and injection rate of wells had to be optimised, as described in section 2.6.

At the start of the optimisation of well location and injection rate, just six injection wells were operated with target injection rates of 2Mt/year. However this rate was not achieved in each well as injection was limited by the bottom hole pressure (BHP) constraint that constrains the BHP to below 90% of the fracture pressure. Despite this limitation on rate through each well **Figure A3.1** shows that some pressure space remained which could be utilised and as a result extra injectors were added until the increase in injection rate through all wells when an extra well was added fell to 0.1Mt/yr. This determined an appropriate well density for near-maximum injection.

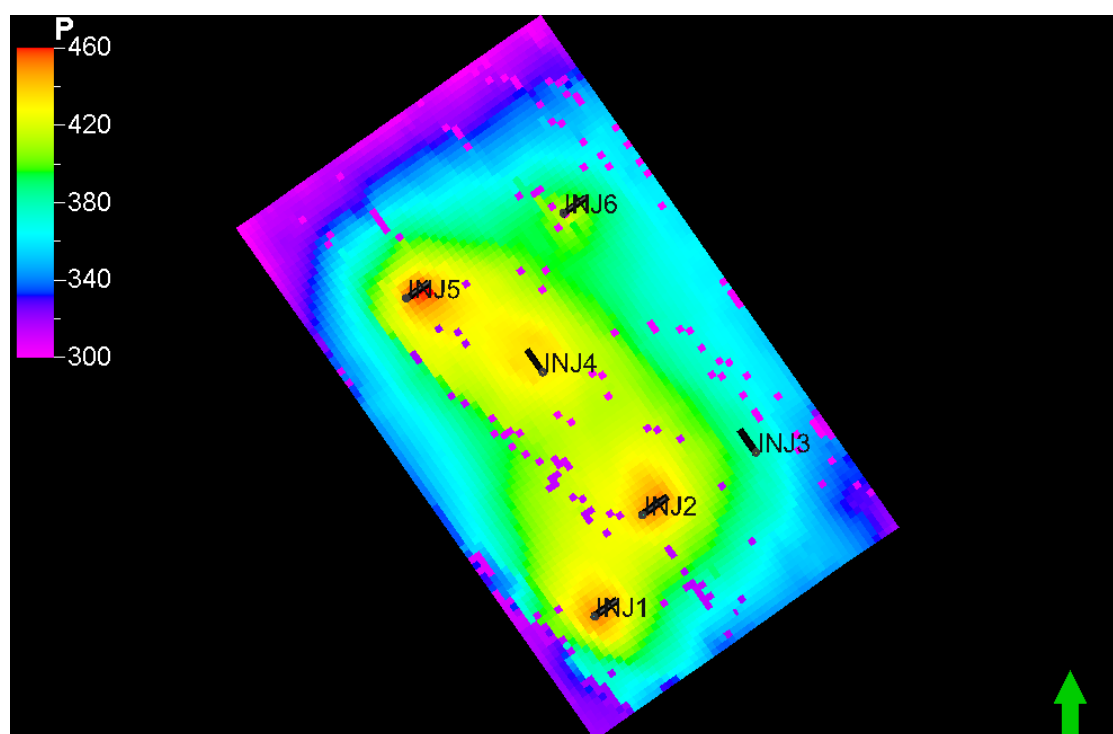


**Figure A3.1: Pressure (bars) profile at top layer at 50 years in a preliminary 6 well injection scenario. Purple 'specs' are shales that were treated as inactive cells in early simulations. Pressures around 400bars (=40MPa) and below indicate some limited pressure space, suggesting that using more wells would lead to higher storage capacities. Wells are shown in black**

This limitation on well density was due to pressure interference between wells. Although pressure was seen to be relieved by the open flow boundaries of the model, pressure interference between wells increased with further injection over time. The effect of this is

shown in **Figure A3.2** where increased interference led to decreased injection over time. In a realistic storage case, constant injection over the time period would be more likely. For the assessment of storage capacity though, it is assumed that capacity is not affected by the time or rate of injection, and this decay in rate is observed.

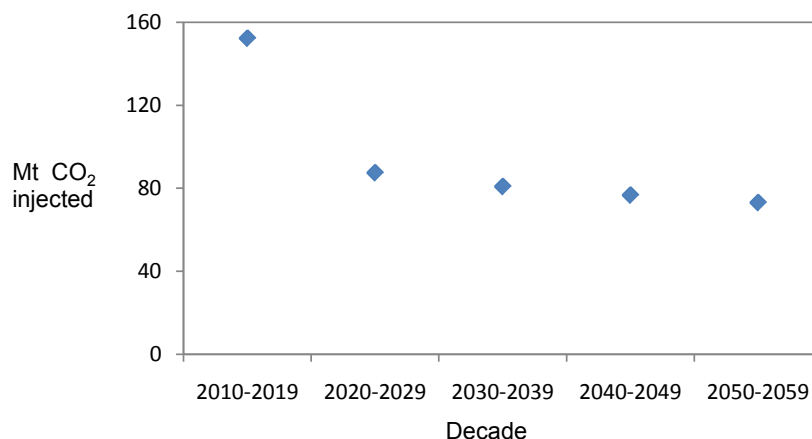


**Figure A3.2: The total mass of CO<sub>2</sub> (Mt) injected into the base case geological model per decade using 11 wells**

While increasing the well density, as explained above, it was simultaneously necessary to try to satisfy the 99% storage constraint and migration velocity constraint. Due to the low average permeability of the aquifer, the extent of the CO<sub>2</sub> that could be injected under the BHP constraint was only around 5 km and had velocities less than 10m/year. This allowed that wells could still be located fairly close to the boundary. With the ability to place wells fairly freely under the storage and migration velocity constraints, they had little impact upon injection and capacity was constrained rather by how much it was possible to inject due to BHP and well density.

The final injection setup for the model is described and shown in section 2.6 where it is noted that horizontal wells were used to avoid injection into shale layers. To summarise, the storage was constrained by a combination of the BHP constraint, which broadly determined the well density, and to a lesser extent the 99% storage constraint, which determined how near to the boundary could be injected. This combination of the two factors is behaviour typical of an open aquifer from storage regime 1 or 2. Good injectivity that could be achieved through any one well alone, as well as the permeability of 11mD being slightly greater than the notional 10mD boundary, would tend to categorise it as storage regime 2.

### 3.2 Base case Exemplar – Storage Capacity and Trapping Mechanism

Having determined well locations and rates into the section of the Forties sandstone member, as outlined in section 3.1, its capacity was estimated as 471 Mt representing a storage pore volume utilisation of 3.5%. The final distribution of saturations at 1000 years is presented in **Figure A3.3**, and **Figure A3.4** shows which mechanisms trapped this CO<sub>2</sub>, using the method explained in section 2.4.

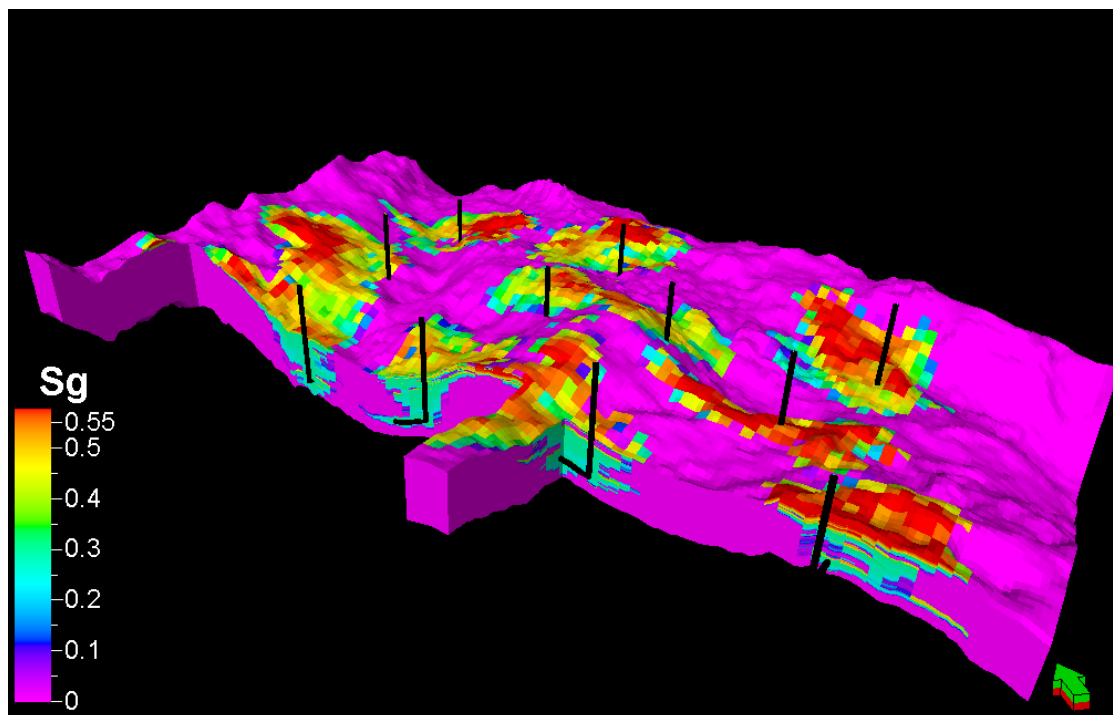


Figure A3.3: CO<sub>2</sub> saturation in Forties base case model at 1000 years. Maximum gas saturation is 0.577. Model length 36km, viewed from south and vertically exaggerated by a factor of 15. Wells are shown in black

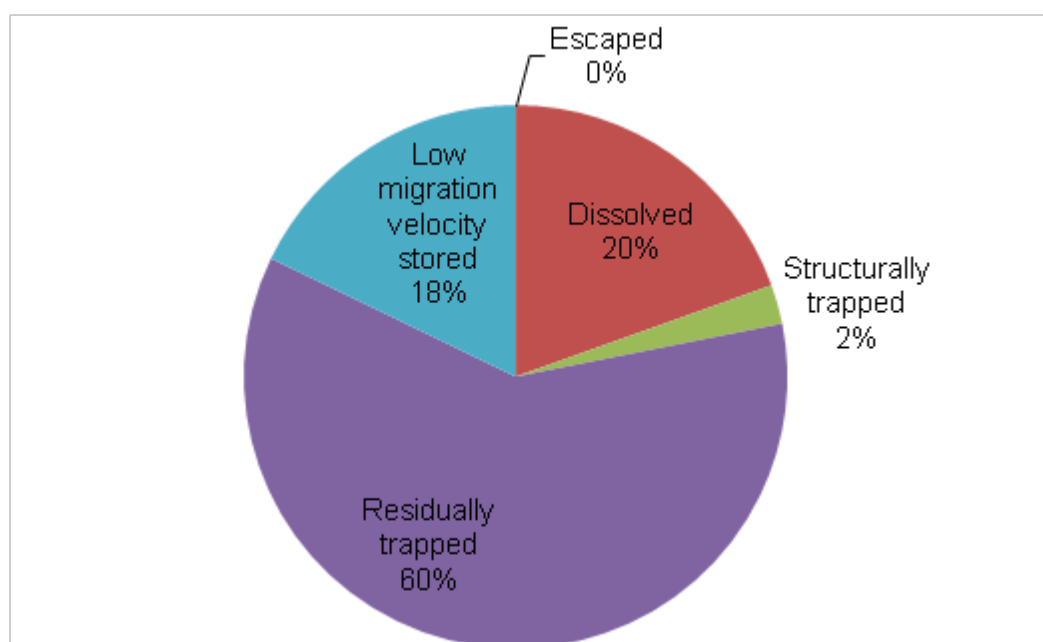


Figure A3.4: Mechanisms trapping CO<sub>2</sub> in the base case model at 1000 years. Percentages show the proportion of the total amount trapped by different mechanisms

In this case residual trapping is most significant. However, it is important to note that due to the low migration rates, it was possible to store 18% of the injected CO<sub>2</sub> without residual, structural trapping or dissolution which are more permanent trapping mechanisms, since low velocity CO<sub>2</sub> is still mobile and unconfined. The low permeability of this model explains this

high amount of low migration velocity storage as it leads to low migration velocities such that this CO<sub>2</sub> is migrating less than 10m/year.

In **Figure A3.5** it is seen that over time this low velocity CO<sub>2</sub> becomes increasingly trapped by the other mechanisms, however even at 10,000 years 7% of CO<sub>2</sub> is still mobile.



**Figure A3.5: Mechanisms trapping CO<sub>2</sub> at 1000 years and 10,000 years**

### 3.3 Base Case Exemplar Verification

The base case model was investigated to check its sensitivity to user chosen inputs. In particular, two studies were considered, the sensitivity of results to grid resolution and the boundary condition.

#### 3.3.1 Sensitivity to Grid Resolution

In order to reduce simulation runtimes (of up to many months) grid resolution was reduced from the original geocellular model. To assess the sensitivity of model results to grid resolution it was considered how a number of measures were affected when using a lower resolution model. The original 1.7m cell model was compared with the 450,450 cell version that coarsened the 1.7m cell model by a factor of two in both the x and y horizontal directions, but maintained resolution in the vertical direction. In both cases well locations were the same and rates were determined to maximise storage under the constraints mentioned previously.

The effect upon the following areas were considered:

### 3.3.1.1 Porosity and Permeability Distribution

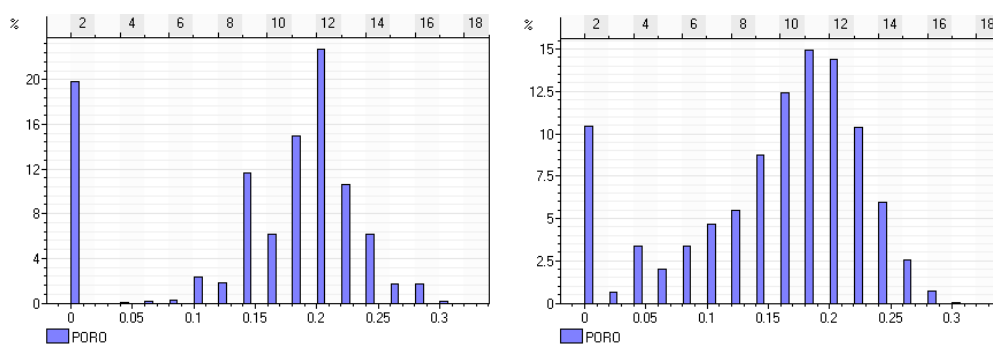


Figure A3.6a: Porosity distribution for 1,733,400 (left) and 450,450 (right) cell models

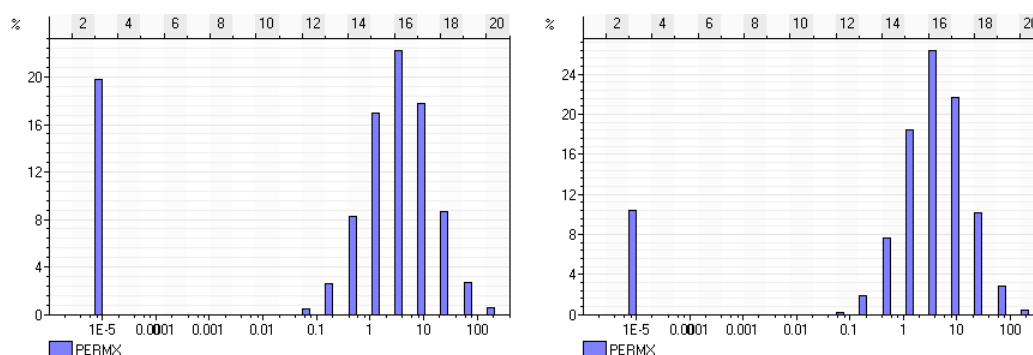


Figure A3.6b Permeability distribution for 1,733,400 (left) and 450,450 (right) cell models

The general distribution shapes for each model stayed the same – as shown in **Figures A3.6a and Figure A3.6b** – however the standard deviation of each model decreased, from 23 to 22 for the permeability, and from 0.086 to 0.075 for porosity. The spike for zero porosity and permeability was also reduced by around half leading to smaller zero permeability shale layers. **Figure A3.7** also shows that the channels still remain visually intact.

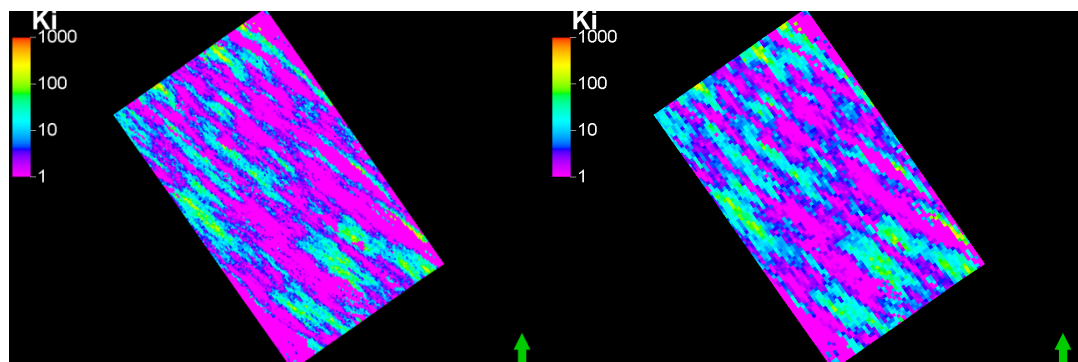
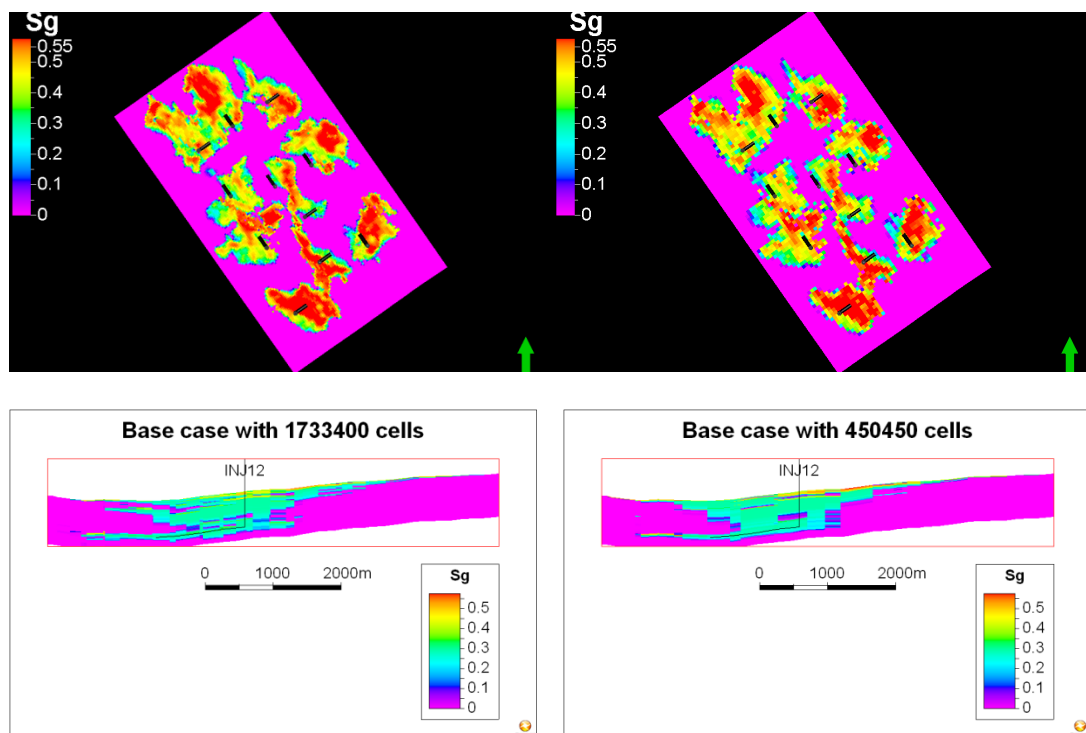


Figure A3.7: Permeability (mD) map for 1,733,400 (left) and 450,450 (right) cell models viewed from above

### 3.3.1.2 Saturation Profiles at 10,000 Years



**Figure A3.8: Saturation profiles at 10000 years for 1,733,400 (left) and 450,450 (right) cell models. Top models show top layer viewed from above. Wells are shown in black. Bottom models show saturation intersections around injection well INJ12**

In **Figure A3.8** the areal spread is captured well by the 450,450 cell model with very similar CO<sub>2</sub> extent to the 1.7m cell model. The cross-sections show slightly greater lateral migration extent within the model with the higher resolution case, which is likely a result of the larger proportion of impermeable shale cells. This may have some effect on the residual trapping, as seen in **Figure A3.10** where there is an increase in residual trapping in the higher resolution model.

### 3.3.1.3 Total CO<sub>2</sub> storage capacity

The total CO<sub>2</sub> injected into the model changed from 536Mt for the 1,733,400 cell model to 471Mt for the upscaled model. This occurred as more injection was possible under the BHP constraint by which both models were constrained. **Figure A3.9** suggests this is because pressure build-up near well was lower in the 1,733,400 cell model and higher localised pressure highs are seen in the 450,450 cell model where injection would be reduced as a result.

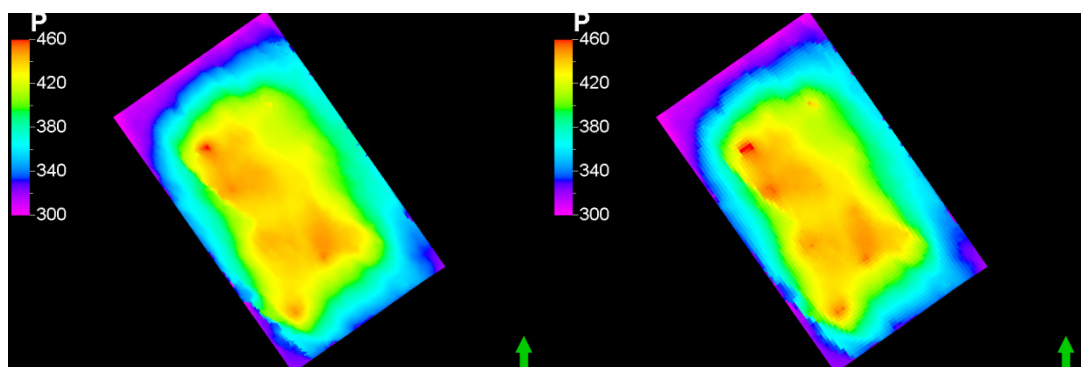


**Figure A3.9: Pressure (in bars) profiles on top layer at 40 years for 1,733,400 (left) and 450,450 (right) cell models. Higher localised pressure is visible in the 450,450 cell model**

Although this change in injection is not insignificant it only represents a change in storage pore volume utilisation from 3.5% to 3.9%. For the investigations presented in section 3.4 and section 4, this order of change is smaller than what is seen for physical sensitivities such as dip and permeability. This change also seems limited to reservoir models where the BHP constraint is the limiting factor on storage capacity such as in this base case. For reservoirs where this is not the case it was seen that the migration distances were not changed significantly from those seen in **Figure A3.8**. Further, for resolutions finer than 200m x 200m, as in the 1,733,400 cell model, it has been seen (see Appendix A5.3) that there is very little change in storage capacity and migration distances.

Trapping mechanisms in each case are also considered. It has been noted above that residual trapping may be increased due to greater lateral movement of CO<sub>2</sub> and an increase is seen in **Figure A3.10**. This increase is also likely due to the increase in total injection volume. Dissolution does not change significantly although proportionally has decreased a little from the higher resolution model.

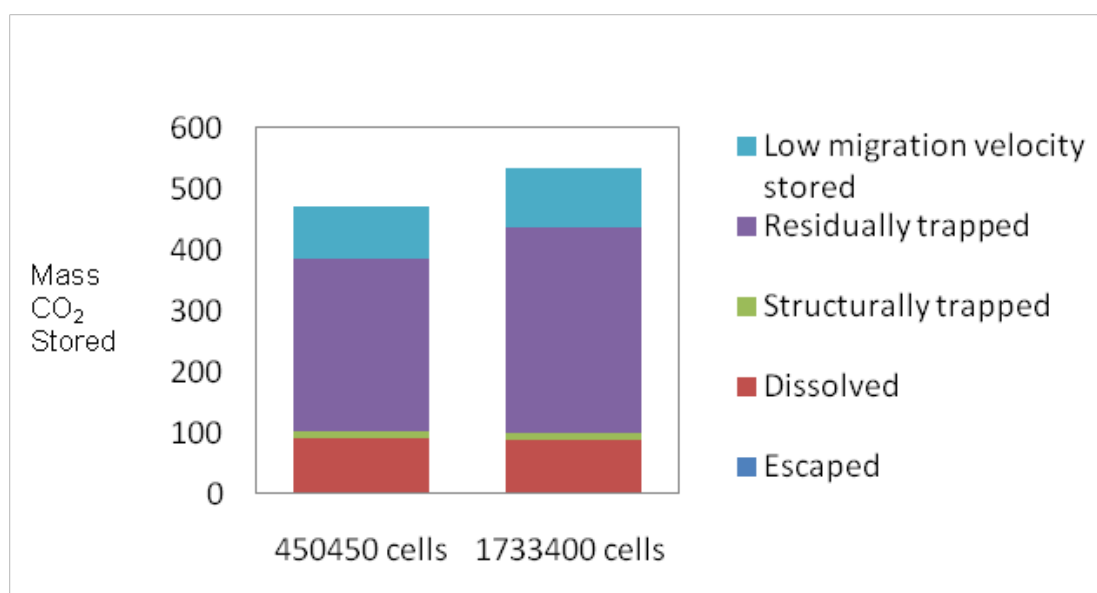


**Figure A3.10: Mass (Mt) of CO<sub>2</sub> stored with different grid resolutions at 1000 years**

The changes that have been observed as a result of a change in grid resolution are not insignificant; however they do not show any signs of changing the way the fundamental dynamics are captured. In particular flow patterns are still captured very well which is important for migration limited storage scenarios. For BHP constrained cases – which are of less interest – it is possible that injection may be underestimated; however compared to physical sensitivities the change is small. In conclusion, the coarser grid resolution is highly unlikely to affect any of the conclusions from the physical sensitivity studies, supporting the trade-off made to achieve feasible runtimes.

### 3.3.2 Sensitivity to Boundary Condition

Reservoir simulation models require some simplifying assumptions to represent the behaviour outside of the volume modelled and especially the behaviour at the model boundary. The boundary condition for this work is described in section 2.2. To support the use of this boundary condition a preliminary study of the sensitivity of the results to over 20 boundary condition scenarios was considered. These sensitivities were constructed as variations of the 6-well injection preliminary base case which injected 360Mt into the Forties geological model. Four of the most interesting scenarios are described as follows:

**Scenario 1** Base Case (boundary condition described in section 2.2) boundary pore volumes for four sides starting from the north-west side were  $1.0 \times 10^{11} \text{m}^3$ ,  $2.1 \times 10^{10} \text{m}^3$ ,  $8.5 \times 10^{10} \text{m}^3$  and  $7.1 \times 10^{10} \text{m}^3$  respectively compared to the  $2.0 \times 10^{10} \text{m}^3$  volume of the storage unit.

**Scenario 2** Larger connected pore volume –  $9.4 \times 10^{11} \text{m}^3$ ,  $1.6 \times 10^{12} \text{m}^3$ ,  $9.4 \times 10^{11} \text{m}^3$  and  $1.6 \times 10^{12} \text{m}^3$  for four sides starting from the north-west side.

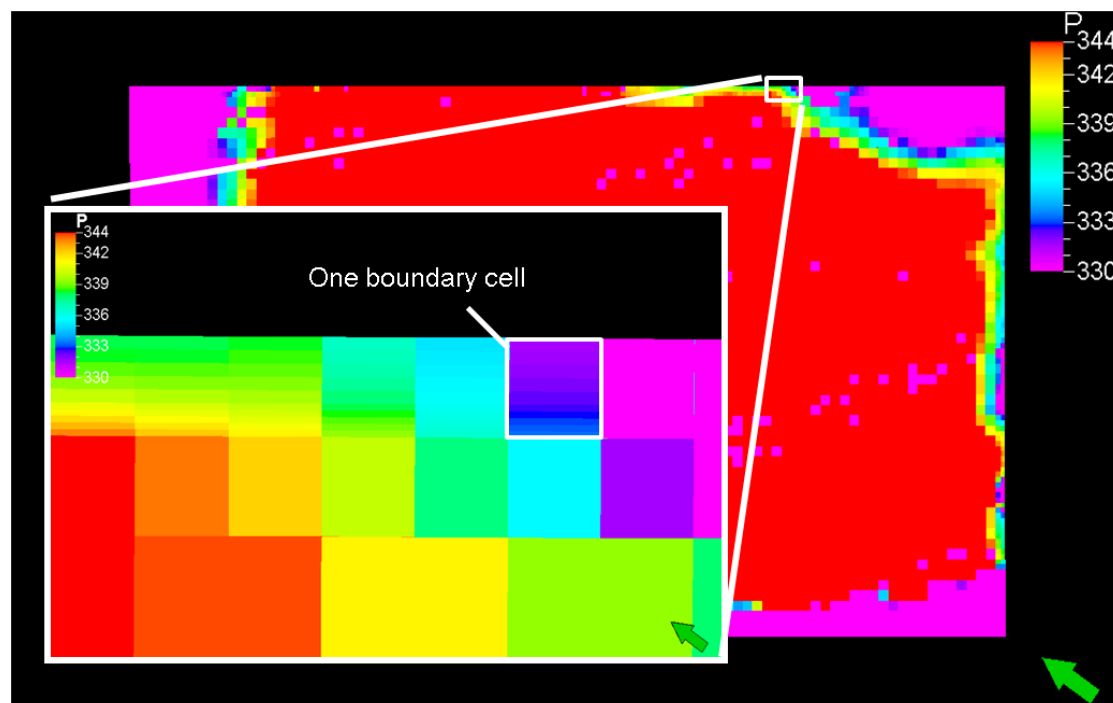


**Figure A3.11: Scenario 3 - The cells at the boundary had large pore volumes to represent the volume of aquifer attached to the model. Visually these boundary cells appear with the same area as their neighbours, however their pore volume is larger. To test the effect of the resolution of these boundary cells, such as the one highlighted**

they were refined. This can be seen by the range of colours inside. This refinement allowed the pressure to be resolved more accurately.

**Scenario 3** The large connected pore volume cells in scenario 2 were highly refined using grid refinement as shown in **Figure A3.11**. Therefore operations within this large pore volume were calculated using a large number of cells. As a result, cells in the connected pore volume were only between 4 and 8 times the width of normal cells.

**Scenario 4** The same as scenario 3 but the boundary cells moved in by 400m – 1400m cells depending upon boundary.

By modelling these scenarios the storage capacity was affected as shown in **Figure A3.12**. Since the base case capacity was limited by injectivity the changes in capacity seen are due to the change in injection rates.

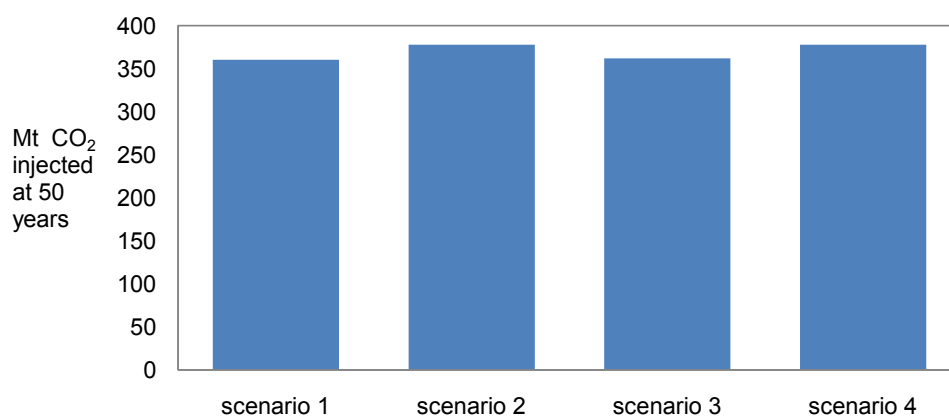


**Figure A3.12: Sensitivity of injected CO<sub>2</sub> volume to changes in boundary condition**

From the range of boundary conditions considered, the greatest change to stored CO<sub>2</sub> was 5% in scenarios 2 and 4. In scenario 2 a far larger pore volume was used to test the sensitivity to pore volume since an open aquifer with a restricted pore volume had been modelled. The larger pore volume caused a 5% increase in capacity since there was a larger volume over which pressure could be dissipated. As mentioned in the grid sensitivity analysis, this was significantly smaller than the effect of grid refinement. In scenario 3 it was shown that refining resolution at which the pressure footprint was resolved outside the domain had little effect upon the injected CO<sub>2</sub> volume. In scenario 4, the boundary cells were moved further into the model reducing the distance between the boundary cells and wells by up to 25%. This was also found to change the injected CO<sub>2</sub> volume by 5% thus showing that decreasing resolution nearer to the well and pressure plume has more of an effect on injected CO<sub>2</sub>.

From these results it was found that the boundary condition had a limited effect upon the injected CO<sub>2</sub> volume and the maximum 5% change in injected volume is considered acceptable under the same reasoning as used with grid sensitivity. Furthermore, as this case was limited by injectivity, it is expected that if the boundary condition was to impact any case it would be this type since the pressure impact of the boundary is most important here. Therefore it seems reasonable to extend this result to models more limited by CO<sub>2</sub> extent rather than injectivity.

### 3.4 Base case Exemplar Sensitivity to Reservoir Dip and Permeability

The sensitivity of capacity results to changes in average reservoir dip and permeability were assessed. This was used to:

- Test the sensitivity results used to form the storage regimes, which showed that dip and permeability had a key influence upon the storage pore volume utilisation of a storage unit (see Appendix A5.3), with a case that has real top-surface structure and heterogeneity.
- Check the analysis of the three broad storage regimes as described in section 1.3 and shown in **Figure A1.1**.

#### 3.4.1 Base case Exemplar sensitivity to permeability

Sensitivities to the average permeability of the base case are run as described in section 2.5, with the results shown in **Figure A3.13** and summarised in **Table A3.1** at the end of section 3. The sensitivities considered were 145mD and 1D representing the storage regime 2 and 3 cases to be investigated, respectively. Given computational time constraints the case with permeability <11mD was not modelled, since the base case is fairly representative of storage regime 1. This is also a rather low permeability and most storage sites are likely to be chosen to have permeabilities of at least 10 mD to avoid – as it has been demonstrated – excessive injectivity constraints.

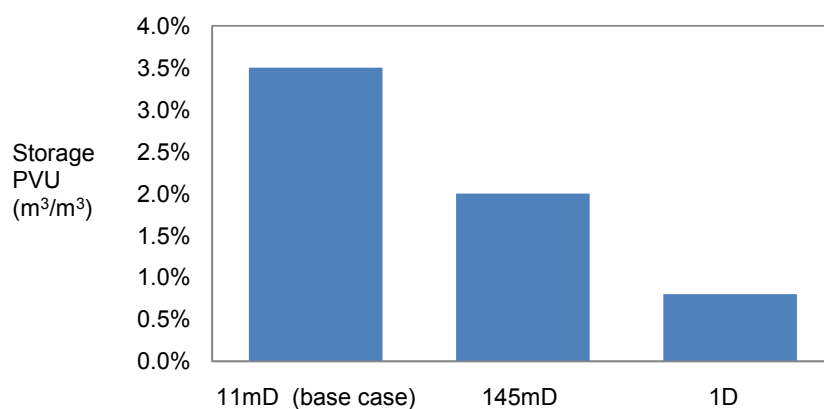


**Figure A3.13: Sensitivity of base case storage pore volume utilisation (PVU) to permeability**

In the 145mD case, representative of storage regime 2, the higher permeability compared to the 11mD case implied that storage pore volume utilisation was no longer limited by the BHP constraint, confirming the change from storage regime 1 to 2. This allowed for potential injection leading to the CO<sub>2</sub> saturation profile shown in **Figure A3.14** where CO<sub>2</sub> equal to 4% of the pore volume was injected; higher than the 3.5% injected into the BHP constraint limited 11mD base case. This injection scenario was suitably designed to meet the 99% storage constraint; however it failed the migration velocity constraint. The resulting final injection scenario that satisfied the migration velocity constraint is shown in **Figure A3.15** with storage pore volume utilisation of 2%. This utilisation was constrained by both the 99% storage constraint and the migration velocity constraint. The result that the migration velocity

constraint has an impact upon this storage regime 2 is interesting and this will be considered in Section 3.4.3.

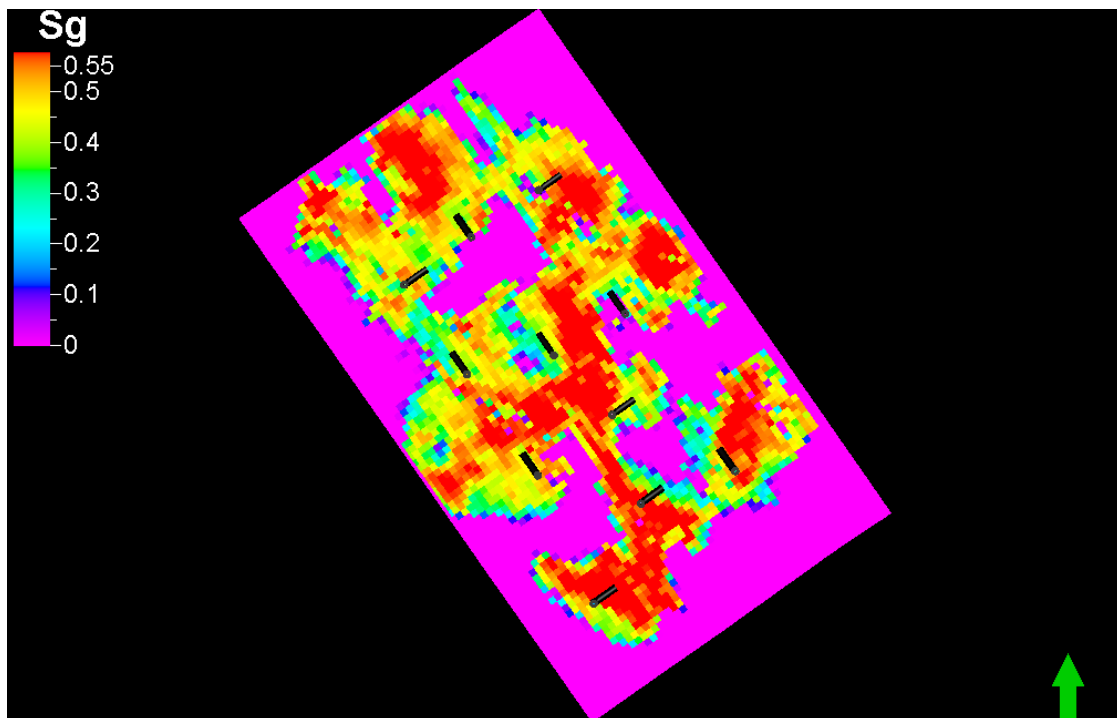
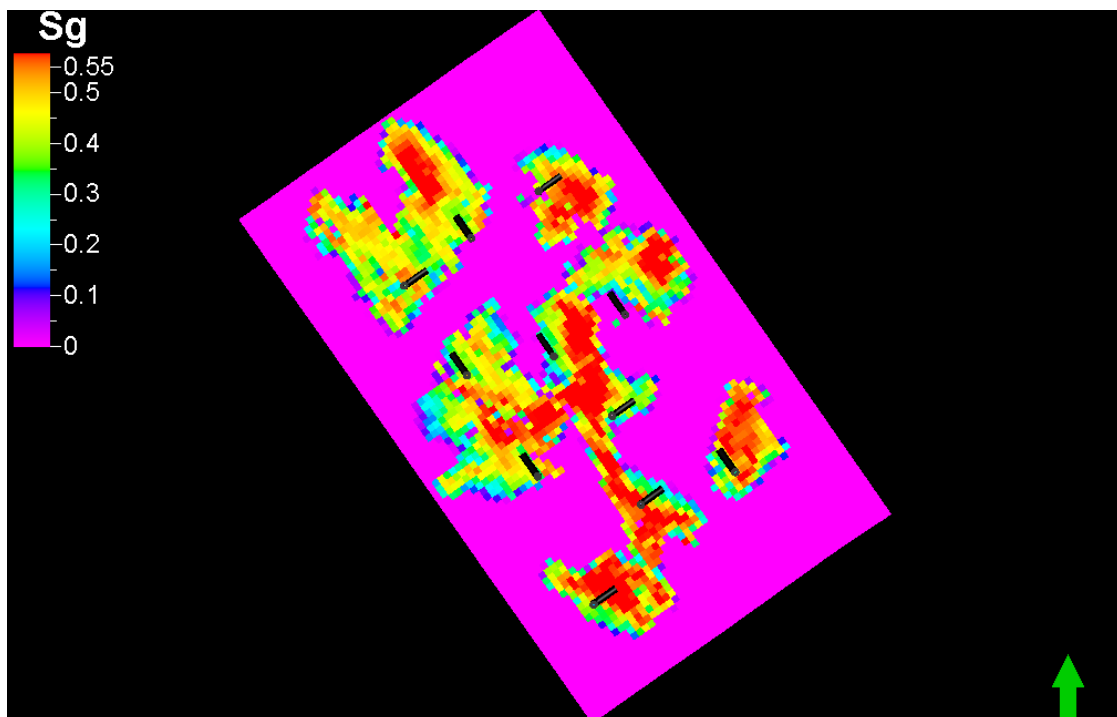


Figure A3.14: Top layer saturation profile at 1000 years for 145mD permeability sensitivity. The injection scenario shows injected CO<sub>2</sub> equal to 4% of the storage unit pore volume. 0.4% of the injected left the model – meeting the 99% storage constraint; however the migration velocity constraint was failed. Wells are shown in black



**Figure A3.15: Top layer saturation profile at 1000 years for 145mD permeability sensitivity. The injection scenario shown injected CO<sub>2</sub> equal to 2% of the storage unit pore volume and met the storage constraints. Wells are shown in black**

This 2% storage pore volume utilisation result confirmed that one could still achieve reasonable storage in a 'storage regime 2' site, and also confirmed an expected decrease in capacity with increasing permeability. In the 1 Darcy average permeability case a further reduction in storage for a storage regime 3 site was seen. The storage capacity in the adapted base case was reduced to 0.8% of the pore volume which was significantly limited by the migration velocity constraint, as expected for regime 3.

### 3.4.2 Base Case Exemplar Sensitivity to Dip

Sensitivities to the reservoir dip of the base case are run as described in section 2.5 and the results are summarised in **Table A3.1** at the end of section 3. The sensitivities considered were 1° and 3° - these dips are larger than the base case that has a value of 0.27°. Since the base case had 11mD permeability, both of these cases still had characteristic velocities representative of storage regime 2, as shown in **Table A3.1**.

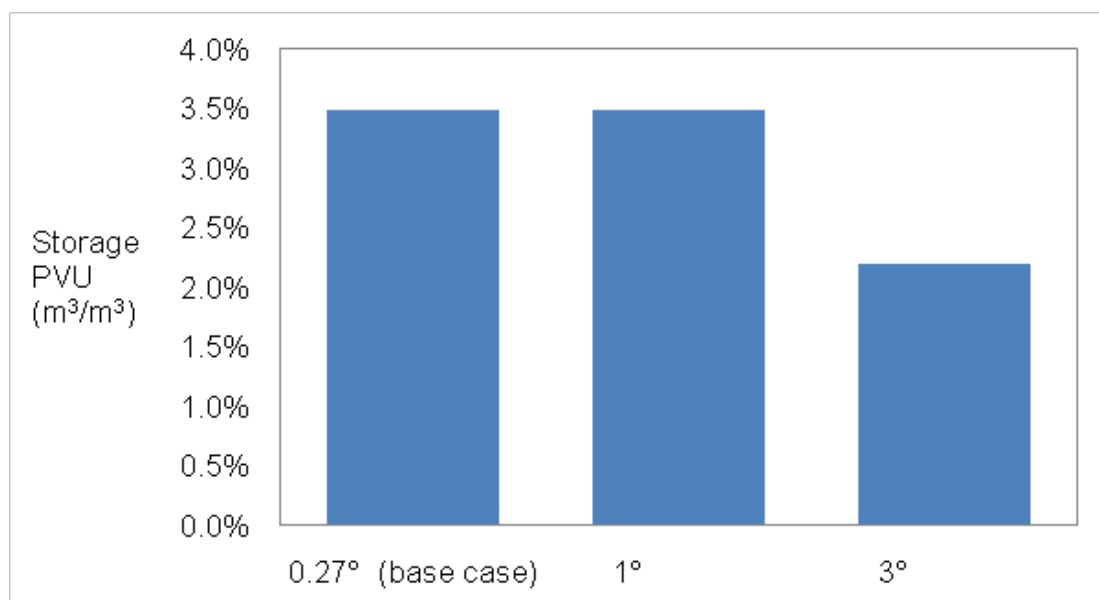


**Figure A3.16: Sensitivity of base case storage pore volume utilisation (PVU) to reservoir dip**

The results of these sensitivities are shown in **Figure A3.16** and do demonstrate a decrease in storage with increasing dip, but only in the 3° case once the migration velocity constraint becomes more important than the BHP constraint. In the 3° case the migration velocity constraint reduced the amount stored as otherwise it was possible to inject more CO<sub>2</sub> than the 2.2% injected and still satisfy the 99% storage constraint. The 2.2% and 3.5% storage pore volume utilisation values still showed that these models had storage pore volume utilisation as it would be expected by the characteristic velocity analysis categorising these models as storage regime 2. However in this case it has been seen again that the migration velocity constraint can have an impact on storage regime 2 as well as storage regime 3 storage units. This will be considered in section 3.4.3.

### 3.4.3 Conclusions and Analysis of the Dip and Permeability Sensitivity and Storage Regime Results

In this section it is shown that the storage regimes approximation still applied when structure and heterogeneity were introduced to dip and permeability sensitivities. The storage pore volume utilisation found in sections 3.4.1 and 3.4.2 have broadly agreed that the storage pore volume utilisation in regime 2 and 3 have come from different distributions with pore volume utilisations below 1% for storage regime 3 and above 2% for storage regime 2. However, it can be seen in **Figure A3.17** that the disparity between the two regimes is noticeably smaller for the realistic heterogeneous model with top-surface structure than in the homogeneous smooth models. Section 4 looks more at the effect of top-surface structure and heterogeneity to explain this.

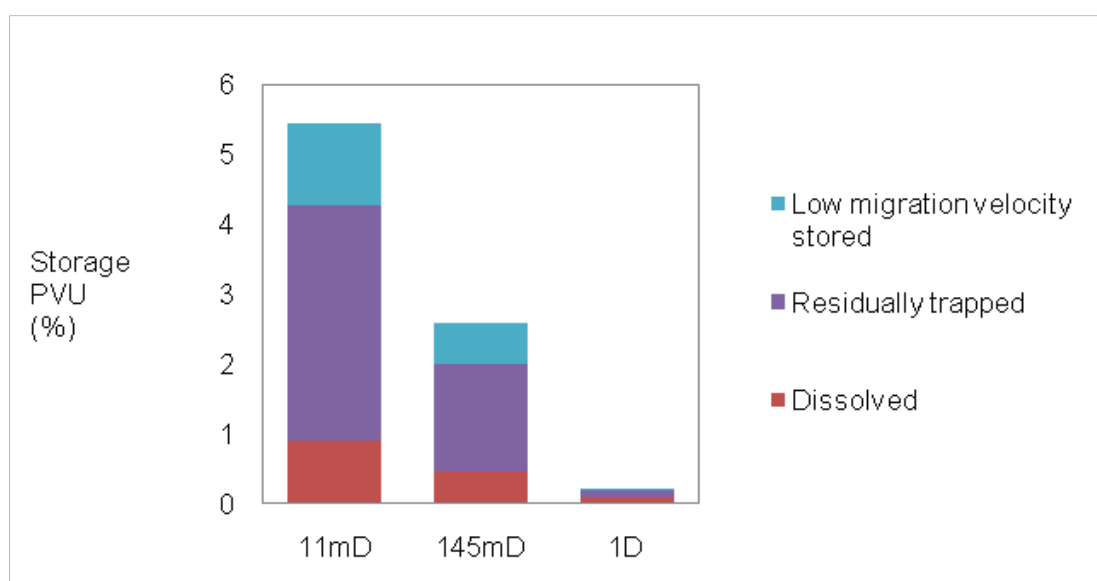


**Figure A3.17: Sensitivity of storage pore volume utilisation (PVU) due to changes in permeability in the 0.270 smooth heterogeneous model**

There is one other distinct issue highlighted in these results - that the migration velocity constraint can constrain capacity in storage regime 2. Based upon the analytic up-dip migration calculation used in Appendix A5.3 this might not be expected. It is possible that this occurs because of high permeability or high dip areas in the heterogeneous base case model, so a smooth homogeneous case is considered to rule this out. The homogenous case considered is the 145mD 0.27° dip case and its saturation profile is shown in **Figure A3.18**.

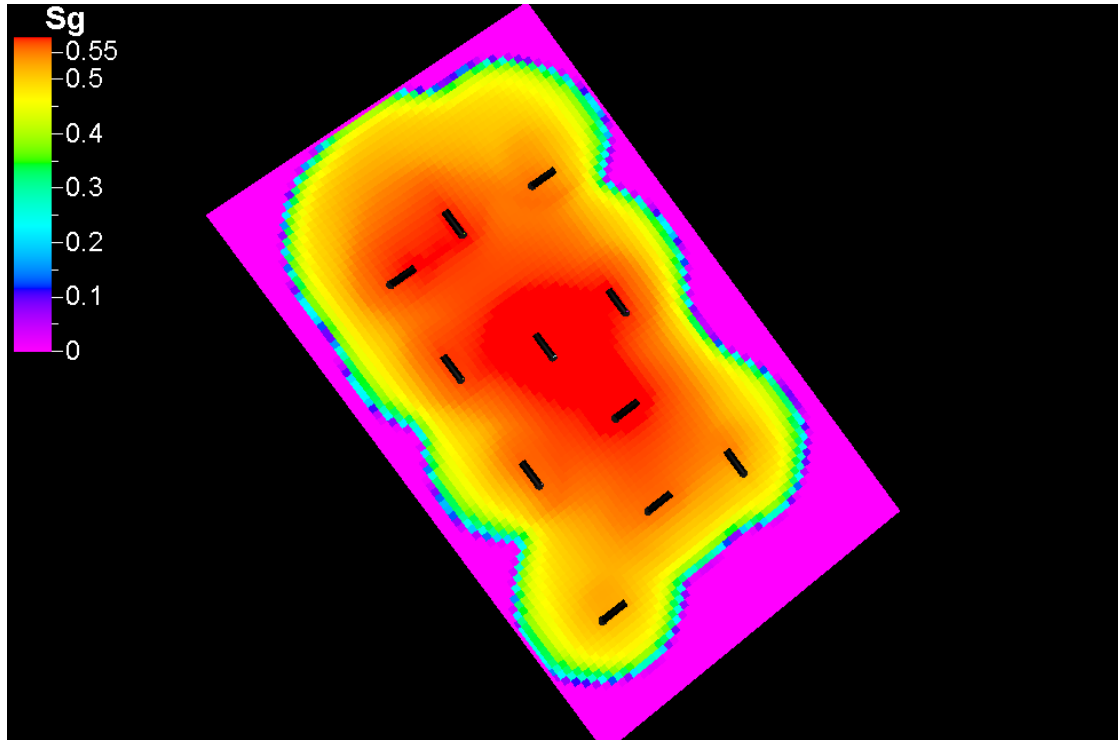


**Figure A3.18: Top layer saturation profile for at 1000 years for 145mD permeability smooth homogeneous model**

The result of this was that both the storage constraint and migration velocity constraint were constraining capacity. To explain why the migration velocity constraint still has an impact in storage regime 2 the analytic analysis of flow velocity is considered.

In the analytic analysis the velocity of spreading of the buoyant CO<sub>2</sub> plume is considered using the form of Vella and Huppert (2006), in addition to the component of flow updip due to gravity that is used to separate the storage regimes 2 and 3 – the first term in equation (3.1). Using this, the velocity  $v$  of CO<sub>2</sub> migration is

$$v = \frac{K\lambda_{CO_2}\Delta\rho g}{(1-S_{WC})\phi} \left( \sin\theta + \frac{dh}{dx} \cos\theta \right) \quad (3.1)$$

Where  $\Delta\rho = \rho_{water} - \rho_{CO_2}$ ,  $h$  is the connected height of CO<sub>2</sub> in the direction perpendicular to the top-surface,  $x$  is the distance along the top-surface,  $\theta$  is the dip angle,  $S_{WC}$  is the connate water saturation,  $\lambda_{CO_2}$  is the mobility of the CO<sub>2</sub> phase and  $g$  is gravity.  $dh/dx$  represents the change in thickness of the CO<sub>2</sub> plume itself with distance – this is difficult to estimate directly from simulation models. The second term in equation 3.1 accounts for the buoyant spreading of CO<sub>2</sub> and explains how storage regime 2 models can have migration speeds of over 10m/year at 1000 years when the first term alone does not predict this.

Although the first term may not always predict the velocity exactly there is still a key difference between the two terms which means that the use of the first term alone is good for dividing models between these storage regimes 2 and 3. This difference is that the updip gravity term is purely dependent upon the dip and permeability whereas the other depends upon the

amount of CO<sub>2</sub> injected via the connected height of CO<sub>2</sub>. This leads to a difference in how the migration velocity constraint acts in storage regime 2 and storage regime 3; since in general the second term is more important in storage regime 2 and the first term is by the definition of storage regime 3 important in this case.

In homogeneous storage regime 2 cases some variable amount of high saturation CO<sub>2</sub> can be stored below the migration velocity constraint threshold, above which the constraint is breached due to the magnitude of buoyant spreading term. In homogenous storage regime 3 cases if high saturation cells were present, they would by definition have too high migration velocities. Thus it is not possible to have any high saturation CO<sub>2</sub> in storage regime 3 and the only low velocity CO<sub>2</sub> must be at lower mobility saturations.

**Figure A3.19** shows that for the set of smooth homogeneous models with permeability variation low migration velocity storage is seen, which is consistent with this understanding. In the 145mD storage regime 2 case, although the migration velocity constraint was limiting as described above, low migration velocity storage was allowed, as it can be seen by the high mobility saturations in **Figure A3.18** and the 80Mt stored in **Figure A3.19**. The 1 Darcy case representing storage regime 3 also fits this analysis only storing 3Mt of low velocity CO<sub>2</sub> and in **Figure A3.20** it can be seen that this is at saturations significantly lower than the highest mobility.

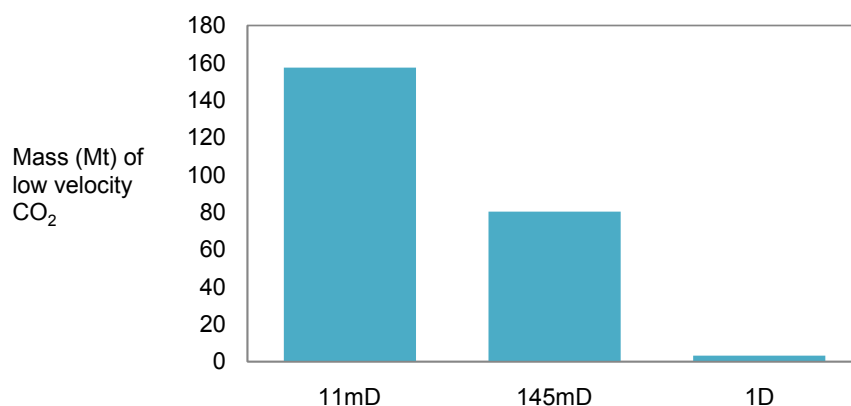


**Figure A3.19: Sensitivity of the stored mass (Mt) of 'Low velocity CO<sub>2</sub>' to permeability in a 0.27° dip, smooth homogeneous scenario. Low velocity CO<sub>2</sub> is defined in Section 2.4**

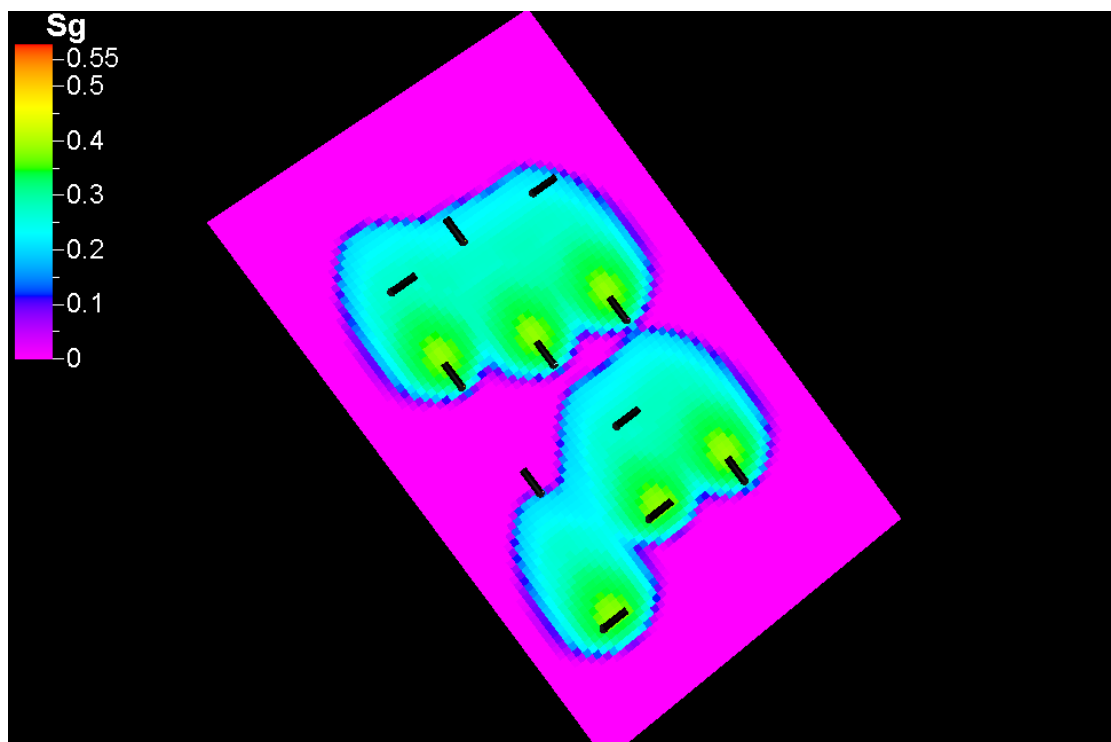


**Figure A3.20: Saturation profile in the top layer of a smooth, homogeneous 1 Darcy model at 1000 years. Most gas saturation is seen to be near residual**

To summarise this analysis, it has been presented that the migration velocity constraint can affect both storage regimes 2 & 3. In storage regime 2 it limits the size of a migrating plume, but in storage regime 3 it essentially prevents any highly mobile CO<sub>2</sub> remaining at 1000 years, or alternatively it virtually stops low migration velocity storage. The impact of preventing low migration velocity storage in storage regime 3 is that less can be injected, reducing the amount of dissolution and residual trapping and ultimately reducing storage pore volume utilisation.

Following the understanding of the migration velocity constraint a general set of possible capacity constraining scenarios can be produced for each storage regime. **Table A3.1** shows a summary of the results.

#### Storage Regime 1

- Limited by BHP combined with 99% storage constraint for location of wells

#### Storage Regime 2

- Limited by BHP combined with 99% storage constraint for location of wells
- Limited by migration velocity constraint due to size of migrating plume with 99% storage constraint for location of wells
- Limited by 99% storage constraint

### Storage Regime 3

- Limited by migration velocity constraint preventing highly mobile CO<sub>2</sub> remaining at 1000 years with 99% storage constraint for location of wells

Finally, it can be observed from Equation 3.1 that in storage regime 2 the migration constraint for spreading CO<sub>2</sub> is still affected by permeability. Therefore within regime 2 once the dip permeability combination is such that the migration velocity is capacity constraining, it is expected that as the permeability increases further migration velocity constraint would restrict plume sizes more and thus lower storage pore volume utilisation.

Average storage unit permeability (mD)	Average storage unit dip (°)	Analytic migration velocity based upon average dip and permeability $\approx 5.5K\sin\theta$ (m/yr)	Storage regime	Storage Pore Volume Utilisation		
				Homogenous smooth	Homogeneous with top-surface structure	Heterogeneous with top-surface structure
11	0.27°	0.3	1/2	5.4%	5.5%	3.5%
145	0.27°	3.8	2	2.6%	1.2%	2%
1000	0.27°	25.9	3	0.2%	0.4%	0.8%
145	1°	13.9	3 (just)	0.9%	0.5%	
145	3°	41.7	3	0.3%	0.3%	
11	1°	1.1	2			3.5%
11	3°	3.2	2			2.2%

Table A3.1: Storage pore volume utilisation (PVU) results

## 4 Impact of Top-Surface Structure and Heterogeneity – Sensitivity Results

In this section the effect of top-surface structure and heterogeneity upon storage pore volume utilisation in dipping open aquifers is investigated. The method described in section 2.5 is used to evaluate the effect that the introduction of top-surface structure and heterogeneity have on the storage pore volume utilisation and compare it to the results for smooth homogeneous models in each of the storage regimes.

### 4.1 Effect of Top-surface Structure upon Storage Capacity

The effect of top-surface structure was evaluated in the three storage regimes, as set in section 5.3.1 in the main report. For the purpose of this analysis the 11mD 0.27° cases modelled as the examples of storage regime 1 are considered, although they slightly fall above the 10mD notional boundary (see section 5.3.1 in the main report). These cases do however have the most important feature of storage regime 1 which is that storage is limited by injectivity due to low permeability.

#### 4.1.1 Effect upon Models with Injectivity Limited Storage Capacity (storage regime 1)

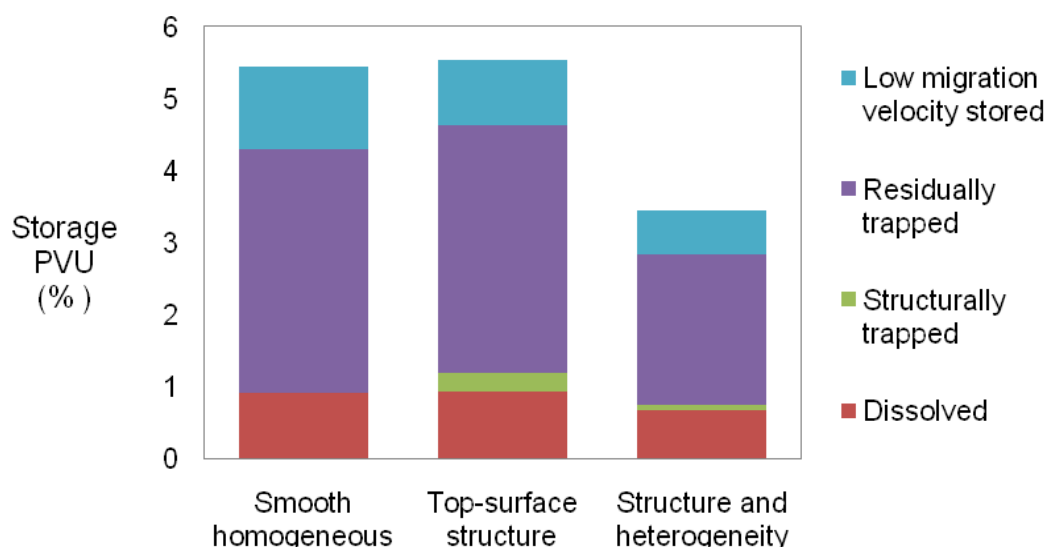


**Figure A4.1: Change in storage pore volume utilisation (PVU) due to the introduction of top-surface structure and heterogeneity to the 11mD 0.27° smooth homogeneous case**

The effect of top-surface structure upon storage capacity in storage regime 1 is minimal as shown by the change in the first two bars in **Figure A4.1** and injectivity still limits storage. It can be seen that some of the CO<sub>2</sub> that was low migration velocity stored at the top of the reservoir in the smooth homogeneous case sits within structural closures when top-surface structure is added. Further, very little difference between the plumes in **Figures A4.2** and **A4.3** can be observed.

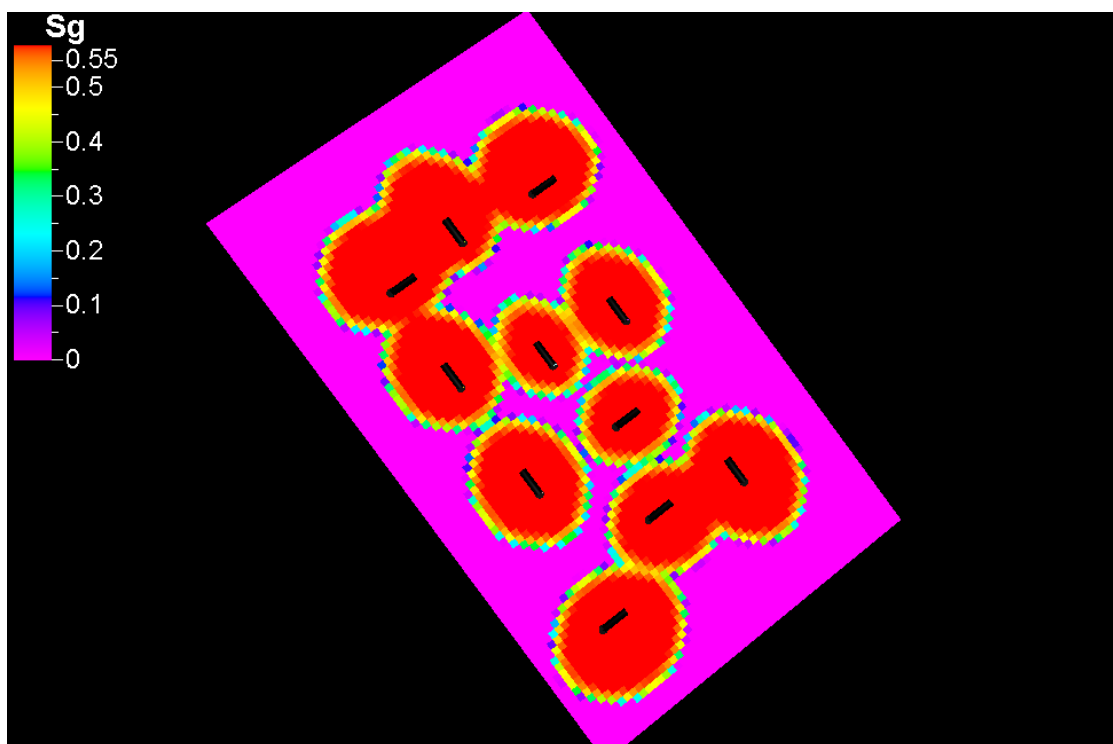


Figure A4.2: Saturation profile showing the top layer of a smooth homogeneous 11mD model with a dip of 0.27° at 1000 years

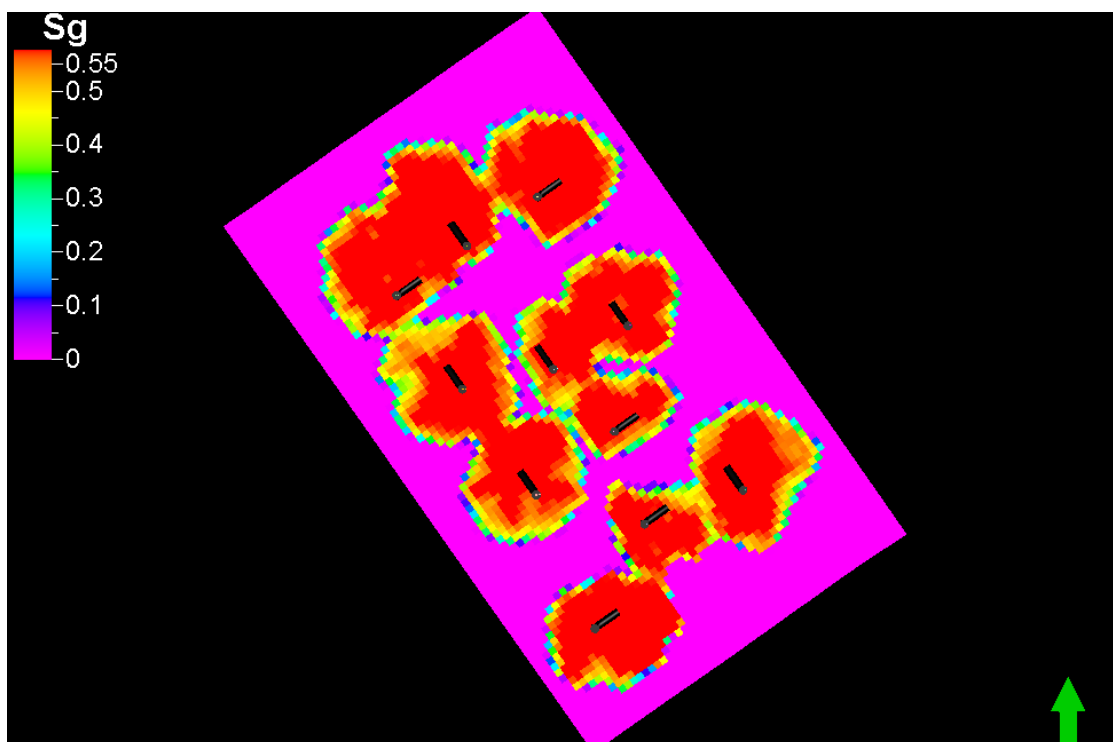
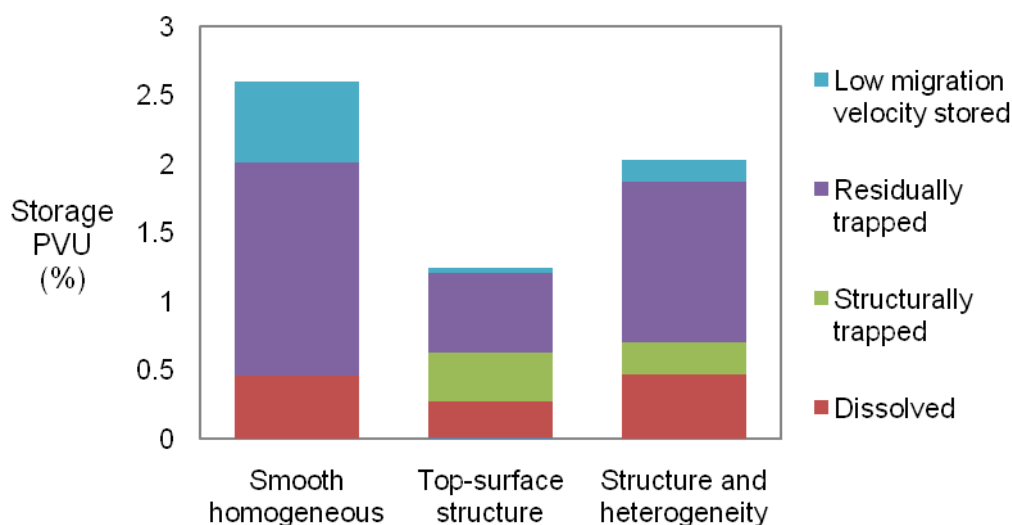


Figure A4.3: Saturation profile showing the top layer of 11mD, 0.27° dip homogeneous model with top-surface structure at 1000 years

#### 4.1.2 Effect upon Models Characterised by Storage Regime 2



**Figure A4.4: Change in storage pore volume utilisation (PVU) due to the introduction of top-surface structure and heterogeneity to the 145mD 0.27° smooth homogeneous case**

The introduction of top-surface structure into the 145mD storage regime 2 model caused a drop in storage pore volume utilisation from 2.6% to 1.2%, as shown in **Figure A4.4**. This reduction occurred during the optimisation of injection into the model with top-surface structure by the need to reduce injection rates into, or even to stop wells in regions with locally higher dip, to comply with both the 99% storage constraint and the migration velocity constraint. For example, **Figure A4.5** shows that it was necessary to shut-in two wells in the north-west (upper left) to meet the migration velocity constraint. In addition, channelling led to poorer coverage of the top-surface.

However, the introduction of structural trapping due to the introduction of top-surface structure provided an additional amount of trapping and, of the CO<sub>2</sub> that was injected, 29% of it became structurally trapped, equivalent to 48Mt. This can be seen in **Figure A4.5** by the red high saturation patches. This extra trapping mechanism along with the less secure high dip regions introduced two features that had competing effects upon the storage capacity. Structural trapping increased capacity whereas high dip regions increased migration velocities as well as distances, leading to a need to reduce injection to satisfy the open aquifer storage constraints.

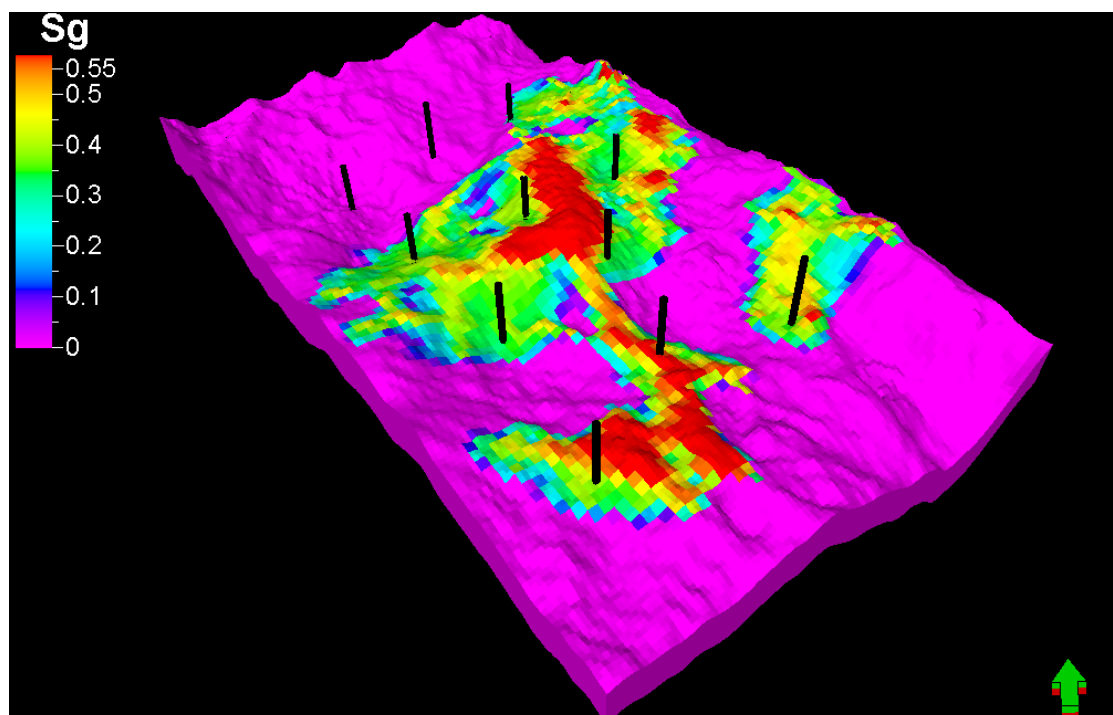


**Figure A4.5: Saturation of a homogeneous 145mD, 0.27° dip model with top-surface structure at 1000 years. Model viewed from south and exaggerated by factor 15 in the vertical direction**

The combined effect of these two impacts is subtle. If the structural closures alone were added above the smooth model one could see a pure 48Mt increase in storage. What can be seen in this realistic example though is that where the geology has created structural closures, there are associated regions that dip away from the structure. In other areas full closure is not formed and, worse, some partial closure or unclosed regions form routes that can either lead to escape or prohibited high velocity migration. The result is that the remaining top-surface area outside the structural closures and the area directly below the structurally stored CO<sub>2</sub> only stores 5Mt through low migration velocity storage - a significant drop from 80Mt. Effectively large portions of this area have gained characteristics more like storage regime 3, and as explained in section 3.4.3 where less CO<sub>2</sub> is low migration velocity stored, less is injected, therefore there is less dissolved or residually trapped CO<sub>2</sub> at 1000 years and ultimately a lower storage pore volume utilisation is achieved.

#### 4.1.3 Effect upon Models Characterised by Storage Regime 3

Two dip and permeability combinations representative of storage regime 3 are simulated, the 1D 0.27° case and the 145mD 3° case. A final 145mD 1° simulated scenario also had analytic estimates of its maximum gas saturation velocity just over 10m/yr, using buoyant migration with the known average dip angle and average permeability, categorising it as storage regime 3, but giving it characteristics in-between storage regime 2 and 3. This case will also be considered.

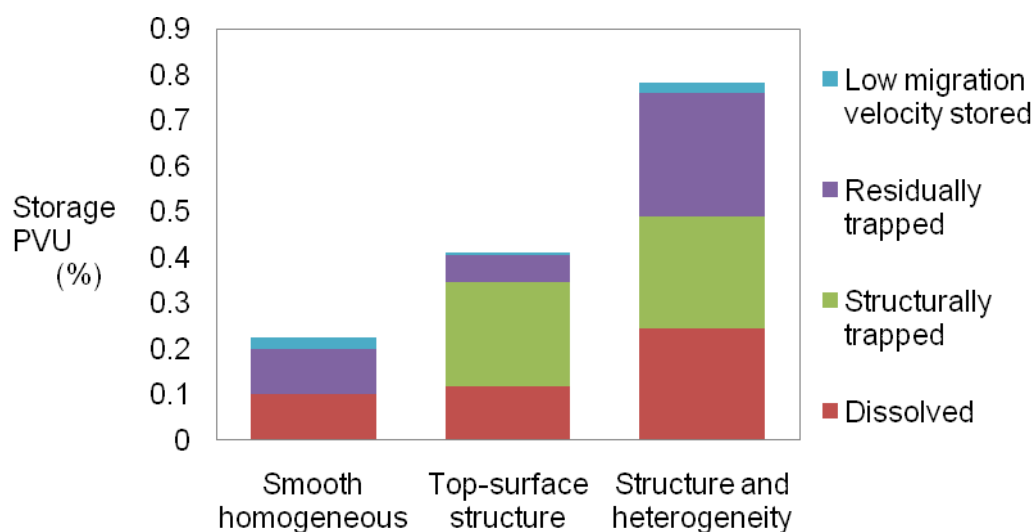


**Figure A4.6: Change in storage pore volume utilisation (PVU) due to the introduction of top-surface structure and heterogeneity to the 1 Darcy 0.27° smooth homogeneous case**

First, the 1D 0.27° case is considered. As seen in section 3.4.3, in the smooth homogeneous model this case had very low storage pore volume utilisation because the migration velocity constraint only allowed low migration velocity storage at saturations approaching residual that have very low mobility. **Figure A4.6** shows that the introduction of top-surface structure increased the storage pore volume utilisation from 0.2% to 0.4%. The increase due to top-surface structure in this case is clear with 55% of the CO<sub>2</sub> stored in structural closures in the top-surface structure scenario - this figure almost directly corresponds to the increase in storage from the smooth case. The other key point is that the effect of high dip areas has been far less pronounced. This is because there was virtually no low velocity CO<sub>2</sub> in the smooth homogeneous case and thus the introduction of higher dip regions were unlikely to cause substantial unpermitted migration velocities and a need for reduced injection.

The second case modelled is the 145mD 3° case. The introduction of top-surface structure into the smooth model actually failed to produce any structural closure due to the 3° dip. This implied that there was no opportunity to see an increase in storage due to structural trapping. However the effect of different and higher dip regions could be evaluated. The result was that there was no change in the storage pore volume utilisation staying at 0.3% as shown in **Table A3.1**. Since the smooth case here was in storage regime 3 and therefore without significant low migration storage, this supports the idea that the higher dip regions have little effect on storage pore volume utilisation if there is not low migration velocity storage in the smooth model.

The final case considered is the 145mD 1° case (**Figure A4.7**), which is categorized in storage regime 3. However gas saturations of only 0.05 below the maximum gas saturation can still flow with velocity less than 10m/yr in the model, so it has some characteristics of storage regime 2. For example at 0.9% the storage pore volume utilisation is substantially higher than the other smooth storage 3 models and the mass of low velocity CO<sub>2</sub> stored is 10 times larger than the mass of low velocity CO<sub>2</sub> stored in the 1Darcy and 3° sensitivity cases. At the same time the pore volume utilisation and low migration velocity storage are still lower than the other storage regime 2 cases. Given this evaluation, the result of including top-

surface structure seems to more closely represent the style of a storage regime 2 scenario. The 7Mt of low velocity CO<sub>2</sub> is reduced to 4Mt due to reduced well rates being approximately halved in all injecting wells to keep within the migration velocity constraint. This low level of low migration velocity storage is similar to that in the 145mD 0.27° model with top-surface structure. In addition, there is a low increase in storage from structural closure as the 1° dip stops most of the closure. The conclusion from this case is that in some cases which are only just across the storage regime 2/3 boundary, modest level of storage due to some fairly high saturation low velocity CO<sub>2</sub> can still occur, and that the introduction of extra dip regions reduces storage pore volume utilisation in the storage regime 3 models.

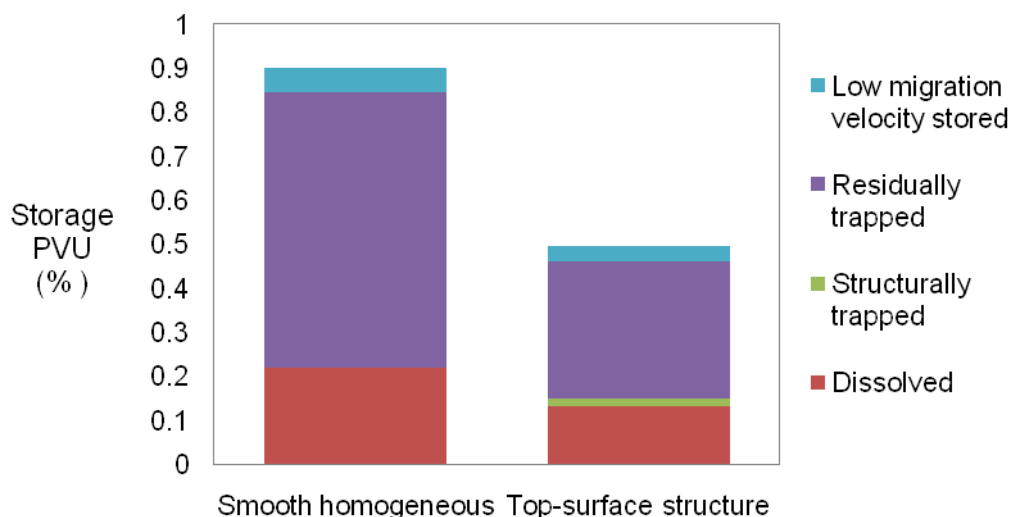


Figure 4.7: Change in storage pore volume utilisation (PVU) due to the introduction of top-surface structure and heterogeneity to the 145mD, 1° smooth homogeneous case

#### 4.1.4 Conclusions on the Effect of Top-surface Structure

The introduction of top-surface structure introduces both structural closures and regions of high dip. The effects of these regions generally compete to increase or decrease storage pore volume utilisation respectively.

The balance of these effects has been assessed by understanding how CO<sub>2</sub> is stored within smooth homogeneous models prior to including structure into the models. This analysis of smooth homogeneous models divides them into those which can store CO<sub>2</sub> through low migration storage at high saturations and those that cannot. This division generally fits well with the separation of storage regime 2 and 3, although one example showed that it is possible to have some modest low migration velocity storage just across the storage regime 2/3 boundary.

For those sites that were seen to be able to store CO<sub>2</sub> through low migration velocity storage a decrease in storage was seen, as the effect of new higher dip regions reducing storage pore volume utilisation was more successful than the addition of structural closures increasing pore volume utilisation. For those sites unable to store CO<sub>2</sub> through low migration velocity storage, either increases or no change in storage pore volume utilisation were seen with the addition of top-surface structure - with no change occurring when the top-surface added no structural closure.

These results show that there is only a sharp drop in storage pore volume utilisation due to the introduction of high dip routes to smooth cases where there was strong low migration velocity storage. This is due to the loss of low migration velocity storage. Therefore it was concluded that there is a qualitative difference between the effect of introducing higher dip routes to smooth model cases with strong low migration velocity storage (storage regime 2) and cases with weak low migration velocity storage (storage regime 3). This result builds on work on Representative Structures in Appendix A5.3 that showed the qualitative difference between the storage pore volume utilisation shown in storage regimes 2 and 3, which were shown in section 3.4 to be characterised by their ability or not to store low velocity CO<sub>2</sub>. The introduction of high dip regions is similar to introducing regions that have the qualitatively lower storage pore volume utilisation of storage regime 3. This result further demonstrates the significance of low migration velocity storage upon storage pore volume utilisation, as shown in section 3.4.3.

Further, the results presented in this section show that the addition of localised structural closure alone will increase storage. In cases where there is virtually no low migration velocity storage of CO<sub>2</sub> such as typical storage regime 3 cases, where the addition of the introduction of high dip regions have little effect upon storage, this may be the dominant effect of the introduction of top-surface structure.

## 4.2 Effect of Heterogeneity upon Storage Capacity

The impact of heterogeneity upon storage pore volume utilisation was also evaluated under each of the storage regimes using the same dip and permeability scenarios as in section 4.1.

### 4.2.1 Effect upon models with Injectivity Limited Storage Capacity (storage regime 1)

The effect of heterogeneity upon a storage unit with injection-limited storage pore volume utilisation is evaluated using the 11mD 0.27° scenario with the results shown in **Figure A4.1**. Here it can be seen that the introduction of heterogeneity significantly reduced the amount injected and the resulting storage pore volume utilisation decreased from 5.5% to 3.5%. The capacity in both examples was constrained by the same BHP constraint so it can be deduced that the pressure near well built up to this pressure with a lower injection rate than in the heterogenous case. To confirm this **Figure A4.8** shows that in the heterogenous case the pressure at the well has built up as high as in the homogeneous case, despite the lower injection. It can also be observed that this is a result of more localised pressure build-ups. These localised pressures can be seen to occur in regions surrounded by low permeability volumes such as shales, and therefore these low permeability volumes cause lower injection and storage pore volume utilisation.

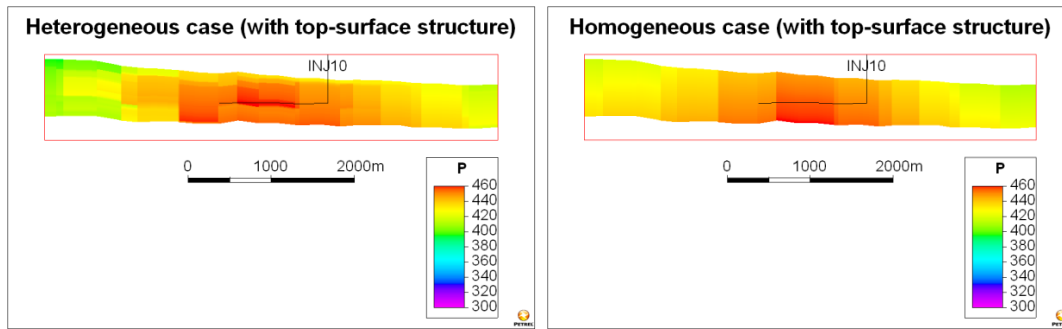


**Figure A4.8: Pressure (in bars) profile around well INJ10 in heterogeneous (left) and homogeneous (right) cases at 50 years. The intersections show that localised high pressure can build up in the heterogeneous model whereas it spreads further in the homogeneous model**

#### 4.2.2 Effect upon Models Characterised by Storage Regimes 2 & 3

The effect of heterogeneity upon storage pore volume utilisation in storage regimes 2 and 3 is considered together since similar results are found in each regime. In particular the two cases considered are the 145mD 0.27° storage regime 2 case and the 1D 0.27° storage regime 3 case. The storage results for these cases were previously shown in **Figure A4.4** and **Figure A4.6** respectively.

From both these figures it can be seen that the introduction of heterogeneity increases storage, from 1.2% to 2.0% and 0.4% to 0.8% respectively. Within this increase dominant rises come from increases in residual trapping and dissolution. The reason for this is that the heterogeneity, such as shale layers, within the model was able to increase the amount of lateral migration of the CO<sub>2</sub> after injection leading to a greater reservoir contact and therefore greater residual trapping and dissolution. This is shown in **Figure A4.9** where far greater lateral migration and sweep is seen in the heterogeneous case, whereas CO<sub>2</sub> in the homogeneous model takes the most direct route to the surface.

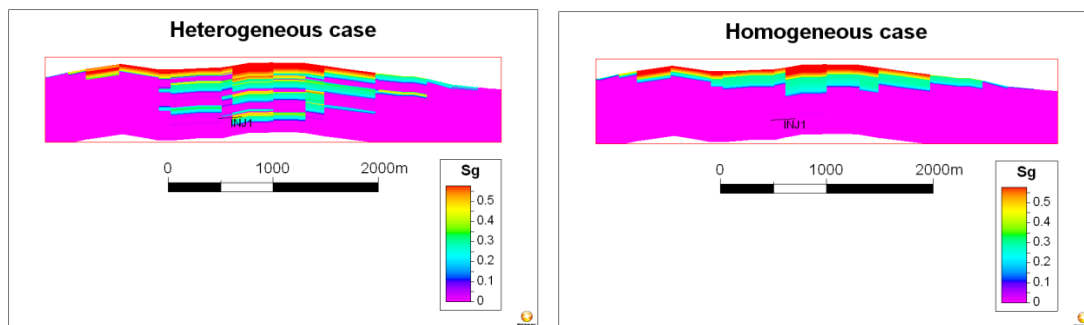


**Figure A4.9: Saturation intersections to show wider lateral migration under shales in the heterogeneous model (left) compared to the homogeneous model (right) at 1000 years. Both models have 145mD permeability and 0.27° dip**

The other increase that is seen is in the low migration velocity storage; however the extra low migration velocity storage is likely to be due to structural trapping under small shale layers deeper within the reservoir, an example of which is shown in **Figure A4.10**.

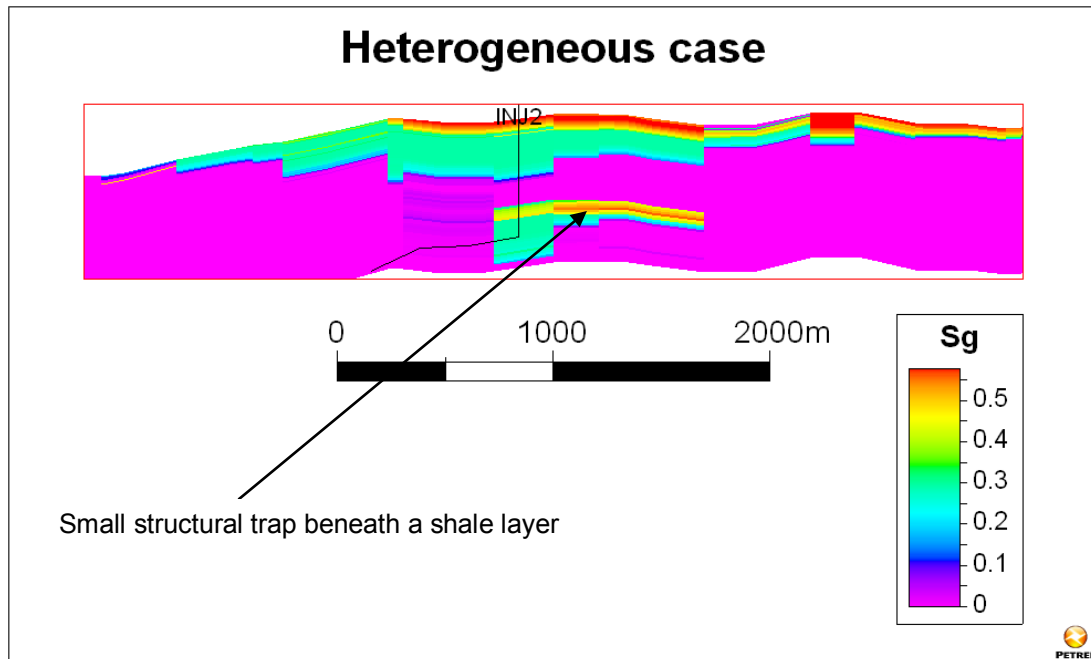


**Figure A4.10: Gas saturation intersection around well INJ2 to show structural trapping under shales at 1000 years for the 11mD heterogeneous case**

#### 4.2.3 Conclusions on the Effect of Heterogeneity

The introduction of heterogeneity has two major effects upon storage pore volume utilisation. In models where injectivity is the limiting factor, such as storage regime 1 and some low permeability storage regime 2 cases, the introduction of heterogeneity reduced the amount that could be injected under a BHP constraint and thus reduced the storage pore volume utilisation. In models where either the 99% storage constraint or migration velocity constraint constrained storage pore volume utilisation, the introduction of heterogeneity was seen to improve storage pore volume utilisation by improving the lateral sweep of CO<sub>2</sub>.

## **5 Discussion**

To assess the implications and significance of the results presented, the limitations of assumptions and the setup used were considered. With these caveats the results reported in this study will then be placed in a broader context for estimating regional storage capacities.

Key new assumptions influencing the results in this study were the constraints within which storage units had their capacity assessed. These interpreted current regulation and guidance, as described in section 5.3.1 in the main report. The constraints allowed for making more realistic capacity estimates in keeping with the interpretation of current regulation, for example allowing mobile but very slowly migrating CO<sub>2</sub> at 1000 years in the capacity, as opposed to requiring fully residually trapped CO<sub>2</sub>. However, regulation can change or current regulation could have been interpreted differently and the results could have some sensitivity to this. Regulatory issues that may affect the results include the time at which CO<sub>2</sub> stability is required, the acceptable migration velocity at that time and the proportion of injected CO<sub>2</sub> that must remain within the storage unit. These are issues for future consideration.

Some assumptions were also required for the assessment of storage capacity within this framework. In particular assessment undertaken in this work was based at the storage site scale, and scenarios with increased dip used tilted versions of the same top-structure.

The first of these assumptions was evaluation at the scale of a storage site that may be considered for licensing and provide operations for a company for years to decades, rather than the entire basin-scale. This provided varying top-surface structure and heterogeneity over a significant 21km x 36km region for assessing the effects of these features. In this work it was assumed that regulation would apply directly to the storage unit scale and therefore the effects of structure and heterogeneity were assessed at this scale. At the basin scale the balance of effects of structure and high dip routes could be altered, for example if the effect of high dip routes is more influential near boundaries, and could be considered for further work. In addition, in this work open boundaries over a storage unit scale were considered, when potentially other units could neighbour this unit, changing the nature of the boundary condition. Given the significant scale of a storage unit, it is not clear how often neighbouring storage units would be in operation at the same time and thus, if over time neighbouring open units were used, there may be a time interval between injection into each, during which pressure dissipation could occur.

Secondly, the effect of top-surface structure on storage sites with larger average dip was assessed using tilted versions of the base-case Forties structure. In the examples with 1° and 3° dip this resulted in very little and no structural closure in the models respectively. This example may or may not be representative of structural closure in higher dip reservoirs. To analyse this further new consideration of a variety of structures would be needed.

Accepting these assumptions, the implications of the results presented in this work to storage capacity estimation are now outlined.

This analysis starts by looking at the implication of introducing high dip regions to smooth models, then structural closure and then the combination of the two as occurs in a realistic top-surface structure.

First the implication of introducing high dip regions is considered. In section 4.1.4 a qualitative difference has been shown between the effect of introducing higher dip routes to smooth model cases with strong low migration velocity storage (storage regime 2) and cases with weak low migration velocity storage (storage regime 3). The implication for storage capacity estimation is that the addition of localised dip that leads to escape or prohibited high migration speeds will:

- Significantly decrease storage pore volume utilisation when low migration velocity storage is high in the equivalent smooth model.
- Make significantly less difference to storage pore volume utilisation if there was little low migration velocity storage in the smooth model.

Secondly, the implication of introducing structural closure is considered. The results obtained in this work have shown that the addition of localised structural closure will increase storage almost independently of low migration velocity storage. Therefore it is expected that the implication for storage capacity estimation is that structural closures will, unsurprisingly, provide additional storage capacity, although the use of this volume depends upon the CO<sub>2</sub> plumes being able to access the correct regions.

With these evaluations of the effect of high-dip routes and structural closure, the general change in storage pore volume utilisation from top-surface structure will depend upon the geological occurrence of structural closures versus high dip routes that the top-surface structure introduces. However, it is more likely that storage units with high amounts of low migration velocity storage (storage regime 2) would have their capacity overestimated by smooth models than storage units with virtually no low migration velocity storage (storage regime 3). This idea is demonstrated in **Figure A5.1**.

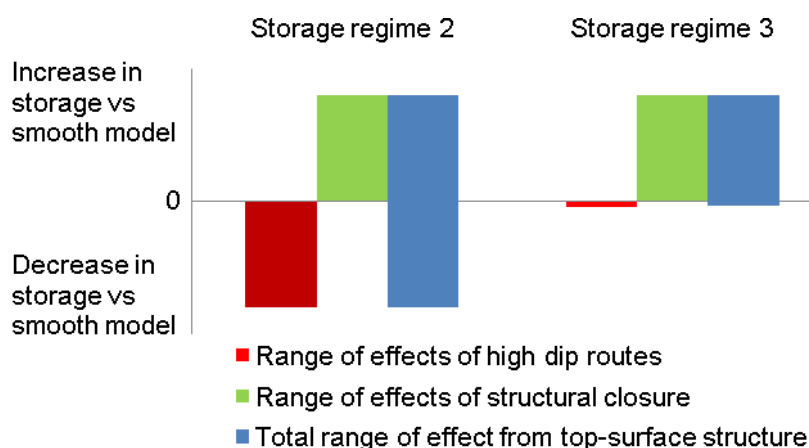


**Figure A5.1: Range of potential general effects of the introduction of top-surface structure to storage regimes 2 and 3**

To extend these ideas further, investigation into the geostatistical occurrence of closure versus high dip routes would be needed. At the national scale this would be useful to avoid systematically overestimating or underestimating storage with smooth models, especially since this study has shown that factor of 2 or more decreases and increases in storage pore

volume utilisation can occur with the introduction of top-surface structure relative to smooth model figures.

There may also be some risk implications arising from the uncertainty in estimates if the effect of top-surface structure cannot be modelled. If the risk is to be avoided more conservative estimates may come from more reliance upon residual trapping, or alternatively estimates that are less influenced by structure may come by considering enhancing residual trapping through the use of brine and CO<sub>2</sub> injection together (Qi et al, 2009).

For heterogeneity similar issues exist with assessing the implications and significance of the conclusions made in this study due to the site-specific permeability distribution. In this study it was observed that heterogeneity can reduce injection significantly in injectivity limited scenarios and increase sweep in the remaining cases. In both cases the shale layers present in the model played an impact upon these, affecting the spread of the pressure footprint and vertical migration of CO<sub>2</sub> respectively and therefore generalising these results is still unclear. For other models where shales are still present the explanation for reduced injectivity due to localised pressure build-up seems likely to be extendable; however further work could be done on this especially when there are no low permeability layers. The result on sweep is supported by a recent paper from Lengler et al. (2010) who show that the breakthrough time of CO<sub>2</sub> is increased by heterogeneity. Given the distances considered in this work are significantly longer than those in the Lengler et al. (2010) study by two orders of magnitude, it is expected that heterogeneity improves sweep in the vast majority of cases by suppressing gravity over-ride and rapid migration along the top of the formation, thus improving storage pore volume utilisation.

In summary this work uses a North Sea example to provide new insights into the effect of top-surface structure on storage pore volume utilisation and gives grounds for further understanding and analysis in the future. Of key significance is that this understanding is based upon analysis of the trapping mechanisms involved in CO<sub>2</sub> storage and helps demonstrate their importance in determining capacity.

This understanding clearly demonstrates that top-surface structure can both increase or decrease storage pore volume utilisation relative to an equivalent smooth model. Whereas in some previous literature heterogeneity has been touted as a source of decreased security through increased migration, and caprock undulation as increased security (Kopp et al., 2009; Juanes et al., 2010), this study has demonstrated that top-surface structure provides a more complex picture and that heterogeneity tends to reduce overall CO<sub>2</sub> plume migration.

## **6 Conclusions**

Top-surface structure and heterogeneity allow for the variation of reservoir dip and permeability, which are the key parameters in determining the storage pore volume utilisation of open aquifers. The effects were evaluated under a realistic interpretation of regulations for capacity estimation using a real North Sea top-surface structure and heterogeneity field and optimisation of injection rates to estimate storage pore volume utilisation. The results were interpreted in terms of three storage regimes. In this Exemplar model case it was seen that the introduction of permeability heterogeneity to a homogeneous model: represent

- reduced storage pore volume utilisation when the storage in the homogeneous model was limited by injectivity, due to localised pressure build-up;
- increased storage pore volume utilisation when injectivity did not constrain storage capacity, by improving sweep of CO<sub>2</sub>,

and the introduction of top-surface structure to smooth storage units:

- decreased storage pore volume utilisation for smooth units with slower characteristic flow velocities for mobile CO<sub>2</sub>;
- increased or maintained pore volume utilisation for smooth units with faster characteristic flow velocities for mobile CO<sub>2</sub>.

In this work it was described how the top-surface structure introduces both structural closures and regions of localised higher dip that either lead to escape or prohibited high migration speeds. The balance of the effects of these features is seen to determine the change in storage pore volume utilisation due to top-surface structure.

Further, the reduction in storage capacity due to localised higher dip is seen to be qualitatively larger and far more significant when top-surface structure is introduced to smooth models that have lower dip and permeability which allow CO<sub>2</sub> to be stored in a mobile and laterally unconfined form at 1000 years relative to those with higher permeability and dip. In the North Sea model studied this dependency was significant enough that the reduction in storage from the introduction of localised higher dip was greater than the increase in storage from the introduction of structural closure when the smooth model was able to store mobile and laterally unconfined CO<sub>2</sub> at 1000 years, but smaller when it was not.

Overall, this work has presented a quantitative framework for assessing storage sites based on different constraints – pressure, migration distance and migration speed and placed different cases into three storage regimes. This work has shown that open aquifers of modest permeability and dip can prove to be favourable storage sites with large storage capacities. These aquifers limit the speed with which the CO<sub>2</sub> migrates while the extensive open pore volume can help dissipate pressure, avoiding pressure problems associated with other types of storage site. This suggests that with careful selection and design, large open aquifers are promising sites for CO<sub>2</sub> storage.

## **7 Acknowledgements**

Particular thanks goes to Surinder Singh Dio for excellent computational support throughout this work.

## 8 References

1. Bachu, S., Bonijoly, D., Bradshaw, J., Burruss, R., Holloway, S., Christensen, N.P., Mathiassen, O.M., 2007. CO<sub>2</sub> storage capacity estimation: Methodology and gaps. *International Journal of Greenhouse Gas Control* 1, 430-443.
2. Bennion, D.B., Bachu, S., 2008. Drainage and imbibition relative permeability relationships for supercritical CO<sub>2</sub>/brine and H<sub>2</sub>S/brine systems in intergranular sandstone, carbonate, shale, and anhydrite rocks. *Spe Reservoir Evaluation & Engineering* 11, 487-496.
3. Bradshaw, B.E., Spencer, L.K., Lahtinen, A.-L., Khider, K., Ryan, D.J., Colwell, J.B., Chirinos, A., Bradshaw, J., Draper, J.J., Hodgkinson, J., McKillop, M., 2011. An assessment of Queensland's CO<sub>2</sub> geological storage prospectivity -- The Queensland CO<sub>2</sub> Geological Storage Atlas. *Energy Procedia* 4, 4583-4590.
4. Bradshaw, J., Bachu, S., Bonijoly, D., Burruss, R., Holloway, S., Christensen, N.P., Mathiassen, O.M., 2007. CO<sub>2</sub> storage capacity estimation: Issues and development of standards. *International Journal of Greenhouse Gas Control* 1, 62-68.
5. Carlson, F.M., 1981. Simulation of Relative Permeability Hysteresis to the Nonwetting Phase, SPE Annual Fall Technical Conference and Exhibition. SPE 10157, San Antonio, Texas.
6. CSLF, 2008. Task Force for Review and Identification of Standards for CO<sub>2</sub> Storage Capacity Estimation.
7. Dahowski, R.T., Li, X., Davidson, C.L., Wei, N., Dooley, J.J., Gentile, R.H., 2009. A Preliminary Cost Curve Assessment of Carbon Dioxide Capture and Storage Potential in China. *Energy Procedia* 1, 2849-2856.
8. Doughty, C., Pruess, K., Benson, S.M., Hovorka, S.D., Knox, P.R., Green, C.T., 2001. Capacity investigation of brine-bearing sands of the Frio formation for geologic sequestration of CO<sub>2</sub>. eScholarship Repository.
9. Evans, D., Graham, C., Armour, A., Bathurst, P., 2003. *The Millennium Atlas: Petroleum geology of the central and northern North Sea*. The Geological Society of London.
10. Flett, M., Gurton, R., Weir, G., 2007. Heterogeneous saline formations for carbon dioxide disposal: Impact of varying heterogeneity on containment and trapping. *Journal of Petroleum Science and Engineering* 57, 106-118.
11. Goodman, A., Hakala, A., Bromhal, G., Deel, D., Rodosta, T., Frailey, S., Small, M., Allen, D., Romanov, V., Fazio, J., Huerta, N., McIntyre, D., Kutcho, B., Guthrie, G., 2011. U.S. DOE methodology for the development of geologic storage potential for carbon dioxide at the national and regional scale. *International Journal of Greenhouse Gas Control* In Press, Corrected Proof.
12. Gorecki, D., Sorensen, J.A., Bremer, J.M., Knudsen, D.J., Smith, S., Steadman, N., Harju, J.A., 2009. Development of Storage Coefficients for Determining the Effective CO<sub>2</sub> Storage Resource in Deep Saline Aquifers, SPE International Conference on CO<sub>2</sub> Capture, Storage and Utilization, San Diego, California, USA,.
13. Gluyas, J.G., Hitchens, H.M., 2002. United Kingdom oil and gas fields: commemorative millennium volume. Geological Society (London) Memoir 20.

14. Hayek, M., Mouche, E., Mugler, C., 2009. Modeling vertical stratification of CO<sub>2</sub> injected into a deep layered aquifer. *Advances in Water Resources* 32, 450-462.
15. Holloway, S., 2009. Storage capacity and containment issues for carbon dioxide capture and geological storage on the UK continental shelf. *Proceedings of the Institution of Mechanical Engineers, Part A: Journal of Power and Energy* 223, 239-248.
16. Holloway, S., Garg, A., Kapshe, M., Deshpande, A., Pracha, A.S., Khan, S.R., Mahmood, M.A., Singh, T.N., Kirk, K.L., Gale, J., 2009. An assessment of the CO<sub>2</sub> storage potential of the Indian subcontinent. *Energy Procedia* 1, 2607-2613.
17. IEAGHG, 2009. Development of Storage Coefficients for Carbon Dioxide Storage in Deep Saline Aquifers, Report no. 2009/13.
18. Jin, M., Pickup, G., Mackay, E., Todd, A., Monaghan, A., Naylor, M., 2010. Static and Dynamic Estimates of CO<sub>2</sub> Storage Capacity in Two Saline Formations in the UK, SPE 131609, SPE EUROPEC/EAGE Annual Conference and Exhibition, Barcelona, Spain.
19. Juanes, R., MacMinn, C., Szulczewski, M., 2010. The Footprint of the CO<sub>2</sub> Plume during Carbon Dioxide Storage in Saline Aquifers: Storage Efficiency for Capillary Trapping at the Basin Scale. *Transport in Porous Media* 82, 19-30.
20. Kopp, A., Class, H., Helmig, R., 2009. Investigations on CO<sub>2</sub> storage capacity in saline aquifers--Part 2: Estimation of storage capacity coefficients. *International Journal of Greenhouse Gas Control* 3, 277-287.
21. Kuuskraa, V.A., Koperna, G.J., Riestenberg, D., Esposito, R., 2009. Using reservoir architecture to maximize CO<sub>2</sub> storage capacity. *Energy Procedia*, 3063-3070.
22. Land, C.S., 1968. Calculation of Imbibition Relative Permeability for Two- and Three-Phase Flow From Rock Properties, SPE Number 1942. *SPE Journal* 8, 149-156.
23. Lengler, U., De Lucia, M., Kühn, M., 2010. The impact of heterogeneity on the distribution of CO<sub>2</sub>: Numerical simulation of CO<sub>2</sub> storage at Ketzin. *International Journal of Greenhouse Gas Control* 4, 1016-1025.
24. Lewis, D., Bentham, M., Cleary, T., Vernon, R., O'Neill, N., Kirk, K., Chadwick, A., Hilditch, D., Michael, K., Allinson, G., Neal, P., Ho, M., 2009. Assessment of the potential for geological storage of carbon dioxide in Ireland and Northern Ireland. *Energy Procedia* 1, 2655-2662.
25. Li, X., Wei, N., Liu, Y., Fang, Z., Dahowski, R.T., Davidson, C.L., 2009. CO<sub>2</sub> Point Emission and Geological Storage Capacity in China. *Energy Procedia* 1, 2793-2800.
26. MacMinn, C.W., Szulczewski, M.L., Juanes, R., 2010. CO<sub>2</sub> migration in saline aquifers. Part 1. Capillary trapping under slope and groundwater flow. *Journal of Fluid Mechanics* 662, 329-351.
27. MacMinn, C.W., Szulczewski, M.L., Juanes, R., 2011. CO<sub>2</sub> migration in saline aquifers: Regimes in migration with dissolution. *Energy Procedia* 4, 3904-3910.
28. Obi, E.-O.I., Blunt, M.J., 2006. Streamline-based simulation of carbon dioxide storage in a North Sea aquifer. *Water Resour. Res.* 42.
29. Ogawa, T., Nakanishi, S., Shidahara, T., Okumura, T., Hayashi, E., 2011. Saline-aquifer CO<sub>2</sub> sequestration in Japan-methodology of storage capacity assessment. *International Journal of Greenhouse Gas Control* 5, 318-326.

30. Pickup, G.E., Jin, M., Olden, P., Mackay, E., Todd, A.C., Ford, J.R., Lawrence, D., Monaghan, A., Naylor, M., Haszeldine, R.S., Smith, M., 2011. Geological storage of CO<sub>2</sub> : Site appraisal and modelling. *Energy Procedia* 4, 4762-4769.
31. Pruess, K., 2005. A TOUGH2 Fluid Property Module for Mixtures of Water, NaCl, and CO<sub>2</sub>. Earth Sciences Division, Lawrence Berkeley National Laboratory, University of California, Berkeley CA 94720, LBNL-57952.
32. Qi, R., LaForce, T.C., Blunt, M.J., 2009. Design of carbon dioxide storage in aquifers. *International Journal of Greenhouse Gas Control* 3, 195-205.
33. Radoslaw, T., Barbara, U.M., Adam, W., 2009. CO<sub>2</sub> storage capacity of deep aquifers and hydrocarbon fields in Poland - EU GeoCapacity Project results. *Energy Procedia* 1, 2671-2677
34. Szulczewski, M., Juanes, R., 2009. A simple but rigorous model for calculating CO<sub>2</sub> storage capacity in deep saline aquifers at the basin scale. *Energy Procedia* 1, 3307-3314.
35. Ukaegbu, C., Gundogan, O., Mackay, E., Pickup, G., Todd, A., Gozalpour, F., 2009. Simulation of CO<sub>2</sub> storage in a heterogeneous aquifer. *Proceedings of the Institution of Mechanical Engineers Part a-Journal of Power and Energy* 223, 249-267.
36. USDOE, 2010. Carbon Sequestration Atlas of the United States and Canada.
37. van der Meer, L.G.H., Yavuz, F., 2009. CO<sub>2</sub> storage capacity calculations for the Dutch subsurface. *Energy Procedia* 1, 2615-2622.
38. Vangkilde-Pedersen, T., Anthonsen, K.L., Smith, N., Kirk, K., Neele, F., van der Meer, B., Le Gallo, Y., Bossie-Codreanu, D., Wojcicki, A., Le Nindre, Y.M., Hendriks, C., Dalhoff, F., Christensen, N.P., 2009. Assessing European capacity for geological storage of carbon dioxide - the EU GeoCapacity project. *Energy Procedia* 1, 2663-2670.
39. Vella, D., Huppert, H., 2006. Gravity currents in a porous medium at an inclined plane. *Journal of Fluid Mechanics* 555, 353.